Urban Green Infrastructure: Modelling and Implications to

Environmental Sustainability

by

Jiachuan Yang

A Dissertation Presented in Partial Fulfillment
of the Requirements for the Degree
Doctor of Philosophy

Approved November 2016 by the
Graduate Supervisory Committee:

Zhihua Wang, Chair
Kamil Kaloush
Soe Myint
Huei-Ping Huang
Giuseppe Mascaro

ARIZONA STATE UNIVERSITY

December 2016

ABSTRACT

The combination of rapid urban growth and climate change places stringent

constraints on multisector sustainability of cities. Green infrastructure provides a great

potential for mitigating anthropogenic-induced urban environmental problems;

nevertheless, studies at city and regional scales are inhibited by the deficiency in

modelling the complex transport coupled water and energy inside urban canopies. This

dissertation is devoted to incorporating hydrological processes and urban green

infrastructure into an integrated atmosphere-urban modelling system, with the goal to

improve the reliability and predictability of existing numerical tools. Based on the

enhanced numerical tool, the effects of urban green infrastructure on environmental

sustainability of cities are examined.

Findings indicate that the deployment of green roofs will cool the urban

environment in daytime and warm it at night, via evapotranspiration and soil insulation.

At the annual scale, green roofs are effective in decreasing building energy demands for

both summer cooling and winter heating. For cities in arid and semiarid environments, an

optimal trade-off between water and energy resources can be achieved via innovative

design of smart urban irrigation schemes, enabled by meticulous analysis of the water-

energy nexus. Using water-saving plants alleviates water shortage induced by population

growth, but comes at the price of an exacerbated urban thermal environment. Realizing

the potential water buffering capacity of urban green infrastructure is crucial for the long-

term water sustainability and subsequently multisector sustainability of cities.

Environmental performance of urban green infrastructure is determined by land-

atmosphere interactions, geographic and meteorological conditions, and hence it is

recommended that analysis should be conducted on a city-by-city basis before actual

implementation of green infrastructure.

ACKNOWLEDGMENTS

Finally, yet most importantly, I would like to express my sincere gratitude to my friends, relatives, and family for their constant understanding, support, and help throughout my life.

TABLE OF CONTENTS

LIST OF TABLES

LIST OF FIGURES

Figure   Page

CHAPTER 1 INTRODUCTION

1.1. Literature Review

Global population has become increasingly urbanized: about 52% of the world's population live in cities in 2012, and this proportion is projected to increase to 67% by 2050 (United Nations 2012). During the past decades, natural terrains have been continuously converted to urban landscapes to meet the ever-increasing demand of the expanding urban population (Seto et al. 2011). Urbanization changes the surface energy and moisture balances (Yang et al. 2013), leading to higher temperatures in urban areas as compared to surrounding rural areas, which is known as the Urban Heat Island (UHI) effect and has been considered as one of the major challenges posed to human beings in the 21st century (Arnfield 2003, Rizwan et al. 2008). The adverse effects induced by UHI include but are not limited to, elevated temperatures (Tran et al. 2006, Imhoff et al. 2010), increased energy consumption (Fung et al. 2006, Hirano and Fujita 2012), air pollution (Sarrat et al. 2006, Nazaroff 2013), heat-related mortality and morbidity (Tan et al. 2010, Mishra and Ramgopal 2013), and disruption to ecosystems (Eigenbrod et al. 2011). On the other hand, global climate change is forecasted to cause more frequent occurrences of climatic extremes, such as heat waves and severe floods, imposing additional challenges on urban environment (Field et al. 2014). The synergistic interactions between UHIs and heat waves (Li and Bou-Zeid 2013) make cities become unprecedentedly vulnerable to environmental problems in the future that adaptation and mitigation strategies are critical to alleviate UHIs and their subsequent adverse environmental effects.

1

During the past decades, numerous strategies have been proposed, developed and implemented to mitigate UHIs, including reflective materials (Synnefa et al. 2006, 2008), materials with high optical and thermal performances (Ma et al. 2002, Karlessi et al. 2009, Yang et al. 2016b), green roofs (Dvorak and Volder 2010), urban parks and trees (Bowler et al. 2010, Shashua-Bar et al. 2011), heat sinks (Geros et al. 2005), to name a few. Among these techniques, green roofs, urban parks, and shade trees can be grouped as the urban green infrastructure. Green infrastructure is recognized as an effective method for mitigating UHIs that provides multi-scale ecological, economic and social benefits for the urban environment (Mell 2010). Maximum surface temperature of vegetated surface can be more than 20 K cooler than that of engineering materials (Wilmers 1988). Urban green infrastructure cools the built-up environment mainly through two mechanisms, i.e. evapotranspiration and shading. Via evapotranspiration, vegetation redistributes the available solar energy incident on the land surface for latent heat of vaporization and reduces the sensible heat flux. In terms of the shading effect, tree canopies block transportation of solar radiation that the shaded areas receive less heat and subsequently have a lower surface temperature.

Recent years have seen rapidly increasing number of studies on green infrastructure. A systematic quantitative review identified a total of 115 original research papers on urban trees published between 1981 and 2011 (Roy et al. 2012). Another review study found 74 articles that had measured ground-level cooling effect of urban green infrastructure (Bowler et al. 2010). Though the cooling effect is affected by patch sizes, geographical and climatic conditions, a meta-analysis of data suggested that an urban park would be around 1 °C cooler than a non-green site on average (Bowler et al. 2010).

With its capacity to reduce temperatures, urban green infrastructure can decrease building energy consumption (Niachou et al. 2001, Wong et al. 2003, Yang and Wang 2015, Wang et al. 2016) and enhance outdoor thermal comfort of pedestrians (Lin et al. 2010, Park et al. 2012). A simulation study found that the installation of green roof can save the annual energy consumption of a five-story commercial building in Singapore by 0.6 – 14.5% (Wong et al. 2003). The high surface area and roughness of green infrastructure make it an effective sink for urban air pollutants. Using a dry deposition model, Yang et al. (2008) suggested that 198000 m^2 of green roofs could remove a total of 1675 kg air pollutants in one year for Chicago. The soil layer of urban green infrastructure also provides benefits for stormwater runoff retention (Mentens et al. 2006).

Most of the existing studies on urban green infrastructure has been limited to field measurements and simulation results at neighbourhood scales, upscaling the results of these studies for guidance on green infrastructure for a city or regional scale is difficult, due to the substantial influence of surface heterogeneity (Ramamurthy et al. 2014). For city and regional scales, a modelling approach is more feasible than in-situ experiments as building green infrastructure involves high capital cost and stakeholder communication. The lack of studies of green infrastructure at city and regional scales is mainly owing to the complexity of coupled water and energy transport inside urban canopies. Numerical simulations of urban green infrastructure necessarily require realistic representations of urban surface processes and land-atmosphere interactions (Song and Wang 2015). Among the available urban land surface models, the family of urban canopy models (UCMs) have been demonstrated as a useful tool for capturing the coupled water and energy budgets over urban areas (Kusaka et al. 2001, Martilli et al. 2002, Wang et al.

2013). An international effort was conducted to compare a wide range of these urban canopy models and to evaluate them against site observations (Grimmond et al. 2010, 2011). It is identified that the latent heat flux is the one for which the models demonstrated the least capability. This is because most models are inadequate in calculating urban water budgets due to the oversimplified representation of complex urban hydrological processes and urban vegetation. Various problems exist: for example, Masson (2000) modelled surface intercepted water as small reservoirs and took snow effects into consideration in urban areas, but without resolving the anthropogenic water budget explicitly. Lee and Park (2008) and Wang (2014a) included tall trees in the urban canopy model but neglected subsurface moisture transport. Outdoor irrigation, the important moisture source for urban green infrastructure, is also neglected in most of the existing urban canopy models (Yang and Wang, 2015). The net effect of the simplified representations is that the root-mean-square error between the predicted and observed latent heat fluxes can be up to the same order of magnitude as the latent heat flux per se (Grimmond et al. 2010, 2011). This significant deviation consequently introduces errors into the modelling of urban climate and impacts the reliability and accuracy of predicted effects of urban green infrastructure.

1.2. Study Objectives

Based on the background and identified deficiency in studies of urban green infrastructure discussed in Chapter 1.1, this study is intended to implement physically-based representation of urban green infrastructure into the urban canopy model. Subsequently, by coupling the urban canopy model with a mesoscale atmospheric model,

regional impact of urban green infrastructure can be quantified. The dissertation will mainly address the following key issues on environmental performance of urban green infrastructure:

1) Impact of green roofs on building energy efficiency and urban climate at the city scale under different geographical and climatic conditions;

2) Potential of adjusting irrigation schemes for urban lawn to achieve optimal water-energy trade-off;

3) Seasonal variation of the effect of green roofs on regional hydroclimate in a coupled land-atmosphere system;

4) Potential water buffering capacity of urban green infrastructure and its implications for water management towards a city of multisector sustainability.

1.3. Organization of this Dissertation

This dissertation is organized as follows. Chapter 2 describes the implementation of urban hydrological processes into the urban canopy model and its impact on predicting the coupled water and energy budgets over built terrains. Chapter 3 investigates the relationship between water and energy consumption in the urban environment, and discusses the potential of developing a smart irrigation scheme for the optimal water-energy trade-off in a desert city. Chapter 4 presents the effect of green roofs on urban hydroclimate in a coupled land-atmosphere system. The impact of urban hydrological processes at the regional scale is assessed for two major metropolitan areas in the United States. Chapter 5 explores the water buffering capacity of urban green infrastructure in the Phoenix metropolitan area and discusses the long-term water sustainability under the

challenge of future climate change and population growth. Chapter 6 summarizes the

entire study and concludes the key findings on environmental performance of urban green

infrastructure. Recommendations for future research directions are also given in Chapter

6.

CHAPTER 2 IMPACT OF GREEN ROOFS ON BUILDING ENERGY EFFICIENCY
AND URBAN CLIMATE

2.1. Introduction

Green roof, rooftop with a vegetation layer, has been proved as an effective system
to alleviate some urban environmental problems under a wide range of climate conditions
through field observations (Santamouris et al. 2007, Jim and He 2010). However, at the
city and regional scale, a numerical model that well captures energy as well as water
budget on green roof in the urban environment is still missing. On the other hand, while
existing urban canopy models have shown overall good performance in capturing urban
surface energy balance and boundary-layer structure, they are inadequate in calculating
urban water budgets due to the oversimplified representation of complex urban
hydrological processes (Grimmond et al. 2010, 2011). To understand the environmental
effect of green roofs, implementing a physically-based parameterization into the urban
canopy model with an accurate representation of the hydrological processes is therefore
critical.

Compared to natural landscapes, urban environments consist of a considerable
fraction of paved surfaces. Though a pavement is able to store water due to surface
porosity, local slope gradient and surface depressions, evaporation from paved surfaces
has been largely neglected in urban canopy models. Evaporation arising from water-
holding pavement surfaces, especially during and shortly after precipitation, contributes a
substantial fraction of moisture fluxes arising from a built environment (Ramamurthy and
Bou-Zeid 2014). Another dimension of complexity in urban hydrology arises from the
anthropogenic sources, examples including water release from commercial buildings

(Moriwaki et al. 2008) and urban irrigation (Johnson and Belitz 2012). In addition, in contrast to natural terrains, a considerable fraction of urban vegetation presents as isolated patches, such as hedges, roadside trees, and garden plants. Along the upwind edge of a vegetation canopy surrounded by a lower roughness surface, due to the lack of obstacles to both radiation and airflow, the advection and 'clothesline effect' (Hagishima et al. 2007) lead to higher rates of evapotranspiration. Patchy urban vegetation has therefore higher rate of potential evapotranspiration, a phenomenon known as the oasis effect (Oke 1979).

To address the challenges in modelling the urban water cycle, Wang et al. (2011a, 2013) developed an improved urban canopy model to incorporate detailed hydrological processes, including evaporation over vegetated and engineered surfaces, sub-facet heterogeneity for water transport, and green roof systems. Capability of the model has been validated by field measurements under different climate conditions (Sun et al. 2013, Wang et al. 2013). More recently, Miao and Chen (2014) formulated urban irrigation, oasis effect, and anthropogenic latent heat into a single layer urban canopy model. It is noteworthy that their evaporation parameterization over impervious surfaces was based on an empirical decay function, and the model was only tested for the Beijing metropolitan area. Inspired by the recent work, the aim of our study in this Chapter is to further improve and test the reliability and predictability of the urban canopy model. We adopted the single layer urban canopy model (SLUCM), a widely-used urban parameterization scheme in the Weather Research and Forecasting (WRF) system, as the basis for incorporating physically-based representation of urban hydrological processes. Our objectives are to: (1) enhance and evaluate the modelling of urban hydrological

8

processes in the current SLUCM, and (2) assess the capacity of physical parametrizations of multilayer green roofs in mitigating urban environmental problems at the city scale. Numerical simulations are driven by meteorological forcing and compared against surface energy budgets, both obtained from eddy-covariance measurements at four metropolitan areas, namely Beijing (China), Montréal (Canada), Vancouver (Canada), and Phoenix (U.S.).

2.2. Representation of Urban Hydrological Processes

2.2.1 Single layer urban canopy model

A schematic of the single layer urban canopy model is shown in Fig. 2.1a. Building arrays are represented as a two-dimensional and longitudinally infinite street canyon. To better capture the urban water cycle, we include the following hydrological processes in the new model: (1) energy and water balance of multilayer green roofs, (2) evaporation from engineered pavements, (3) urban irrigation, (4) anthropogenic latent heat, and (5) urban oasis effect. A detailed description of each process is provided below. Compared to the current SLUCM scheme in the WRF model, the urban canopy model developed here explicitly accounts for the surface heterogeneity. In particular, building roofs consist of green roofs and engineered roofs with different hydrothermal properties (Fig. 2.1b). The surface energy balance in the new SLUCM is given by:

$$R_n + Q_F = LE + H + G, \qquad (0.1)$$

where R_n is the net radiation, Q_F is the anthropogenic heat, LE, H and G are the latent, sensible and ground heat fluxes respectively.

9
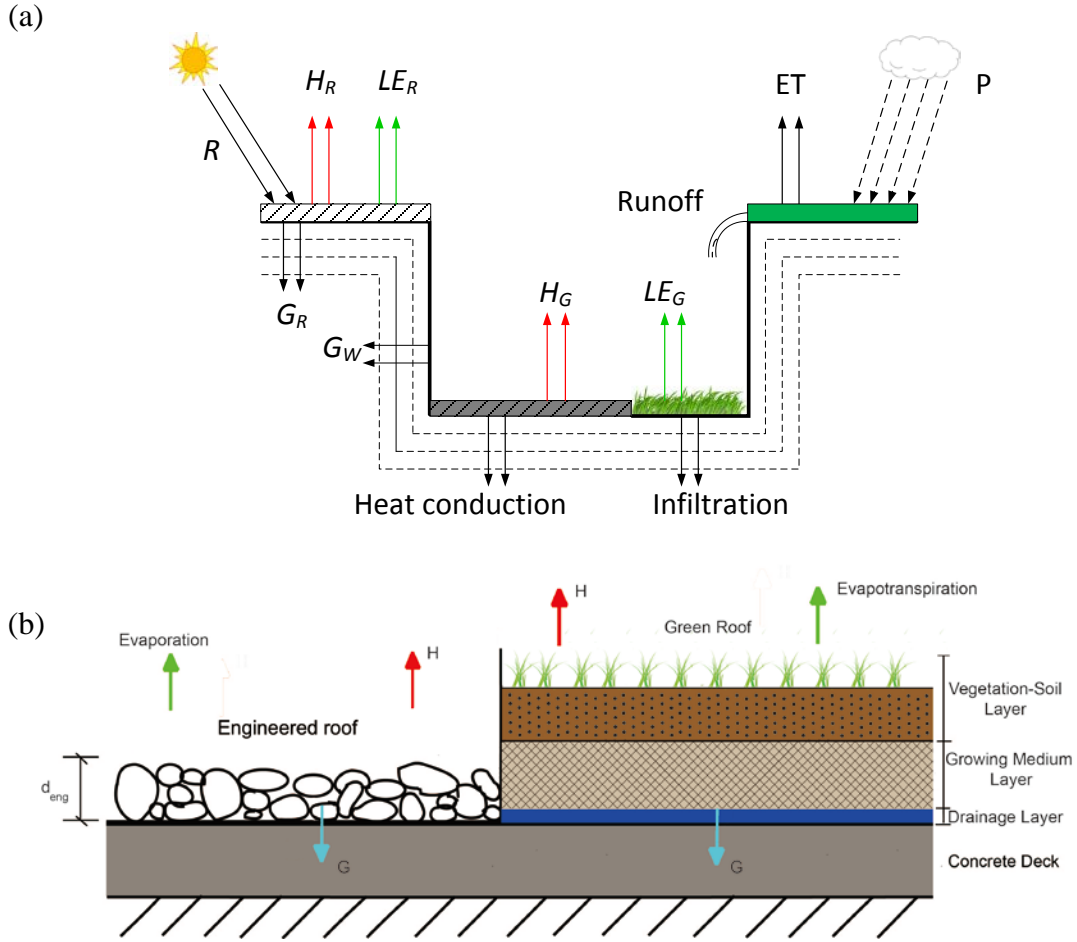
Figure 2.1. Schematics for (a) the single layer urban canopy model, and (b) a green roof and an engineered roof. Subscripts R, W, and G denote properties of roof, wall and ground, respectively; d_eng in (b) is the maximum water-holding depth of the paved surface.

In particular, the latent heat flux arising from a WRF urban grid cell consisting of both urban (impervious) and vegetation landscape is computed as (Chen and Dudhia 2001):

$$LE = (LE_{urb} + Q_{ALH})f_{urb} + LE_{veg}(1 - f_{urb}),$$ (0.2)

$$LE_{veg} = C_H E_p \alpha_{oasis},$$ (0.3)

$$LE_{urb} = rf_{gr}LE_{gr} + r(1 - f_{gr})LE_r + (1-r)LE_g + 2hLE_w,$$ (0.4)

10

where Q_{ALH} is the anthropogenic latent heat, f_{urb} is the fraction of urban landscape; subscripts urb, veg, gr, r, g, and w denote the urban landscape, vegetation landscape, green roof, roof, ground and wall respectively; E_p is the potential evaporation rate; C_H is a coefficient that accounts for the impacts of other variables on the evaporation; α_{oasis} is the oasis parameter; and dimensionless variables r and h represent the normalized roof width and building height respectively. The WRF model adopts a "tile" approach, where latent heat fluxes over built surfaces LE_{urb} is calculated using the single layer urban canopy model and LE_{veg} is computed using the Noah land surface model.

2.2.2 Water balance of multilayer green roofs

A schematic of the multilayer green roof system is shown in Fig. 2.1b. Compared to a conventional roof, it has three additional layers on top of the concrete deck, viz. the vegetation-soil, the growing media and the drainage layers. All three layers consist of porous materials and their volumetric water content θ is computed by vertically discretizing the layer. Temporal and spatial distribution of θ in the intermediate layers is given by the diffusive form of the Richards equation:

$$\frac{\partial \theta}{\partial t} = D(\theta)\frac{\partial^2 \theta}{\partial z^2} + \frac{\partial}{\partial z}K(\theta),$$ (0.5)

where $D(\theta)$ and $K(\theta)$ are the θ-dependent hydraulic diffusivity and conductivity respectively. This form is derived from Darcy's law assuming rigid, isotropic and homogeneous soils. Total latent heat flux over a green roof is then calculated from:

$$LE_{gr} = LE_{dir} + LE_c + LE_t,$$ (0.6)

where subscripts dir, c, and t represent direct evaporation from top soil layer, evaporation of precipitation intercepted by vegetation canopy and transpiration via vegetation. Details of these three components can be found in the community Noah land surface model developed by Chen and Dudhia (2001). Intensive and extensive roofs are two major types of existing green roofs. Within the green roof system, depths of the vegetation-soil layer and growing medium layer are strongly related to plant types and root depths, which can vary from about 0.05 m to more than 1 m depending on vegetation types (Dvorak and Volder 2010). For simplicity, in this Chapter we used a constant thickness of 0.15 m for both growing medium and soil-vegetation layers. The drainage layer is a thin layer constructed to transport drainage moisture away, and therefore its depth is not explicitly modelled.

2.2.3 Evaporation over paved surfaces

In contrast to natural landscapes (soils and vegetation), engineered surfaces admit much simpler hydrological processes. As illustrated in Fig. 2.1b, for a paved roof, a water-holding layer exists above the impervious datum due to the porosity of pavement. The layer also exists on wall and road surfaces. Water is retained within this layer and acts as the source for evaporation. The latent heat flux over engineered pavements is given by (Wang et al. 2013):

$$LE = \frac{\delta}{d_{eng}} \phi E_p,$$ (0.7)

Where ϕ is the porosity of engineered materials, d_{eng} is the maximum water-holding depth dependent on pavement materials, and δ is the water retention depth given by:

$$\phi \frac{\partial \delta}{\partial t} = \begin{cases} 0, & \text{if } \delta > d_{eng} \\ \max(0, P - \phi E_p), & \text{if } 0 \le \delta \le d_{eng}, P > 0, \\ P - \phi E_p, & \text{if } 0 \le \delta \le d_{eng}, P \le 0 \end{cases} \qquad (0.8)$$

where P is the precipitation intensity. Previous studies have assigned different values to

d_{eng}; for example, Grimmond and Oke (1986) used a value of 0.59 mm to represent the

retention capacity of impervious surfaces. Recently, Ramamurthy and Bou-Zeid (2014)

adopted a value of 1 mm for ground concrete and asphalt pavements. In this study, we set

d_{eng} to be 1 mm, 0.2 mm and 1 mm for engineered roof, wall and ground surfaces,

respectively.

2.2.4 Urban irrigation

A number of methods for estimating urban irrigation have been previously

developed, including the use of field measurements, the minimum-month method, and

energy balance formulas (Mayer et al. 1999, Senay et al. 2007). However, many of these

methods are computationally expensive and inaccurate at the city or regional scale

(Johnson and Belitz 2012). The impact of summertime irrigation was qualitatively

discussed in previous studies for several cities, e.g. Beijing (Miao and Chen 2014),

Phoenix (Diem and Brown 2003) and Vancouver (Grimmond and Oke 1986). Timing,

duration and amount of irrigation vary from city to city and are subject to change with

vegetation types as well as local practices and regulations. Irrigation is therefore difficult

to represent at the city scale. For simplicity, here we assume that urban irrigation is

conducted for a 2-h period from 1800 to 2000 local time each day from May to

September in all study cities. When irrigated, moisture of the top two soil layers (0.4 m

thick) of urban lawns or green roofs is set to reach a threshold value of 0.33 where

transpiration is not limited by water availability. Such treatment is used to broadly

represent, rather than exactly match, urban irrigation schemes in a variety of cities.

Development of a physically-based irrigation model remains an open challenge in urban

hydroclimate modelling.

2.2.5 Anthropogenic latent heat

The importance of anthropogenic heat in an urban area has been long recognized

and studied since the 1980s (Oke 1988, Grimmond 1992). To date, however, most studies

have assumed that the anthropogenic heat is sensible heat in nature without accounting

the latent heat component. In the current SLUCM, anthropogenic heat was modelled as a

fixed diurnal profile added to the sensible heat flux. Several recent studies suggested that

water vapour emissions by cooling systems constitute a substantial portion of latent heat

flux in urban areas (Sailor et al. 2007, Miao and Chen 2014); in central Tokyo, this flux

was shown to exceed 500 W m^{-2} during summer (Moriwaki et al. 2008). The diurnal

variation of anthropogenic latent heat follows the schedule of human activity and is

relatively independent of season (Moriwaki et al. 2008). Anthropogenic latent heat in the

surface energy budget is given by:

$$Q_{ALH} = Q_{ALHMAX} f_{ALH} , \qquad (0.9)$$

where Q_{ALHMAX} is the daily maximum anthropogenic latent heat value dependent on the

season and f_{ALH} is a diurnally-varying coefficient. Miao and Chen (2014) developed a

diurnal profile of f_{ALH} for the Beijing metropolitan area based on predicted LE from the

single layer urban canopy model and meteorological observations. Their diurnal profile

14

matches with daily human activities and is similar to that of Tokyo derived by Moriwaki et al. (2008). We adopt this profile to represent the general diurnal variability of urban anthropogenic latent heat and apply it to Vancouver, Montréal and Phoenix in subsequent simulations. Q_{ALHMAX} is estimated to be 17.0, 41.9, 24.4 and 18.0 W m^{-2} for spring, summer, fall and winter in Beijing, respectively (Miao and Chen 2014). In Vancouver, monthly average anthropogenic latent heat is estimated using a top-down methodology developed by Sailor and Lu (2004).

Seasonal anthropogenic latent heat data is not available for Phoenix and Montréal, although previous studies have estimated daily maximum anthropogenic heat values for Montréal (Lemonsu et al. 2010) and Phoenix (Sailor and Hart 2006). In this Chapter, we adopt the approach of Bateni and Entekhabi (2012) to partition the total anthropogenic heat into sensible and latent heat components. Given a small temperature perturbation, based on a linear stability analysis to restore the land surface to thermodynamic equilibrium, the ratio of anthropogenic latent heat to sensible heat is computed as (Yang and Wang 2014b):

$$\frac{Q_{ALHMAX}}{Q_{ASHMAX}} = \beta \frac{\Delta}{\gamma}, \tag{0.10}$$

$$Q_{ALHMAX} + Q_{ASHMAX} = Q_{AHMAX}, \tag{0.11}$$

where Q_{AHMAX} is the daily maximum anthropogenic heat value, Q_{ASHMAX} is the daily maximum anthropogenic sensible heat value, Δ is the slope of the saturation vapour pressure curve, γ is the psychrometric constant, and β is the moisture availability parameter: $\beta = 0$ for completely dry surfaces and 1 for saturated surface. Yang et al. (2013) evaluated the method against field measurements over lake, vegetation, and

suburban land surfaces. It was found that a reasonable choice of β is about 0.5 in fall and about 1.5 in summer over a vegetated surface. The value of β exceeds 1 in summers because of the additional transpiration process by urban vegetation. Assuming the latent heat flux over impervious surfaces is negligible in the absence of rainfall, moisture availability of the city is calculated using:

$$\beta = \beta_{veg}(1 - f_{urb}),$$ (0.12)

where β_{veg} is set as 1.0, 1.5, 0.5 and 0.2 for spring, summer, fall and winter, respectively. This method, albeit not exact, provides a usable scheme to estimate anthropogenic sensible and latent heat where detailed data are not available.

2.2.6 Urban oasis effect

The urban oasis effect on plant transpiration rate has been addressed in several field experiments. A schematic of this effect is shown in Fig. 2.2. Without obstacles to radiation and airflow, patchy vegetation in urban areas has higher rates of potential evapotranspiration than large-area vegetation in natural environment. Oke (1979) found that the actual evapotranspiration from an irrigated suburban lawn was about 1.3 times greater than that from an irrigated rural pasture. Hagishima et al. (2007) conducted experiments using 203 nearly homogeneous potted plants and concluded that scattered small plants had a transpiration rate about 1.6 times that of large vegetation. Miao and Chen (2014) used meteorological observations with the SLUCM and obtained an oasis parameter of about 1.5 for Beijing. Here we adopt a value of 1.5 to account for the oasis effect on potential evapotranspiration rate of urban vegetation.

Urban oasis effect: $PET_{urban} > PET_{rural}$
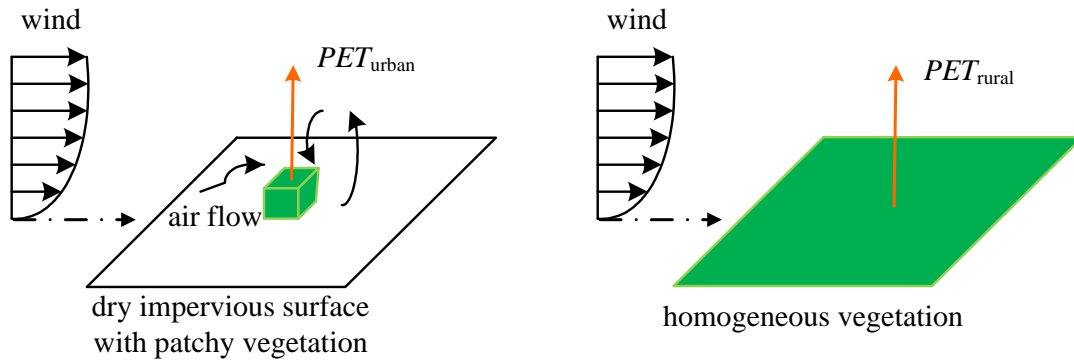
Figure 2.2. Schematics for oasis effect: comparing potential evapotranspiration (PET) over vegetated surfaces in urban and rural areas.

2.3. Study Metropolitan Areas

To evaluate the enhanced single layer urban canopy model, flux measurements were collected from eddy-covariance towers in four metropolitan areas, viz. Beijing, Phoenix, Vancouver and Montréal. Basic meteorological quantities such as wind speed, wind direction, air temperature and relative humidity were also measured at these sites. In the Beijing metropolitan area, three-layer flux observations were carried out at 47, 140 and 280 m of the Chinese Academy of Sciences' 325-m-high Meteorological and Environmental Observation Tower (Miao et al. 2012). Footprint analysis by Wang et al. (2009) demonstrated that the flux measurement at 140 m covered a major fraction of the Beijing metropolitan area (20 km × 20 km). For Vancouver and Montréal, datasets were acquired from the Environmental Prediction in Canadian Cities (EPiCC) network (http://www.epicc.ca), which conducted measurements to evaluate the urban meteorological numerical systems used at the Meteorological Service of Canada. Here we

17

use data from the Vancouver Sunset tower location and the Montréal urban residential

site. More details can be found in Bergeron and Strachan (2012) for the Montréal site,

and in Tooke et al. (2009) and van der Laan et al. (2011) for Vancouver. In Phoenix,

observations were obtained from the eddy-covariance tower deployed at Maryvale, West

Phoenix, through the Central Phoenix Project Long Term Ecological Research program.

Local-scale surface energy balance of the area has been measured for the entire calendar

year 2012 (Chow et al. 2014).

2.4. Model Evaluation and Discussion

Here we present simulation results from the SLUCM with enhanced modelling of

urban hydrological processes, compared against measurement datasets collected at the

four aforementioned metropolitan areas. Hereafter, we refer to the current SLUCM as the

old SLUCM, and the version with proposed hydrological processes as the new SLUCM.

In this Chapter, models are run in an offline (stand-alone) mode. Simulations are driven

by half-hourly meteorological dataset measured from eddy covariance towers, including

wind speed, wind direction, air temperature, relative humidity, atmospheric pressure,

incoming shortwave and longwave radiation, and precipitation. Without records of large-

scale deployment of green roofs in any of these study cities during the measurement

periods, simulations are performed with 0% green roof fraction.

Performance of the SLUCM and coupled hydrological processes relies heavily on

the accurate determination of input parameters (Loridan et al. 2010; Wang et al. 2011b;

Yang and Wang 2014a). As field measurements of all input parameters of the model are

rarely possible, we only collect sensitive parameters of the model. Loridan et al. (2010)

performed an extensive evaluation of the SLUCM and found that the latent heat flux is most sensitive to the vegetation fraction. In Beijing, land cover and building characteristics have been reported by Wang et al. (2009). Urban land-surface parameters were obtained from high resolution lidar data for Vancouver (Goodwin et al. 2009), and from satellite imagery as well as public Geographic Information System data for Montréal (Lantz and Wang 2010). In Phoenix, Myint et al. (2011) developed a set of multi-scale decision rules and supervised approaches using an object-based classifier, and achieved an overall accuracy higher than 90% in urban land cover classification. This method is employed to acquire vegetation fraction of a 1 km × 1 km area centred at the eddy-covariance tower in Phoenix. At each site, area-averaged albedo is estimated from measured incoming and outgoing shortwave radiations during a diurnal cycle on a summer clear day. Facet albedo values are then assigned (i.e., for roof, wall and ground) to achieve the correct overall surface albedo.

In addition to those obtained from field analysis, default values are used for the rest of the parameters. Currently, urban canopy parameters are prescribed in the SLUCM for three urban land-use categories: low-density residential, high-density residential, and industrial and commercial. We use the industrial and commercial category to represent the Beijing study site, and the high-density residential category for Phoenix, Montréal and Vancouver. Properties of different vegetated surfaces are also prescribed in the model. Based on results from Loridan et al. (2010), we select the cropland/grassland category to represent the urban vegetation for Beijing, and the mixed shrubland/grassland category for Phoenix, Montréal and Vancouver. Urban canopy parameters and simulation periods for the four study sites are summarized in Table 2.1. Due to limited data

availability, the simulation for Montréal is only run for 20 and 35 days during spring and
summer 2009, respectively.

Table 2.1. Urban canopy parameters and simulation periods for study metropolitan areas.

Input parameters	Unit	Phoenix	Beijing	Vancouver	Montréal
h (building height)	m	7.5[a]	18.3[d]	4.9[e]	8.35[f]
l_{roof} (roof width)	m	9.4[a]	10[a]	12.3[e]	14[f]
l_{road} (road width)	m	9.4[a]	10[a]	9.4[a]	25.2[f]
f_{urb} (urban fraction)	-	0.844[b]	0.783[d]	0.68[e]	0.72[f]
α_R (albedo of roof)	-	0.16	0.2	0.1	0.12
α_W (albedo of wall)	-	0.16	0.2	0.1	0.12
α_G (albedo of road)	-	0.16	0.2	0.1	0.12
Q_{AHMAX}	W m^{-2}	10.3[c]	*[1]	*[2]	24.0[g]
Vegetation	-	shrubland/ grassland	cropland/ grassland	shrubland/ grassland	shrubland/ grassland
Simulation period	-	04/17/12- 12/31/12	06/30/09- 06/30/10	01/22/09- 10/31/09	04/03/09- 08/31/09[#]
Spring	-	04/17/12- 05/31/12	03/01/10- 05/31/10	03/01/09- 05/31/09	04/03/09- 04/23/09
Summer	-	06/01/12- 08/31/12	07/01/09- 08/31/09	06/01/09- 08/31/09	06/01/09- 08/31/09[#]

a: Default values prescribed in Noah/SLUCM; b: Myint et al. (2011); c: Sailor and Hart (2006); d: Wang et al. (2009);

e: Goodwin et al. (2009); f: Lantz and Wang (2010); g: Lemonsu et al. (2010)

*[1]: Seasonal data of anthropogenic latent heat available from Miao and Chen (2014)

*[2]: Seasonal data of anthropogenic latent heat available from Sailor and Lu (2004)

[#]: Gap exists due to data availability during the simulation period
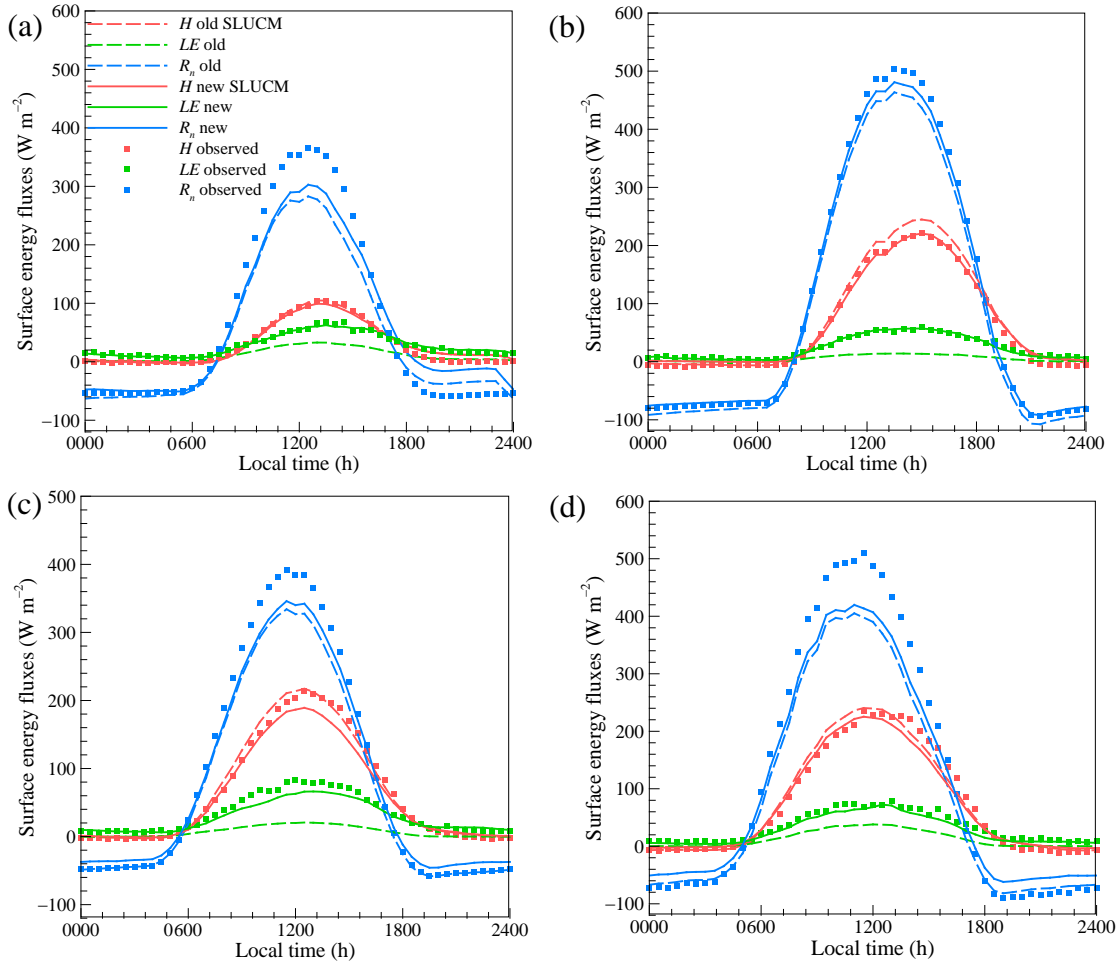
Figure 2.3. Averaged diurnal profiles of modelled and observed H, LE and R_n for (a) Beijing, (b) Phoenix, (c) Vancouver and (d) Montréal.

Model predictions and field observations of H, LE and R_n are compared in Fig. 2.3. Located in a semiarid region, Phoenix has less latent heat flux compared to the other three metropolitan areas. It is clear from Fig. 2.3 that due to the lack of realistic urban hydrological processes, the old SLUCM significantly underestimates LE with a discrepancy of more than 40 W m^{-2} at 1400 local time. With the incorporation of urban hydrological processes, the new SLUCM is able to predict LE with improved accuracy as compared to field measurements, with a deviation of less than 10 W m^{-2} at 1400 local

21

time for all study areas. Constrained by the surface energy balance, the increase in LE in the new SLUCM leads to less available energy for H and G. It is found that (not shown here) about 70% of the reduction is redistributed to H. This implies that the inclusion of hydrological processes in the model has an important impact on the partition of available energy into turbulent fluxes, without significantly altering the soil thermal storage. Figure 2.3 also illustrates that the incorporation of hydrological processes also improves the prediction of daytime net radiation, leading to improved estimates of daytime surface temperatures by the new SLUCM. In addition, the surface energy residual ($R_n + Q_F - H - LE - G$) is calculated over the entire simulation period. Mean residuals for all study sites are less than 0.15 W m^{-2}, indicating the surface energy balance is maintained after the implementation of hydrological processes.

Considering the seasonal variation of urban irrigation, we further evaluate model results against observations at the intra-annual scale. Results from spring and summer periods are plotted in Figs. 2.4 and 2.5, respectively. Predicted LE by the new SLUCM is in good agreement with field observations (with absolute error less than 30 W m^{-2}) except that a substantial deviation of 60 W m^{-2} is found at Vancouver in spring. It is noteworthy that Vancouver has larger LE in spring than in summer due to high precipitation; the opposite is found in other three cities. This discrepancy in spring is possibly related to missing hydrological processes in the current model (e.g. snow melting), necessitating a continuous improvement of the single layer urban canopy model in the future. During summer, the increase of LE is about 100% larger than that in spring due to irrigation in the model; accuracy of prediction of LE is notably improved at all study sites. Nevertheless, a significant deviation in H is observed in Vancouver, which is up to about

50 W m^{-2} around noon. In general, Figs. 2.4 and 2.5 show that the new SLUCM is capable of reproducing seasonal patterns of turbulent heat fluxes at study cities except Vancouver.
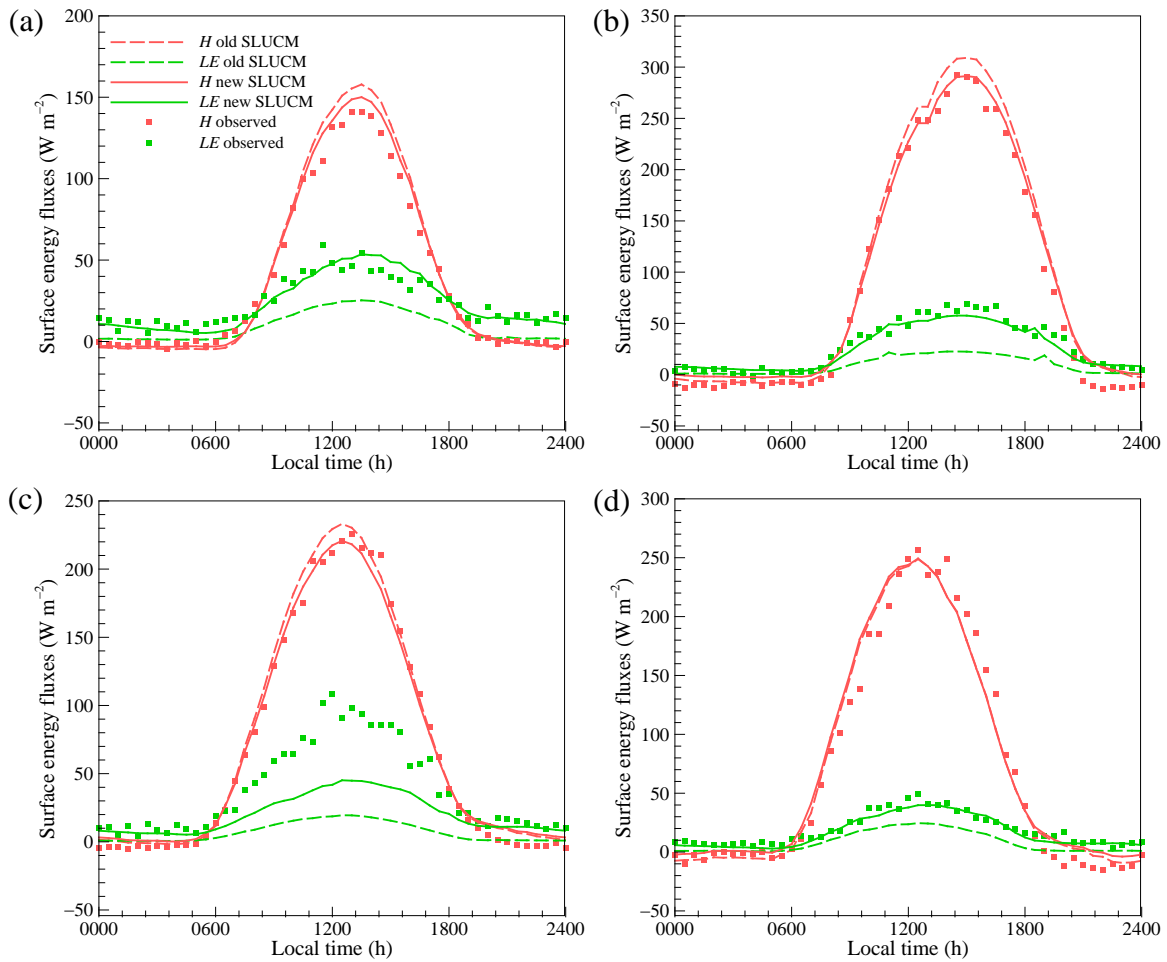
Figure 2.4. Averaged diurnal profiles of modelled and observed H and LE in spring for (a) Beijing, (b) Phoenix, (c) Vancouver and (d) Montréal.
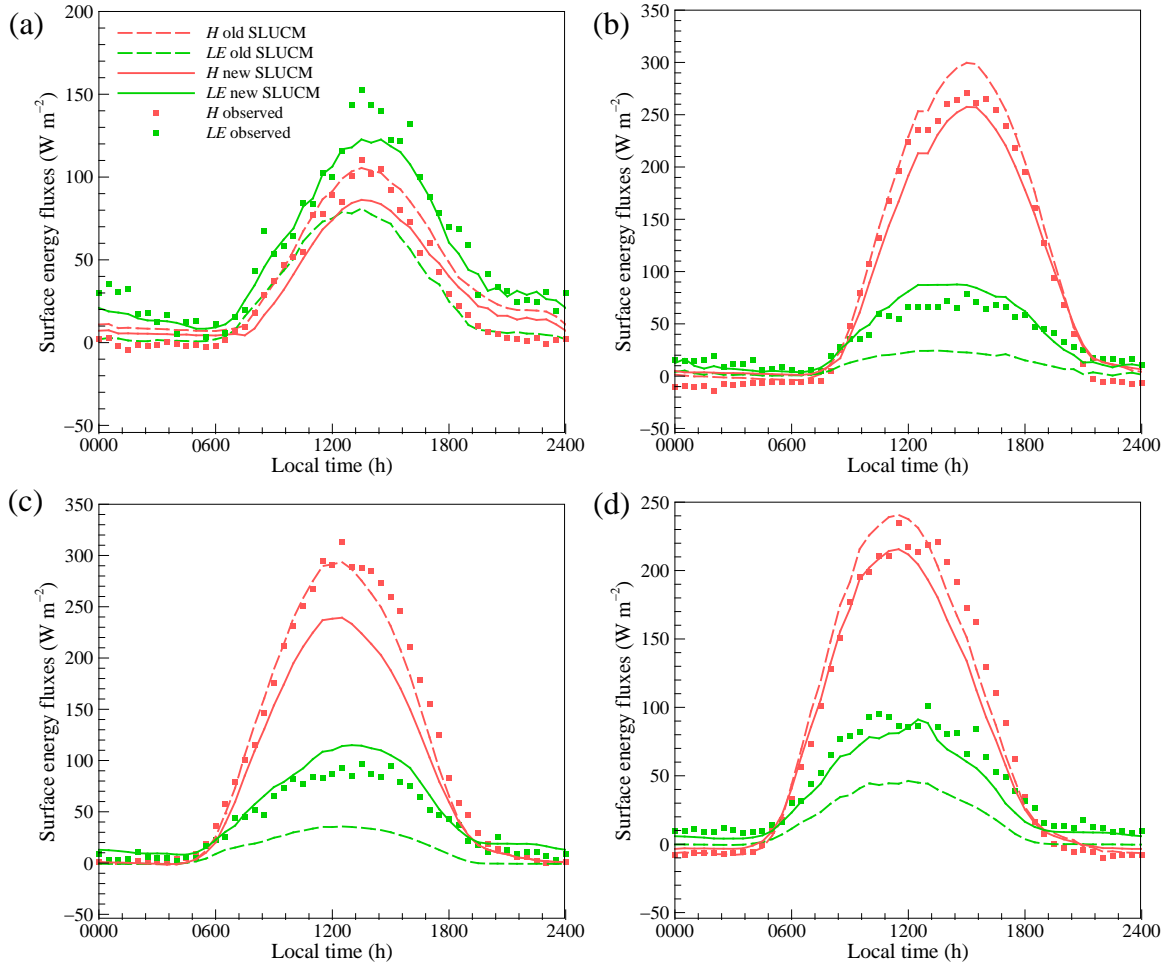
Figure 2.5. Averaged diurnal profiles of modelled and observed H and LE in summer for

(a) Beijing, (b) Phoenix, (c) Vancouver and (d) Montréal.

To quantitatively assess the impact of the proposed hydrological processes, root-mean-square error (RMSE) between observed and modelled results is computed for the entire simulation period. The statistics are summarized in Table 2.2, and are presented in Fig. 2.6 to facilitate visualization of the results. Despite the locations,

Table 2.2. Summary of the median, maximum, minimum, 25th and 75th percentile of the RMSE (W m^{-2}) between model prediction and observation.

Site	Statistics	Old SLUCM			New SLUCM		
		H	LE	R_n	H	LE	R_n
Beijing	Median	2.3	13.5	21.0	4.3	2.7	29.6
	Minimum	0.0	4.6	1.5	0.0	0.1	0.3
	25th percentile	1.2	9.6	7.2	1.3	0.6	5.5
	75th percentile	7.1	21.3	51.6	8.0	4.4	44.1
	Maximum	13.3	37.9	93.7	13.3	7.6	67.4
Phoenix	Median	10.6	11.5	13.1	6.1	1.8	4.5
	Minimum	1.3	1.3	4.1	0.4	0.0	0.0
	25th percentile	5.2	5.7	9.4	4.3	0.8	3.7
	75th percentile	19.4	31.5	30.7	9.2	2.3	11.7
	Maximum	31.8	45.8	42.7	15.3	10.2	14.6
Vancouver	Median	3.3	17.4	3.2	3.9	3.8	11.8
	Minimum	0.0	5.1	0.0	0.0	0.1	1.1
	25th percentile	1.4	8.3	0.6	2.1	1.7	9.7
	75th percentile	10.1	47.2	39.2	14.0	11.1	25.7
	Maximum	17.6	62.5	58.3	33.3	20.7	47.8
Montréal	Median	7.3	15.5	12.6	7.2	5.0	26.7
	Minimum	0.0	6.6	0.3	1.5	0.1	1.2
	25th percentile	2.5	9.1	6.9	4.2	3.3	20.3
	75th percentile	17.7	31.1	73.2	12.4	8.4	56.0
	Maximum	32.6	42.0	111.9	42.5	17.0	96.1

RMSEs from the new SLUCM are notably smaller than those from the old SLUCM with respect to LE. Averaged median RMSE of the four study sites are 14.5 and 3.3 W m^{-2} for the old and new SLUCM, respectively. With respect to H, the old SLUCM has good

overall performance among all study sites, with a median RMSE of 5.9 W m^{-2}; the model performance is slightly better for Beijing and Vancouver, and much improved for Montréal and Phoenix in terms of maximum RMSE. In addition, the averaged median RMSEs for H and LE for the new SLUCM are 5.4 and 3.3 W m^{-2}, respectively, which are significantly better than the corresponding median RMSEs of 22 and 26 W m^{-2} averaged over the group of 32 urban energy balance models at the final stage (where all urban canopy models were fine-tuned with input of most detailed field parameters) (Grimmond et al. 2011).

From Figs. 2.3-2.6, it is evident that the major improvement of the new SLUCM is in its capability of predicting LE, as a result of the enhanced physical representation of urban hydrological processes. Among the proposed hydrological processes, evaporation over pavement surfaces only takes effect during and shortly after precipitation due to the low water-holding capacity. Considering the substantial fraction of paved surface in urban areas, we specifically look into LE during rainfall periods to examine the impact of different parametrization schemes.

The SLUCM is run with old (empirical decay function by Miao and Chen (2014)) and new (resolving water-holding layer in Chapter 2.2.3) schemes respectively. Figure 2.7 shows the result of comparison in summer period in Beijing and Phoenix. It is clear that the old parametrization scheme overestimates LE after the onset of rainfall. Large differences are observed throughout the period with a maximum error of about 80 W m^{-2} in Beijing and about 120 W m^{-2} in Phoenix. In contrast, the new evaporation scheme (Eq. (2.8)) yields more realistic predictions of LE with better agreement with field measurements, with maximum errors less than 40 and 70 W m^{-2} in Beijing and Phoenix,

respectively. This new parametrization scheme for engineered surfaces can markedly enhance prediction of LE and subsequently improve the representation of urban water cycle during and after rainfall events.
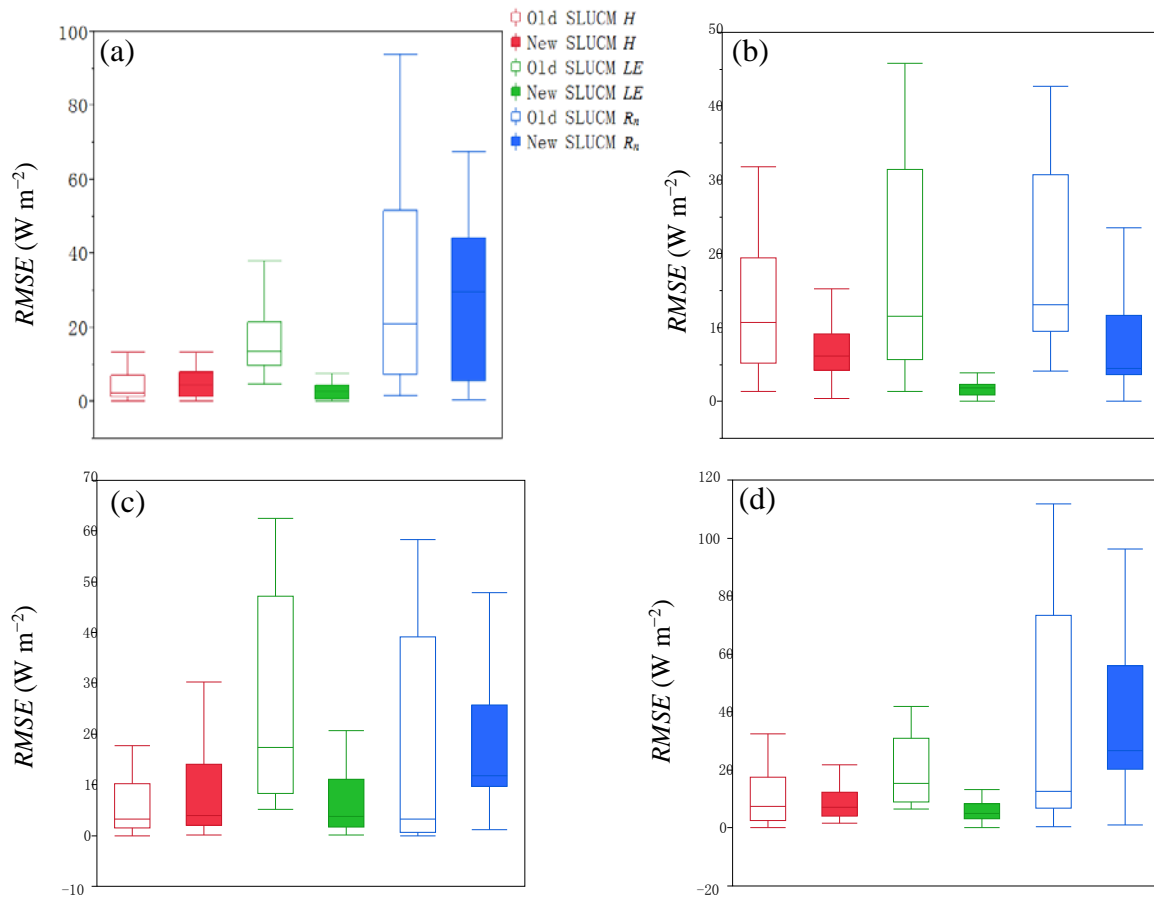
Figure 2.6. Box plots of RMSE between observed and model predicted H, LE and R_n for (a) Beijing, (b) Phoenix, (c) Vancouver and (d) Montréal. Top and bottom of the box represent the 75th and 25th percentile, the horizontal line indicates the median, top and bottom bars are the maximum and minimum values, respectively.
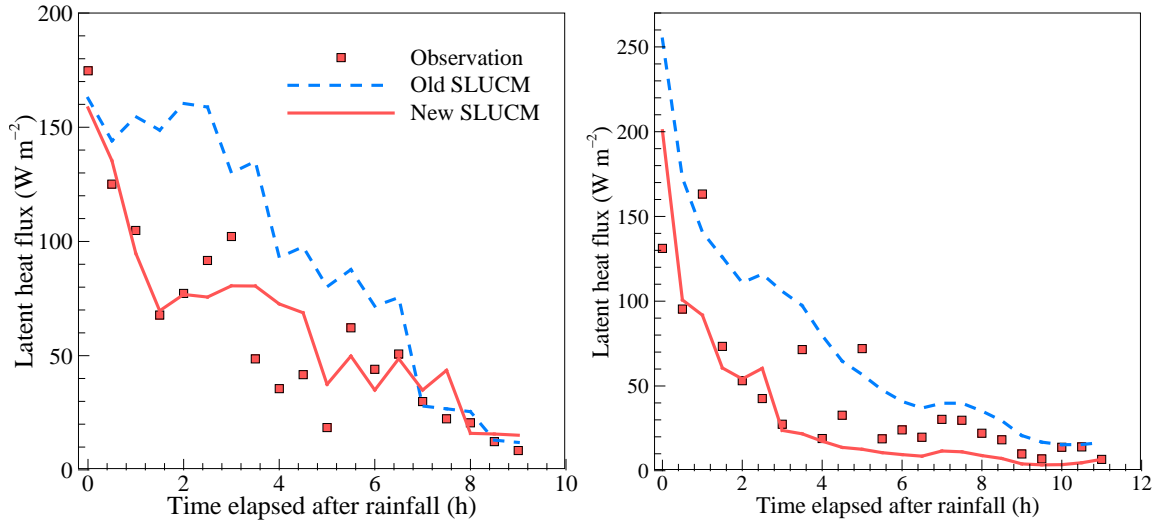
Figure 2.7. Averaged LE after rainfall events during a summer period from two evaporation parametrization schemes for (left) Beijing during 6/30/09-8/30/09 (averaged over 4 major rainfall events), and (right) Phoenix during 7/03/12-8/31/12 (averaged over 4 major rainfall events).

Furthermore, for each hydrological process proposed in this study, the relative contribution is calculated as the ratio (percentage) between the change of LE by turning off the particular process and the overall change of LE by turning on all hydrological processes. It is found that evaporation over engineered pavements has the least relative contribution (less than 0.1%), because it is only effective during and shortly after precipitation. The relative contribution from irrigation varies from about 6.7% in Beijing to about 69.0% in Phoenix. The oasis effect contributes more (> 10%) to the overall LE changes in Phoenix, Vancouver and Montréal, than that in Beijing. It is mainly because the urban cropland/grassland (Beijing) has higher actual rate of evapotranspiration limited by available energy (i.e. supply) rather than the potential rate (i.e. atmospheric

28

demand). The anthropogenic latent heat is determined by population density and the urban category of the measurement site. Therefore its contribution varies vastly for different cities, ranging from about 0.5% in Vancouver to about 50% in Beijing.

2.5. Green Roof Simulations

In this section the new SLUCM model is applied to explore the effect of green roof systems on urban hydroclimate, especially on the modification of urban water/energy budgets. We study five scenarios with different green roof fractions, viz. 0%, 25%, 50%, 75%, and 100% of the total roof area. Simulations are conducted for a five-day period in mid-summer for the four study cities: Beijing, (June 19-24, 2010), Phoenix (July 05-10, 2012), Vancouver (July 16-21, 2009), and Montréal (June 02-07, 2009), driven by measured meteorological forcing. The selected periods were characterized by clear sky conditions with no precipitation. The initial soil moisture of green roofs is assumed to be the same as that of the ground vegetation. Note that urban irrigation is used for subsequent simulations; therefore model results represent the maximum (potential) capacity of evaporative cooling and energy savings by green roofs.
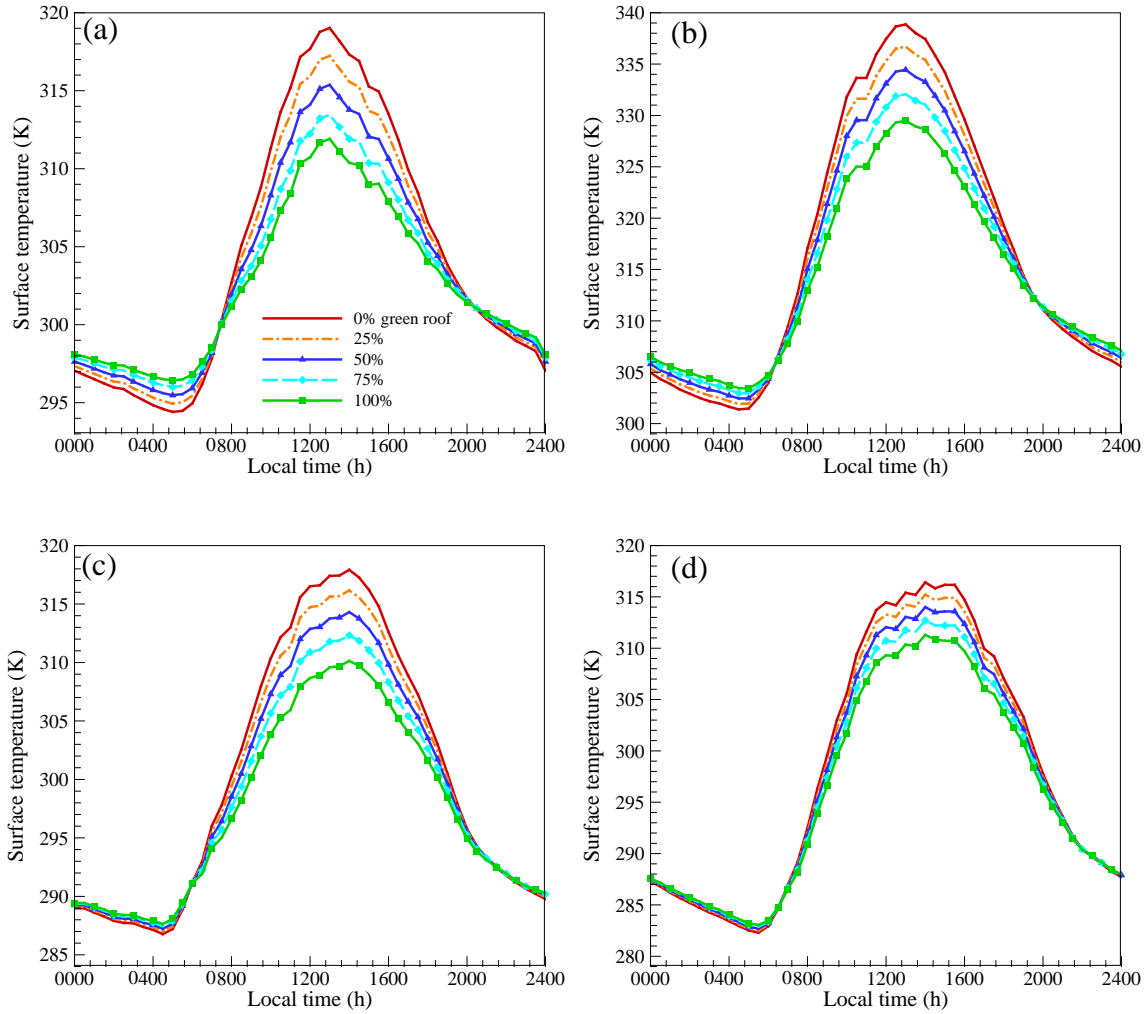
Figure 2.8. Model predicted T_s with various green roof fractions during a 5-day summer period for (a) Beijing, (b) Phoenix, (c) Vancouver and (d) Montréal.

Predicted surface temperature (T_s), sensible and latent heat flux with different green roof area fractions are shown in Figs. 2.8-2.10. With increased green roof fraction and therefore a stronger evaporative cooling effect, urban T_s and H decrease while LE increases, as expected. Figures 2.8-2.10 demonstrate the range of modelled T_s, H, and LE that rooftop modification can produce in each city. Replacing 25% of the rooftop with green roofs can reduce daily peak T_s by 1 to 2 °C in study areas. If green roofs are

implemented over the entire city, reduction in daily peak T_s can be up to 5 to 10 ^{o}C, consistent with values reported by Santamouris (2014). Compared to Beijing and Montréal, Phoenix and Vancouver have larger reductions in T_s. In Phoenix, the reduction is partly due to the presence of a larger roof fraction (see Table 2.1), which provides more area for green roof systems. In addition, the dry atmosphere in the semi-arid environment in Phoenix induces higher potential evapotranspiration, which in turn leads to more significant cooling. In Vancouver, though its urban fraction is the lowest among all study cities, it has the highest roof- to urban-area ratio, leading to more effective cooling per unit urban area by green roofs. Greater available surface energy, as a result of more solar radiation in Phoenix and lower albedo in Vancouver, also contributes significantly to larger increase of LE and reduction of T_s in the two cities.

Figure 2.9 illustrates that green roofs are capable of substantially reducing sensible heat flux in urban areas. As H is determined by the difference between surface and air temperature, the magnitude of reduction in H follows the trend of reduction in T_s. Installation of green roofs over the entire available rooftop area can decrease daily peak H by about 100 W m^{-2} in Beijing and Montréal, and about 160 W m^{-2} in Phoenix and Vancouver. At night, the cooling effect becomes insignificant as the energy source for evaporation, i.e. solar radiation, vanishes. Due to the larger heat capacity of moist soils as compared to pavement materials, nighttime T_s and H on green roofs are higher than conventional roofs. The warming effect of green roofs at night is more evident in low-latitude areas that accumulate more thermal energy during daytime. Among study cities, the nighttime warming (as compared to the case without green roofs) is less than 1 ^{o}C in

Vancouver and Montréal, but can be more than 2 °C in Beijing and Phoenix. Overall, the

nighttime temperature increase is much smaller than daytime temperature reduction.
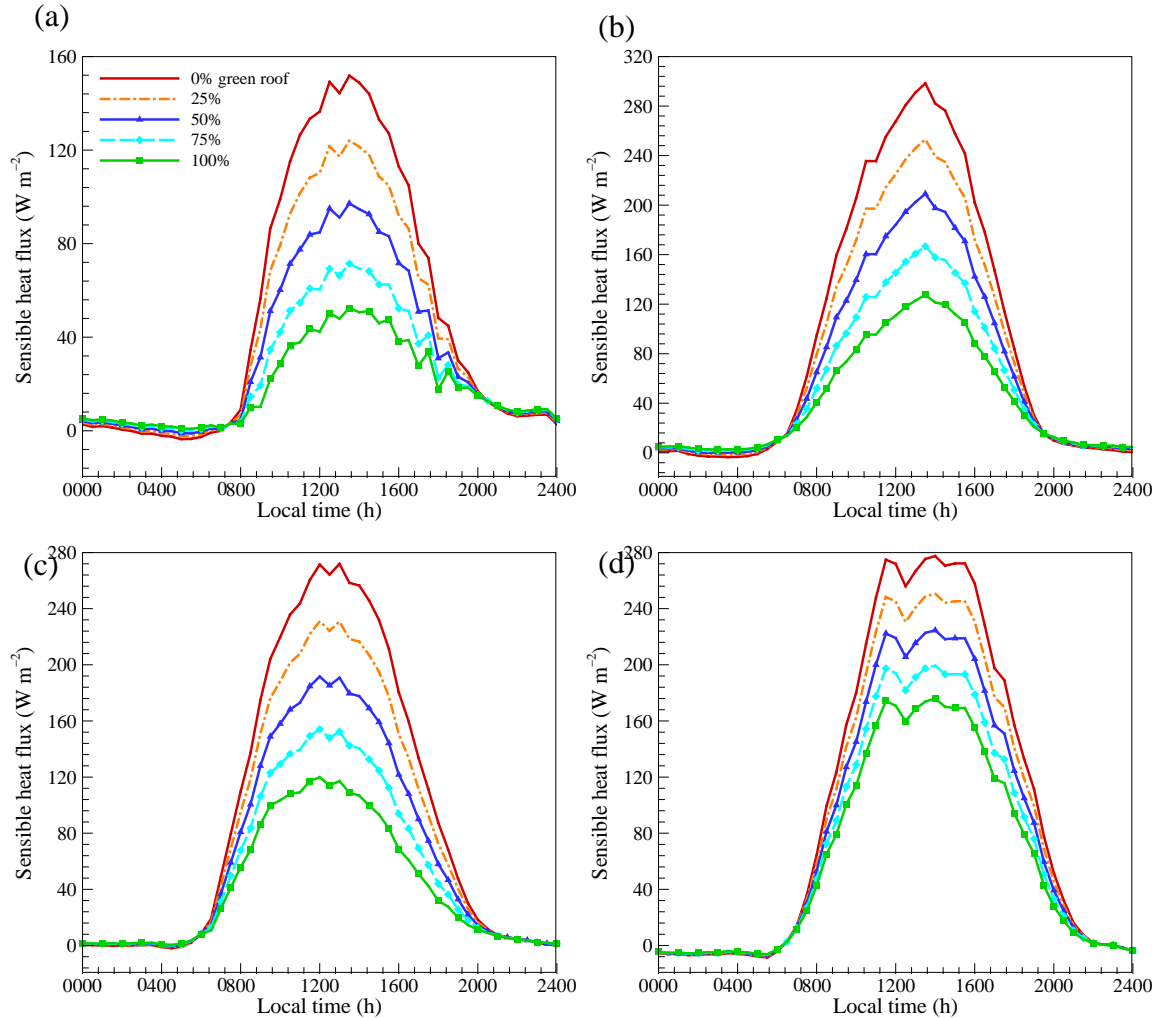
Figure 2.9. Model predicted H with various green roof fractions during a 5-day summer

period for (a) Beijing, (b) Phoenix, (c) Vancouver and (d) Montréal.

In addition, green roofs can lead to an increase of more than 70 W m^{-2} in peak LE

values in all four cities (Fig. 2.10), up to 130 W m^{-2} in Phoenix. It is noteworthy that

increase of LE is relatively linear when green roof fraction rises from 0% to 75%,

consistent with the result of a previous sensitivity study (Yang and Wang 2014a).

However, as green roof fraction increases from 75% to 100%, the increment of LE

becomes much smaller, revealing a complex mechanism of surface energy partitioning

for green roof systems in this range.
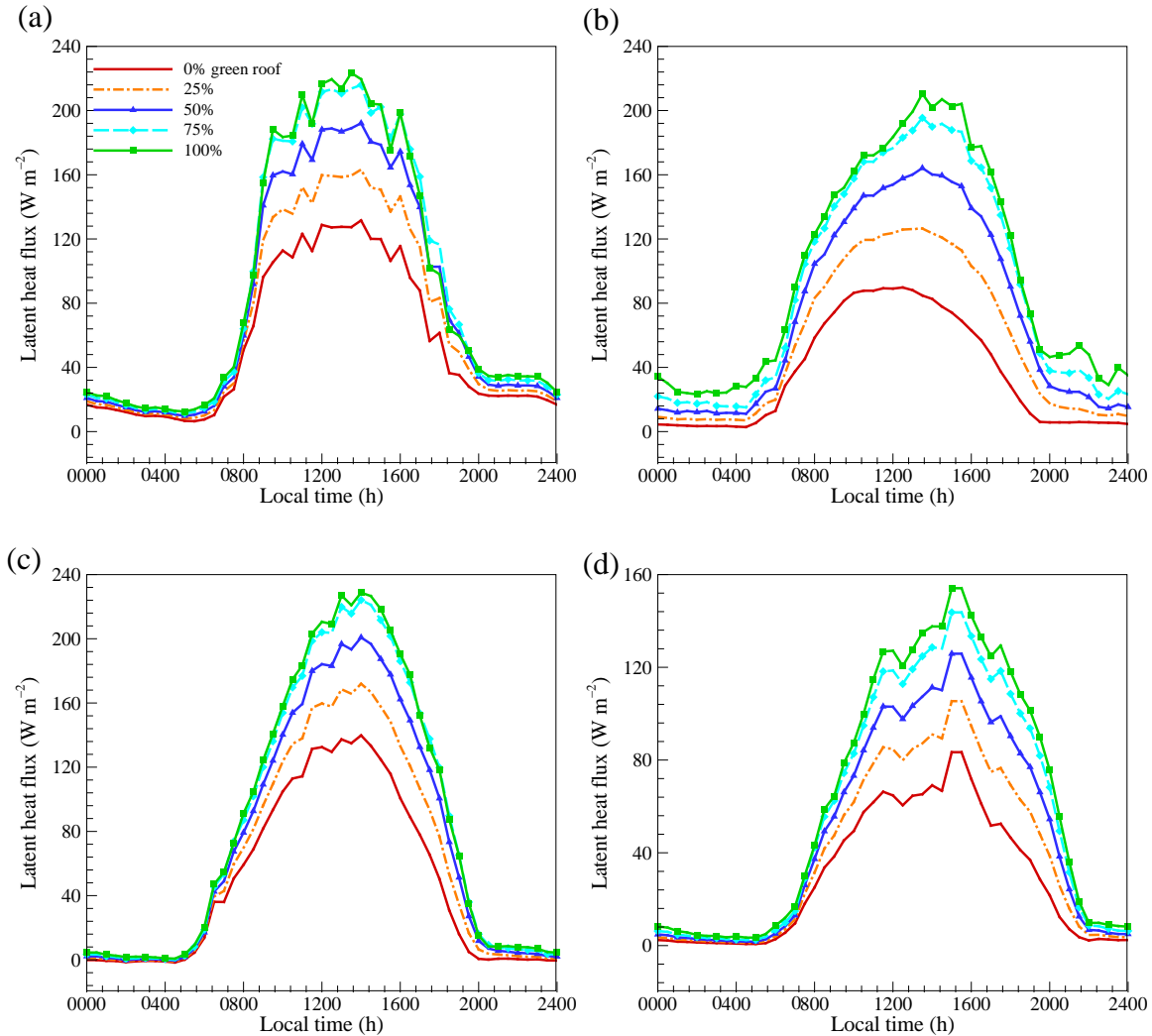
Figure 2.10. Model predicted LE with various green roof fractions during a 5-day

summer period for (a) Beijing, (b) Phoenix, (c) Vancouver and (d) Montréal.

On one hand, the decreased H due to surface cooling contributes more available energy for evapotranspiration (LE increases), whereas the associated reduction in buoyancy weakens the turbulent mixing and retains more moisture at the surface (LE decreases). Results in Fig. 2.10 indicate the existence of a threshold capacity, beyond which further increasing green roof fraction will have negligible effect on LE.
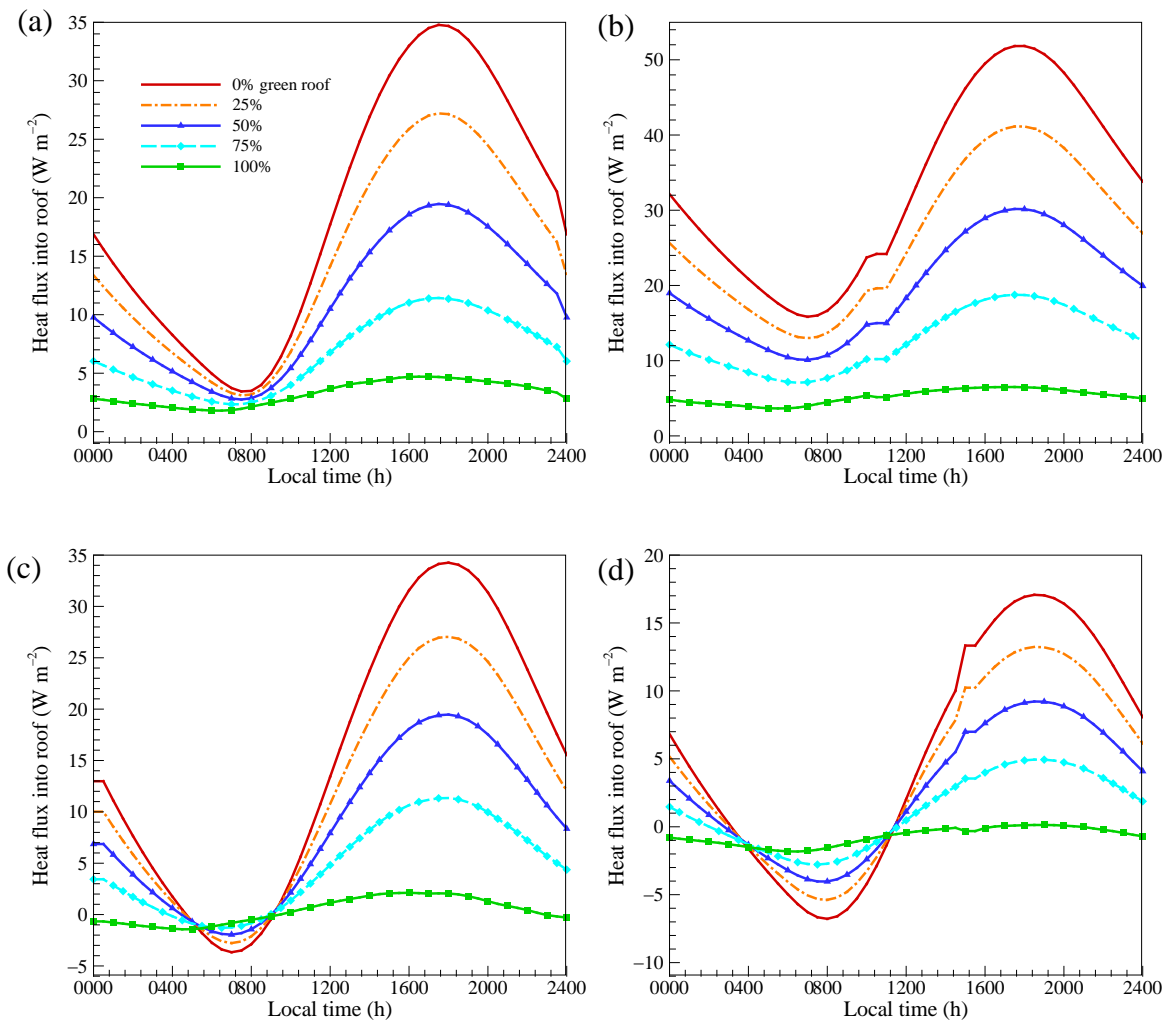
Figure 2.11. Model predicted Q_{in} with various green roof fractions during a 5-day summer period for (a) Beijing, (b) Phoenix, (c) Vancouver and (d) Montréal.

34

Moreover, the cooling effect by green roofs in turn leads to saving of cooling energy consumption of buildings, especially in summers. To assess green roofs' impact on the building energy consumption, we calculate the heat flux conducted into the building through the roof (Q_{in}). A roof thermal insulation value of R30 is used in all simulations.
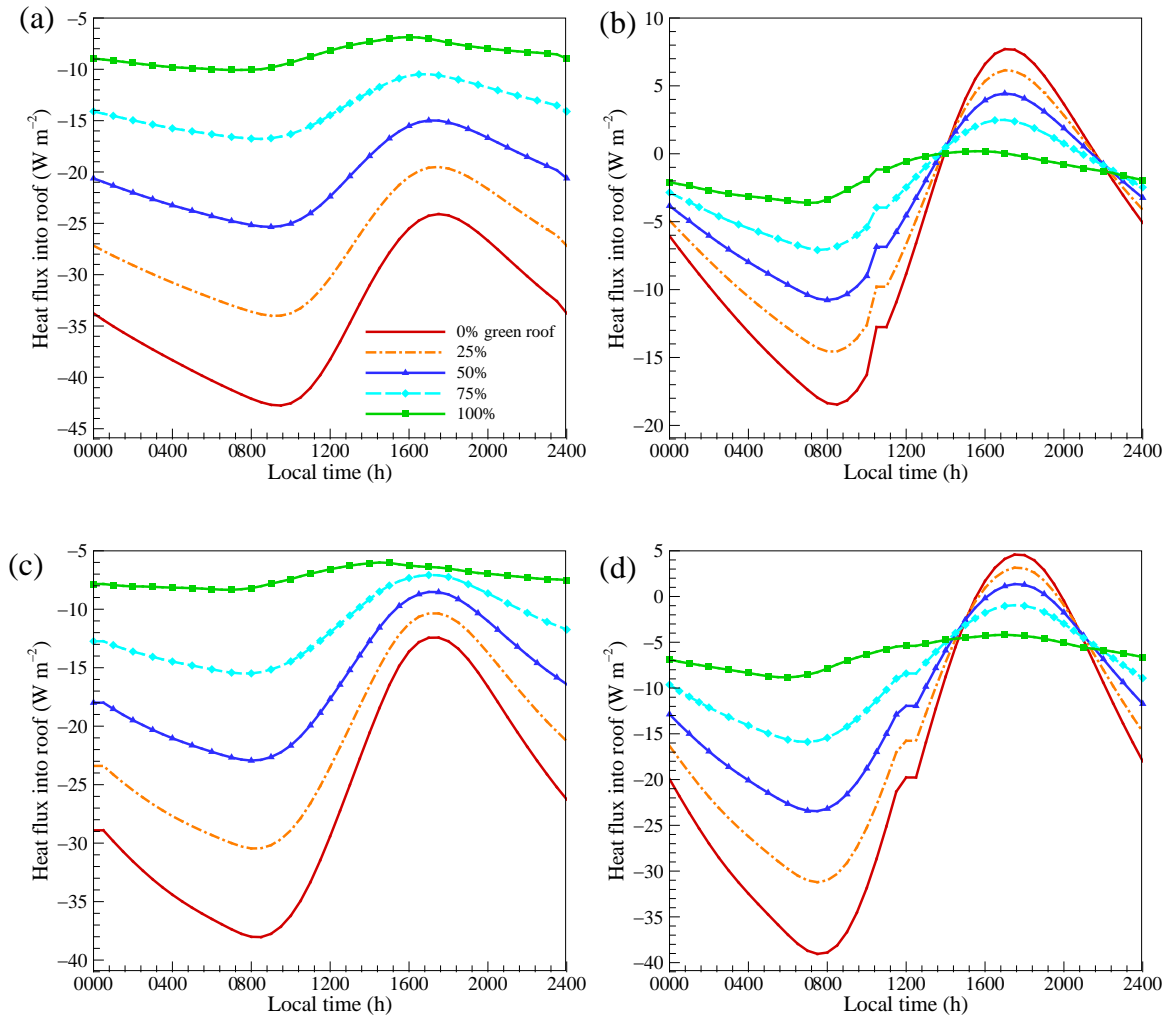
Figure 2.12. Model predicted Q_{in} with various green roof fractions during a 5-day period for (a) Beijing from January 20-25, 2010, (b) Phoenix from December 06-11, 2012, (c) Vancouver from March 08-13, 2009 and (d) Montréal from April 06-11, 2009.

Model predicted Qin with different green roof area fractions in various cities are shown in Fig. 2.11 for the summer period. The peak Qin occurs around 1800 local time, whereas daily peak Ts occurs at about 1400 local time. The time lag of about 4 hours implies the temporal gap between the hottest time and the largest cooling demands of buildings (Wang 2014b). During the study period, diurnal peak Qin values without green roofs are greater than 15 W m^{-2} at all study areas, up to 50 W m^{-2} in Phoenix. With green roofs, Qin can be reduced to nearly zero throughout the day in Vancouver and Montréal, and to less than 7 W m^{-2} in Beijing and Phoenix, implying significant potential saving of building cooling energy in summers.

To illustrate the impacts of green roofs on building energy consumption in cool seasons, a second set of 5-day simulations (different from previous simulation periods in mid-summers) are conducted for Vancouver (March 08-13, 2009), Phoenix (December 6-11, 2012), Beijing (January 20-25, 2010), and Montréal (April 06-11, 2009). In Fig. 2.12, diurnal profiles of Q_{in} exhibit a similar trend to those in summers, where negative values indicate outward heat fluxes with a heating demand for building interiors. During the simulation period, highest peak Q_{in} of 18 W m^{-2} and lowest peak Q_{in} of 43 W m^{-2} are observed in Phoenix and Beijing, respectively. Implementation of green roofs can increase these peaks to about 4 W m^{-2} and 9 W m^{-2} in corresponding cities, suggesting a considerable saving of heating loads. This demonstrates that the insulation effect from additional layers in a green roof system is important in improving building energy efficiency under cool-to-cold climates.

2.6. Summary

In this Chapter, physical urban hydrological parametrizations were implemented into the single layer urban canopy model, including (1) anthropogenic latent heat, (2) urban irrigation, (3) urban oasis effect, (4) evaporation over engineered pavements, and (5) multilayer green roofs. Comparisons against field measurements show that the enhanced SLUCM has improved accuracy in predicting turbulent fluxes over urban areas, especially the latent heat flux. The new model is able to capture not only the diurnal cycle but also intra-annual variations of H and LE in various cities. With the parametrization of water holding capacity of paved surfaces, actual LE is better captured during and shortly after rainfall periods.

It is shown that when well irrigated, green roofs are effective in enhancing latent heat flux, and reducing surface temperature and sensible heat flux through evaporative cooling. For building energy efficiency, green roofs are found to be effective in decreasing not only summer cooling but also winter heating demands, through the combined evaporative cooling and insulation effect. Though environmental benefits of green roofs are encouraging based on the simulation results, their actual performance is sensitive to geographic and meteorological conditions and is critically limited by the availability of water resources.

In general, results of the new SLUCM are promising, even with a large number of default urban parameters, as prescribed in the WRF model. Nevertheless, for specific cities, e.g. Vancouver, the presence of model-measurement deviation requires more meticulous determination of the input parameter space to achieve optimal values. In addition, the lack of snow/ice hydrology in current urban modelling systems necessitates

37

further development of physically-based urban parametrization schemes, especially those

related to the coupled energy-water transport mechanisms.

CHAPTER 3 OPTIMIZING URBAN IRRIGATION FOR THE TRADE-OFF

BETWEEN ENERGY AND WATER CONSUMPTION

3.1. Introduction

Urban areas account for 67-76% of global energy use (Seto and Dhakal 2014), with

the percentages expected to increase under future urban expansion. Buildings are the

dominant energy consumers in the cities, around 40% of the total final energy

consumption in the United States and the European Union is in the building sector

(Retzlaff 2008, European Commission 2012). In recent years there has been a growing

concern about the energy consumption as it is the largest contributor to global CO_2

emissions, which is the leading cause of climate change (Seto and Dhakal 2014).

Building energy consumption in cities is closely related to environmental temperatures

(Akbari 2009), on which urban irrigation has indirect effects by controlling the supply of

surface moisture for evapotranspiration of urban green infrastructure.

While numerous means for reducing building energy consumption have been

investigated, the impact of various urban irrigation schemes on building energy efficiency

has been less explored. Irrigation-induced cooling on near-surface temperature over

agricultural land has been extensively documented in both observational (Sacks et al.

2009) and modelling (Bonfils and Lobell 2007, Lobell and Bonfils 2008) studies. In

summers, daily maximum air temperature over 100% irrigated area can be 5 ºC cooler

than that over non-irrigated area in California (Lobell and Bonfils 2008). On the other

hand, though the importance of irrigation in modelling urban energy and water budget

has been recognized (Mitchell et al. 2008, Vahmani and Hogue 2014), the explicit impact

of irrigation on urban environmental temperature and building energy consumption has

rarely been studied. Irrigation of private gardens consumes 16-34% of the total water supplied to an urban area, let alone the water used for irrigating large open space such as public parks and golf courses (Mitchell et al. 2001). For residential areas within the city of Los Angeles, nearly 225×10^6 m^3 of water was used for irrigation per year (LADWP 2001). Such amount of irrigation can increase evapotranspiration and cool the urban environment considerably, leading to significantly lower cooling load, especially in densely built areas.

Under the challenge of future climate change, water becomes a more precious resource in cities (Vairavamoorthy et al. 2008). Current irrigation practices in most cities are scheduled between sunset and sunrise in order to avoid rapid moisture loss. However, from an energy saving perspective, irrigation should be conducted during daytime as evaporative cooling is driven by available solar radiation at the surface. In this case, irrigating urban vegetation leads to improved building energy efficiency, albeit the trade-off and balance between water and energy resources need to be carefully measured. Different from agricultural irrigation whose objective is mainly on the yield of produces (Topak et al. 2010), urban irrigation apparently needs a new paradigm by considering the environmental sustainability of cities (e.g. mitigate urban heat islands and save building energy consumption).

Understanding the relationship between water and energy consumption in the urban environment is essential to develop an optimal urban irrigation scheme. In this Chapter the single layer urban canopy model, described in Chapter 2 with realistic representation of urban hydrological processes, is employed to identify the environmental impact of urban irrigation in the Phoenix metropolitan area. A variety of uncontrolled and

controlled irrigation schemes is investigated, including (1) daily constant scheme, (2) soil-moisture-controlled scheme, and (3) soil-temperature-controlled scheme. Considering the seasonal variation of meteorological conditions and irrigation demands, the net saving of individual scheme is quantified at an annual scale. The trade-off between water and energy consumption are addressed by adopting the combined monetary saving as a measure of environmental co-benefit. The indirect benefit of irrigation on outdoor thermal comfort of pedestrians is also discussed.

3.2. Numerical Experiment Design

3.2.1 Irrigation schemes

The Phoenix metropolitan area is selected as the study area for this Chapter. The simulation period was one entire calendar year, 2012. Phoenix has a population of more than 1.5 million in 2015, and is the sixth most populous city in the United States (U.S. Census Bureau 2016). Located in a semi-arid environment, Phoenix has a tremendous demand for cooling compared to other cities (Sivak 2008), thus providing a large potential for building energy saving through optimizing irrigation schemes (Gober et al. 2010). In Phoenix, xeric and mesic are two typical vegetated residential landscapes. Xeric sites usually comprise drip-irrigated, low water-use native and/or desert-adapted plants, while mesic sites mainly consist of turf grass and shade trees (Middel et al. 2014). Though xeric landscaping helps to conserve water resource, mesic landscaping provides valuable environmental services by, e.g. reducing urban warming and improving stormwater management, and is aesthetically appealing (Chow and Brazel 2012).

A schematic of irrigation in the single layer urban canopy layer is shown in Fig. 3.1. Focusing on irrigation of mesic neighborhoods, four different urban irrigation schemes are tested for Phoenix. Scheme 1 is the baseline case with no irrigation during the entire simulation period. Scheme 2 is a daily constant scheme that represents current irrigation practice over mesic residential landscapes in Phoenix. Daily irrigation amount is estimated by dividing monthly irrigation data from an in-situ measurement by the number of days in each month. Following a previous study, irrigation is scheduled at 2000 local time every day in this scheme (Yang et al. 2015a). Sensitivity analysis finds that the irrigation time at night has limited impacts on model results. Scheme 3 is a soil-moisture-controlled scheme proposed as a potential urban irrigation paradigm. The idea is to maintain soil moisture at a certain level to keep evaporative cooling effective all the time. Whenever the moisture content of top soil layer (θ_{top}) drops below a critical value, irrigation is carried out to increase the moisture. The amount of irrigation each time is set to be the same as that in the daily constant scheme. Scheme 4 is similar to the soil-moisture-controlled scheme but uses the soil temperature as the controlling variable. Targeted on reducing urban environmental temperature during hot periods, the scheme activates urban irrigation once the temperature of top soil layer exceeds a threshold value. Each time the irrigation amount also equals to the daily irrigation amount of scheme 2. During prolonged daytime period of hot summers, this scheme may easily lead to over irrigation. To avoid waste of water resource, the irrigation amount is then regulated by either the daily irrigation amount of scheme 2 or the difference between θ_{top} and saturated soil moisture, whichever is smaller. For cool to cold months where soil temperature is

42

consistently lower than the threshold value, essential irrigation is conducted to maintain

soil moisture above the wilting point to support biological functions of mesic vegetation.

Volo et al. (2014) has conducted a comparative analysis of the impact of irrigation

scheduling at both mesic and xeric sites in Phoenix. Typical wilting point for mesic site is

found to be from 0.15 to 0.24. In this study, the lower bound value 0.15 is used as the

wilting point and the upper bound value 0.24 is used as the controlling moisture for the

soil-moisture-controlled irrigation scheme. Residual and saturated soil moisture is set to

be 0.10 and 0.50. With respect to the threshold soil temperature for irrigation activation

in the soil-temperature-controlled scheme, a value of 22 $^{\circ}$C is adopted as the first step to

illustrate performance of the scheme.
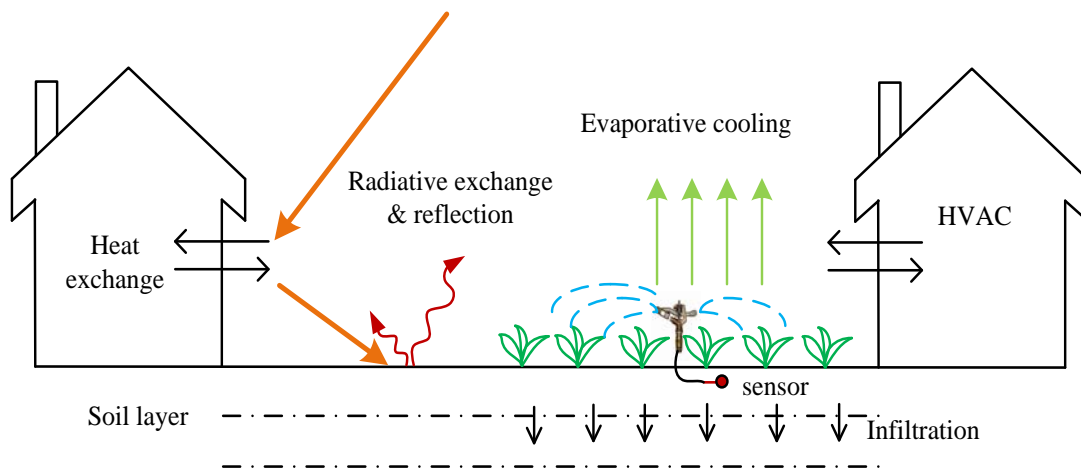
Figure 3.1. A schematic of lawn irrigation in residential areas. The two-dimensional "big

canyon" representation is adopted to represent the urban area with the longitudinal

dimension (canyon length) much larger than the planar dimensions (building height and

road width).

3.2.2 Model evaluation

The single layer urban canopy model developed in Chapter 2 is used to quantify the impact of urban irrigation. Accuracy of the UCM in capturing the energy and water budgets of Phoenix is crucial to accurately assess the impact of urban irrigation on environmental temperature and building energy consumption. In Chapter 2 the performance of the UCM for Phoenix has been evaluated using annually averaged diurnal profiles of turbulent heat fluxes. Considering the variation of meteorological conditions and irrigation demands, the UCM is tested with calibrated parameters at a daily basis in this Chapter. Half-hourly meteorological forcing is obtained from the eddy-covariance tower deployed at Maryvale, West Phoenix. The experiment site has a footprint area of about 1 km $\times$ 1 km, of which about 48.4% is impervious surface, 36.8% is bare soil, and 14.6% is vegetation (Yang et al. 2015a). Daily constant irrigation (i.e. scheme 2) is added into the model to represent practical supply for soil moisture.

Comparison of predicted and observed average ground temperature (T_g), canyon air temperature (T_{can}), sensible heat flux (H), and latent heat flux (LE) is shown in Fig. 3.2. Gaps in data points are due to failure and maintenance of individual sensors. It is clear from the graphs that model predictions agree with observations reasonably well except for LE in certain months. Discrepancy between observed and predicted LE is about 30% in October and November. This deviation is largely caused by the spatial variability and uncertainty in precipitation and irrigation data. For the entire simulation period, root mean square errors are 1.39 $^{\circ}$C, 1.02 $^{\circ}$C, 12.51 W m^{-2}, and 7.36 W m^{-2} for T_g, T_{can}, H, and LE, respectively. The calibrated input parameters are then adopted for subsequent analysis in this Chapter.

44
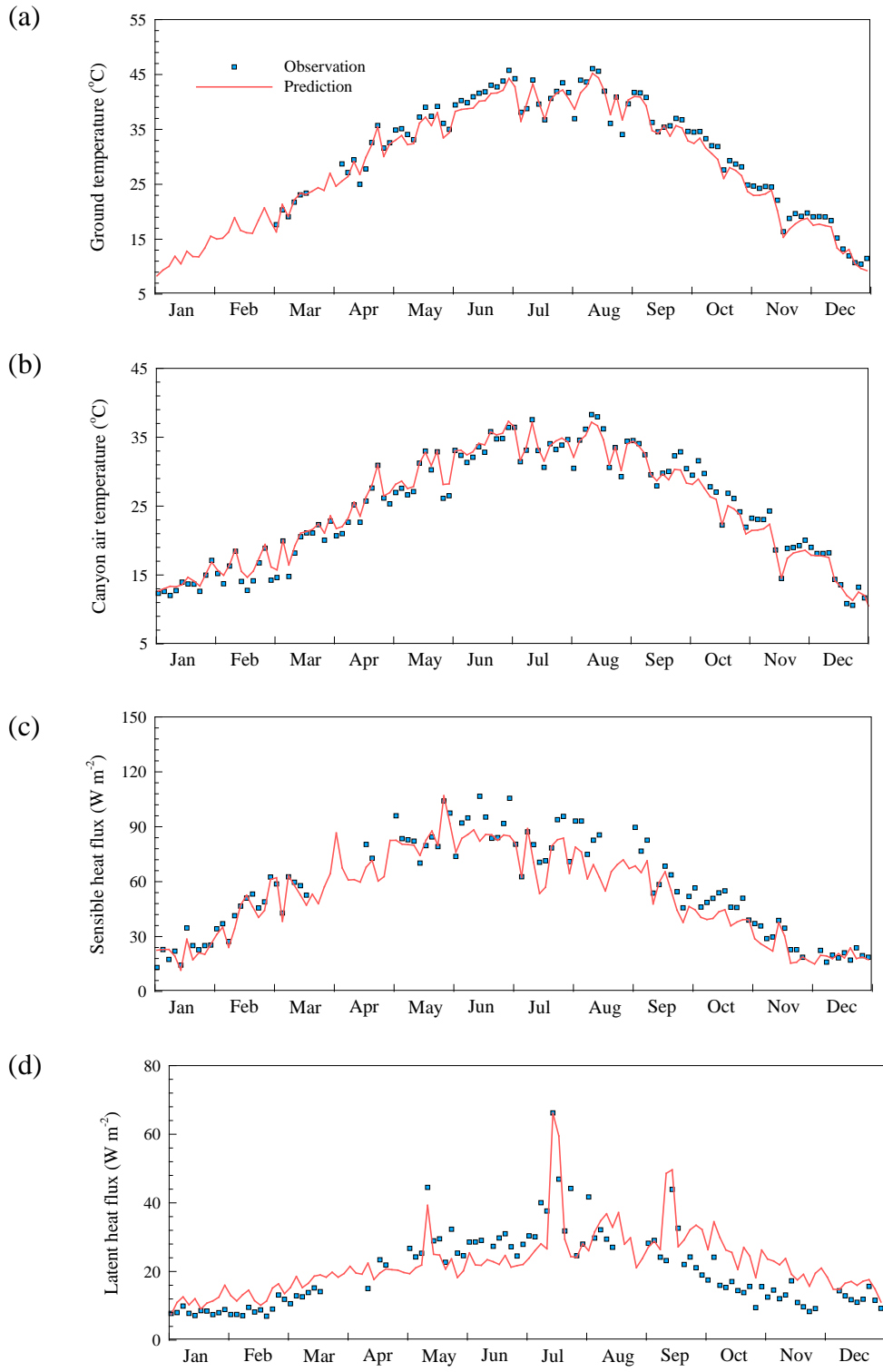
Figure 3.2. Comparison of predicted and observed average (a) T_g, (b) T_{can}, (c) H, and (d) LE in Phoenix during the entire simulation period.

3.3. Results and Discussion

3.3.1 Comparison between different irrigation schemes

On the basis of the demonstrated skill of the UCM in reproducing energy and water budgets for Phoenix, a series of simulations was conducted to investigate the effect of various irrigation schemes on environmental temperature, building energy consumption, and outdoor thermal comfort at an annual scale. In 2010, vegetative cover of the Phoenix metropolitan area was estimated to be about 12% (City of Phoenix, 2010). Aiming to create a healthier, more livable and prosperous desert city, the City of Phoenix has initiated a Tree and Shade Master Plan to achieve the recommended average tree coverage of 25% by American Forest for southwestern cities (City of Phoenix, 2010). Projecting the increase onto residential areas, mesic neighborhoods may have a vegetative cover of more than 30%. For subsequent simulations, a combination of 35% vegetative cover and 65% impervious surface is used to represent mesic residential landscape in the near future.

Figure 3.3 shows the temporal distribution of θ_{top} and water consumption of all schemes. The annual variability is markedly different for different schemes: for daily constant irrigation scheme, water use pattern roughly follows a bell curve, with the peak consumption in the pre-monsoon summer, June; the soil-moisture-controlled scheme maintains θ_{top} at a relatively constant level, water consumption increases with soil temperature and the trend is similar to that of daily constant scheme. Irrigation of the soil-temperature-controlled scheme has the most drastic seasonal variation, with water use mainly concentrated in the summer owing to elevated temperatures. Peak water

46

consumption in July and August for the soil-temperature-controlled scheme is 4 times more than that of other two schemes.
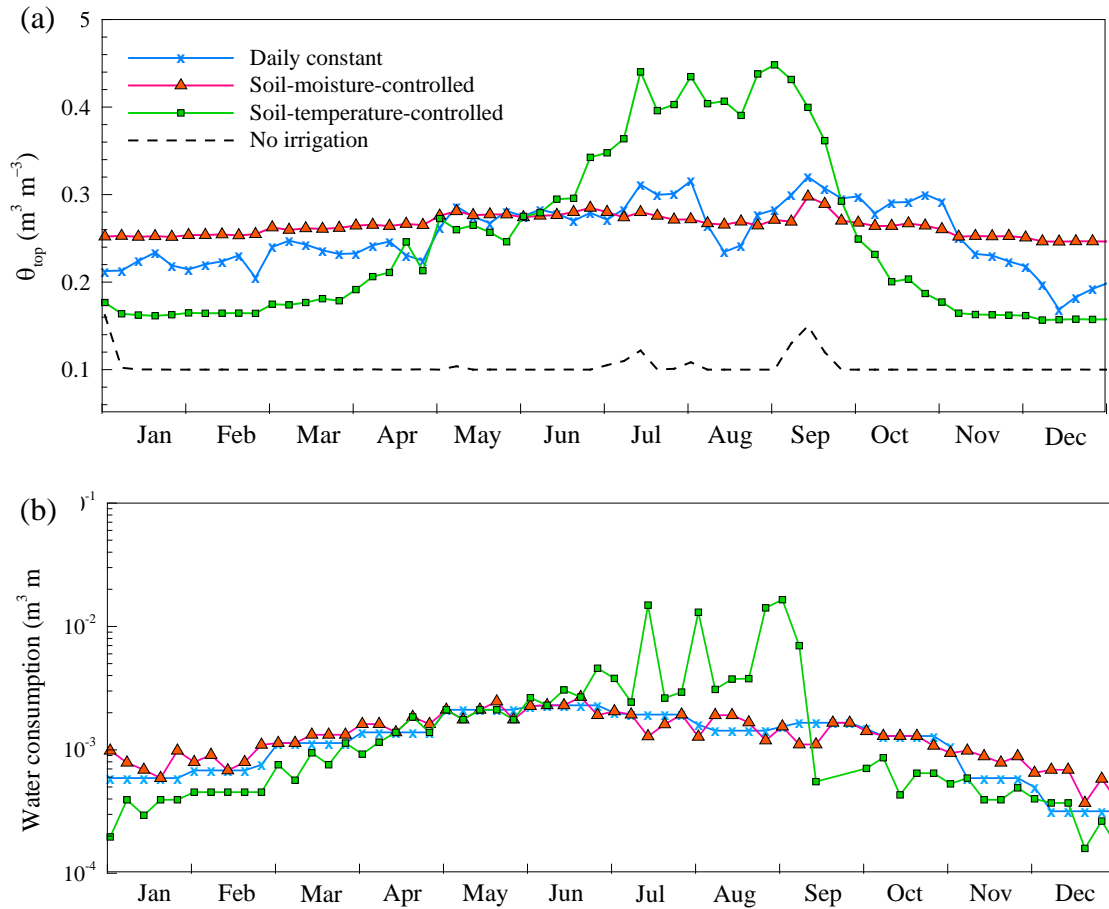
Figure 3.3. Simulated temporal distribution of (a) θ_{top}, and (b) water consumption among different irrigation schemes in Phoenix in 2012.

With vastly different profile of θ_{top} and water consumption, it is expected that soil-temperature-controlled and soil-moisture-controlled irrigation have significantly different impacts on thermal condition in the urban canyon. First, various irrigation schedules modify surface heating and turbulent mixing in the urban canyon, subsequently changing

the heat exchange between wall surface and canyon air. Second, different cooling of the ground surface impacts the amount of longwave radiation emitted towards building surface. Detailed results and discussion on the difference in heat transfer are shown in subsequent sections.

3.3.1.1 Effect of irrigation schemes on environmental temperatures

By replenishing soil moisture for evapotranspiration, urban irrigation has direct cooling impacts on the ground temperature. Note that the UCM does not dynamically simulate the growth and wilt of vegetation. Vegetation is assumed to be fully functional as long as θ_{top} is maintained above the wilting point of mesic landscape. Figure 3.4 demonstrates the reduction of T_g, T_{can}, and wall temperature (T_w) by various irrigation schemes as compared to the no-irrigation case. Calculation of these temperatures involves complicated energy and moisture transport in cities due to urban geometry and thermal interaction. Please refer to Wang et al. (2013) for detailed computational process. Under the same meteorological condition, evaporative cooling is determined by the volumetric moisture content of top soil layer. Consequently, the magnitude of reduction in T_g among different schemes (Fig. 3.4a) follows closely the relative magnitude of θ_{top} in Fig. 3.3a. The soil-moisture-controlled scheme has a larger reduction of T_g than other schemes during the winter, whereas the soil-temperature-controlled irrigation induces the greatest cooling in the summer. Maximum monthly reduction in T_g is about 2.1 ^oC in the winter and about 6.3 ^oC in the summer. When moisture content is relatively constant (e.g. the soil-moisture-controlled scheme), evapotranspiration of urban vegetation is regulated by

48

available radiation at the surface, resulting in the larger cooling in summer compared to other seasons.

(a)

(b)

(c)
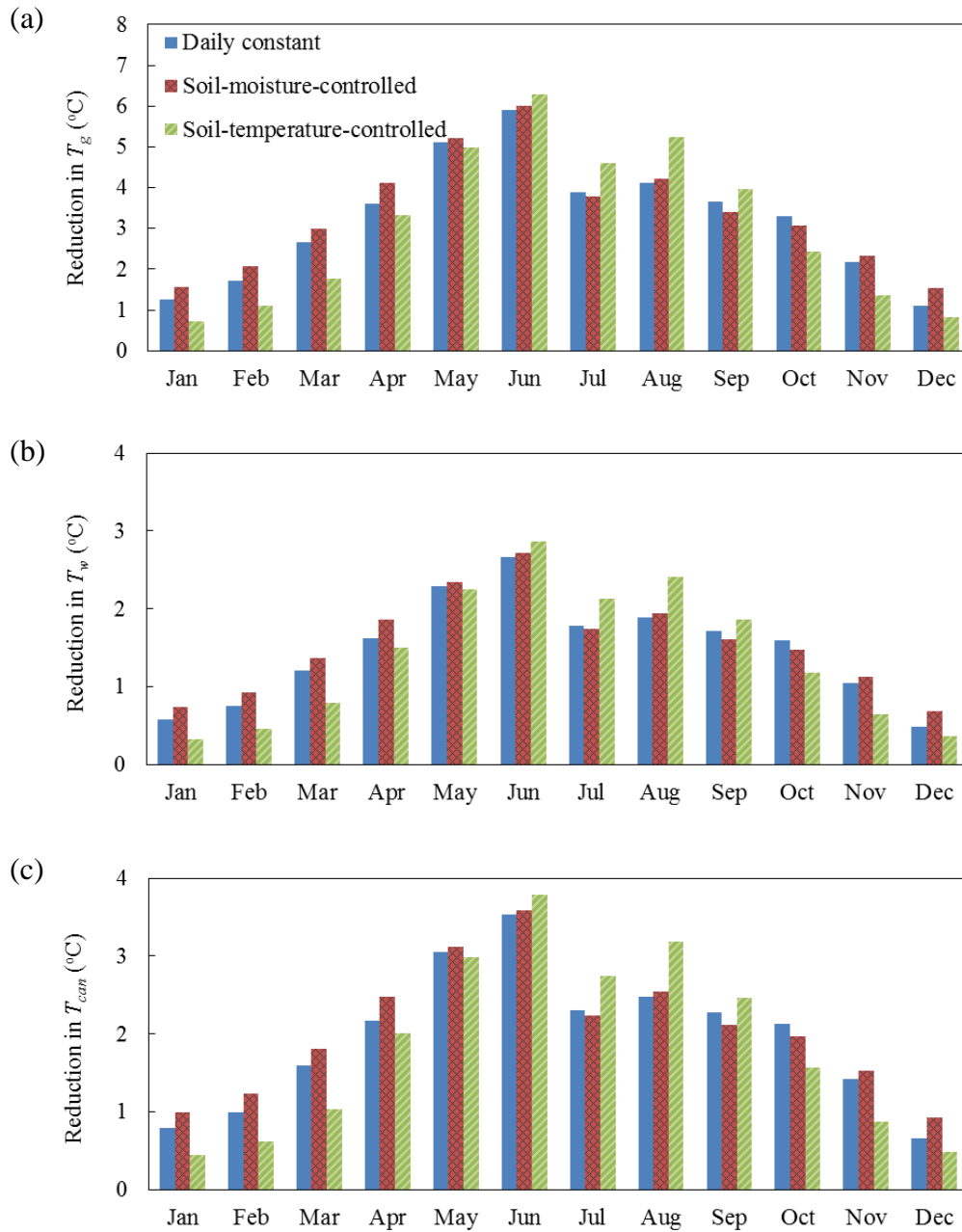
Figure 3.4. Monthly reduction in (a) T_g, (b) T_w, and (c) T_{can} by various irrigation schemes as compared to the baseline (no-irrigation) case. Scale of the vertical axis is different for subplots.

Through the thermal interaction inside the street canyon, urban irrigation has indirect cooling impacts on building surface as lower ground temperature reduces thermal radiation emitted towards the wall. Reduced temperatures subsequently weaken the sensible heat flux arising from ground and wall surfaces, leading to the cooling of canyon air. Effect of different irrigation schemes on T_{can} and T_w is plotted in Figs. 3.4b and 3.4c, respectively. Monthly variation of the reductions in T_{can} and T_w is nearly identical to that of reduction in T_g. Maximum monthly cooling in June is less than 4.0 °C for T_{can} and 3.0 °C for T_w, which is significantly lower than the direct cooling effect on T_g. It is noteworthy that the cooler canyon air and wall surface in turn affect the evapotranspiration process of ground vegetation, thus results here represent the effect of urban irrigation in a built environment with interactive exchange of thermal energy.

3.3.1.2 Effect of irrigation schemes on building energy consumption

Figure 3.4 clearly illustrates that urban irrigation cools the built environment throughout the annual cycle. Reduced environmental temperature can save cooling load of buildings during warm to hot seasons, it nevertheless increases heating demand of buildings in cool to cold seasons. To quantify the net impact of urban irrigation on building energy efficiency, the one-dimensional heat conduction equation through walls is solved as:

$$\frac{\partial T(x,t)}{\partial t} = \alpha_w \frac{\partial^2}{\partial x^2} T(x,t), \tag{1.1}$$

where T is temperature inside the building envelop as a function of position x and time t, and $\alpha = k / \rho c$ is the thermal diffusivity, with ρ the density, c the specific heat, k the

50

thermal conductivity, and the subscript w denoting walls. The heat equation can be

solved analytically using Green's function approach (Wang et al. 2011a) using

convolution integral. Given the temporal scale of this study (annual), and the fact that

convolution requires the saving of all temporal history of the thermal field evolution

inside the wall (for 1 year) and is not computationally effective, the finite difference

method is adopted to solve the heat equation, by discretizing the wall into a finite number

of layers. The temperature profile inside the wall in the i-th layer at time instant j is

solved as:

$$T_i^j = T_i^{j-1} + \alpha_w \frac{T_{i+1}^{j-1} - 2T_i^{j-1} + T_{i-1}^{j-1}}{(\Delta x)^2} \Delta t , \tag{1.2}$$

where x and t are the space and time intervals respectively. This equation is solved with a

constant inner wall surface temperature boundary condition.

Building energy consumption consists of thermal load, plug load, equipment load,

and lighting load. The analysis here focuses on thermal load as the rest is relatively

independent of outdoor meteorological condition. Thermal load is the amount of heating

and cooling energy that needs to be added to or removed from the building to maintain

thermal comfort and control moisture for occupants. Thermal load of buildings is

determined by the combination of external thermal load and internal thermal load.

External loads are made up of heat transmitted through the envelope (roof, wall, and

ground), solar gain through windows, heat loss/gain through leaks, infiltration and

ventilation, while internal loads include heat generated by people, lighting, and

equipment. Note that though the UCM is capable of reproducing energy and water

budgets for urban area, its ability in simulating building structural details is limited. Therefore, several factors are neglected when estimating building energy consumption.

Firstly, internal thermal load of buildings is neglected. For the studied residential area in Phoenix, single family house is the major building type (Chow et al. 2014). Sparsely populated with little activity and energy-intensive equipment, single family house is generally dominated by external thermal loads. Secondly, latent load of buildings is ignored. This assumption is acceptable for Phoenix as latent load constitutes only about 21% of the annual ventilation load under hot and dry climate (Harriman III et al. 1997). Thirdly, the contribution of heat flux transmitted through roof and ground floor is not accounted for, as pilot analysis indicates that irrigation in the street canyon has limited effects on roof temperature and soil temperature under building ground floor. Fourthly, due to model limitation, windows are not simulated that subsequent results represent buildings without windows. Lastly, the efficiency of air conditioning system and the variation of the building interior temperature are not considered. Because the efficiency of air conditioning system is always less than 1, actual energy used for heating and cooling would be larger than the heat flux transmitted through building envelope. Based on these assumptions, building energy consumption is estimated as the heat flux transmitted through the wall in this study, given by:

$$Q_{in}^{j} = \frac{k_w \left(T_{in}^{j} - T_b \right)}{d_{in} / 2},$$

(1.3)

where Q_{in}^{j} is the heat flux entering the building via walls at time step j, d_{in} is the thickness of the innermost (discrete) layer, T_{in}^{j} is temperature of the innermost layer at the same time calculated using Eq. (3.3), and T_b is the inner wall surface temperature. A

positive Q_{in} indicates a cooling demand of the building, while a negative value means a heating demand.
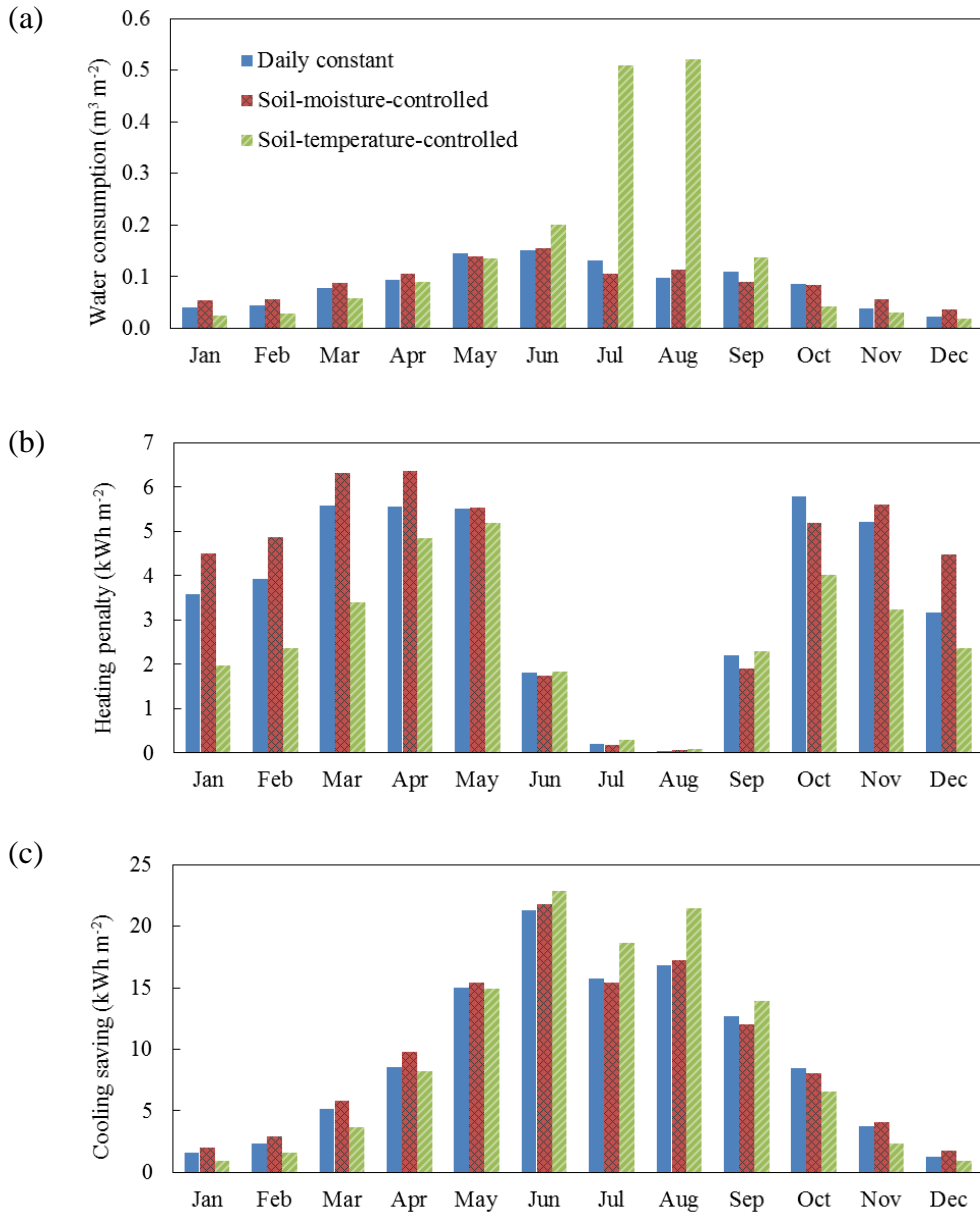
Figure 3.5. Monthly (a) water consumption, (b) heating penalty, and (c) cooling saving by various irrigation schemes as compared to the no-irrigation case.

53

In the UCM, heat transfer within building wall is computed using a multi-layer algorithm, which enables capturing evolution of temperature and heat transfer within the wall as compared to a single-layer algorithm. Here a R5 insulation wall sheathing is considered based on Energy Star recommendation and a typical value of 0.9 W m^{-1} K^{-1} is used for k_w. Inner wall surface temperature is assumed to be maintained at 24 °C by indoor heating, ventilation, and air-conditioning (HVAC) systems for the entire simulation period.

Figure 3.5 presents the monthly water consumption, heating penalty (additional building heating demand), and cooling saving (reduced building cooling demand) by different irrigation schemes as compared to the no-irrigation case. In cool to cold season (November to March), the soil-moisture-controlled scheme consumes about 0.29 cubic meter water per square meter vegetated ground area for irrigation, notably larger than 0.22 m^3 m^{-2} in daily constant scheme and 0.16 m^3 m^{-2} in the soil-temperature-controlled irrigation. Relatively high moisture level maintained by the soil-moisture-controlled scheme significantly increases the heating demand of buildings. Monthly maximum penalty can be up to about 6.3 kWh m^{-2} in early spring and the annual heating penalty is more than 45 kWh m^{-2}. On the other hand, with irrigation concentrated in summer, the soil-temperature-controlled scheme has the least heating penalty as well as the largest cooling saving. Total water consumption of the scheme in summer is 1.23 m^3 m^{-2}, which is about tripled compared to the consumption of 0.38 m^3 m^{-2} in other two schemes. Compared to the control case (no-irrigation), the maximum monthly saving is more than 20 kWh m^{-2} in June. For the entire simulation period, total heating penalty and cooling saving is about 32 and 116 kWh m^{-2}, respectively.

3.3.1.3 Effect of irrigation schemes on net cost

The saving of summer cooling load by lawn irrigation is concomitant with the cost of increased water usage: it takes water to cool an arid city. The trade-off between water and energy consumption naturally leads to the classic question of cost-benefit: Is the saving of cooling energy from urban irrigation worth the cost of water resources? Water conservation has been a primary concern in Phoenix as the city receives water from upstream basins and groundwater pumping. Outdoor water use per capita in Phoenix surpasses rates in other cities. A cost-benefit analysis by combing water and energy consumptions can provide a quantitative estimate, serving as a reasonable economic measure of the environmental sustainability of various irrigation schemes. For unit consistency, total cost is given by:

$$\text{cost}_{\text{total}} = P_{\text{water}} \left(\frac{w}{h} \right) f_{veg} \sum_t W + P_{\text{electricity}} \sum_t |Q_{in}|, \tag{1.4}$$

where P_{water} and $P_{\text{electricity}}$ are the unit prices of water and electricity usage respectively, w/h is ration between ground and wall areas, f_{veg} is the areal fraction of vegetation over ground surface, and W is the water consumption rate. The absolute value function is used to account for electricity consumption by both cooling and heating demand of the building. Note that water cost has a unit of cubic meter water per square meter vegetated ground area, and is multiplied by the fraction of vegetated ground area to wall surface area $(w/h)f_{veg}$ for unit conversion. The resulted total cost is in dollar per square meter wall area.

Electricity price is obtained from the basic plan of local company Salt River Project (http://www.srpnet.com/prices/home/basicfaq.aspx#2) and water price is acquired from

55

the city of Phoenix (htttps://www.phoenix.gov/waterservices/customerservices/rateinfo).

Table 3.1 summarizes the electricity and water prices for Phoenix, both prices have a strong seasonal variation with high charges in summer. Note that the Salt River Project also offers a Time-of-Use plan and an EZ-3 plan in which electricity price is higher during on-peak hours. The choice of electricity plans may affect the results of total monetary saving, however, comparison between different plans is beyond the scope of this study.

Table 3.1. Summary of electricity and water prices in Phoenix.

Month	Electricity price ($¢$ kWh^{-1})	Water price ($\$$ m^{-3})
January	8.03	1.00
February	8.03	1.00
March	8.03	1.00
April	8.03	1.19
May	12.31	1.19
June	12.31	1.32
July	12.83	1.32
August	12.83	1.32
September	12.31	1.32
October	12.31	1.19
November	8.03	1.19
December	8.03	1.00

Monthly saving in total cost of different irrigation schemes as compared to the no-irrigation case is shown in Fig. 3.6. Results show that during hot seasons, irrigating more water leads to more total saving. Maximum monthly saving can be up to about $2.5 m^{-2} in the soil-temperature-controlled scheme for June and August. In cool to cold months when heating demand dominates, additional moisture from irrigation results in increased total cost (negative values in Fig. 3.6). Monthly cost of the soil-moisture-controlled scheme is about $0.13 m^{-2} higher than that of the soil-temperature-controlled scheme throughout the winter. Table 3.2 summarizes the annual water use, electricity consumption, and total cost of all schemes. Among investigated schemes, the soil-moisture-controlled scheme has the largest total cost. Compared to daily constant irrigation, it consumes more water and has higher total cost, primarily due to the increased heating penalty during cool seasons. The soil-temperature-controlled scheme has a significantly larger annual water usage, which is 60% more than that of other two schemes. However, the cost of water can be offset by the saving in cooling energy. Overall, the soil-temperature-controlled irrigation scheme is the most efficient in reducing annual total cost of mesic neighborhoods.

Table 3.2 shows that saving by the soil-temperature-controlled irrigation is relatively insignificant as compared to the total cost of daily constant irrigation. One plausible reason is that the current irrigation practice in Phoenix is well planned as water is a precious resource for the desert city. It is important to keep in mind that the soil-temperature-controlled irrigation is more effective in reducing urban temperatures during the summer than the current irrigation scheme, thus providing benefits of a better living

57

environment to residents, and being more cost-effective. At last, it is worth to point out that results on net cost are achieved based on the assumption and simplification listed in section 3.3.1.2. Modification of any condition, especially the efficiency of air conditioning system, may revamp the energy-water trade-off and lead to significant variation in efficiencies of investigated irrigation schemes.

Figure 3.6. Monthly total saving by various irrigation schemes as compared to the no-irrigation case.

Table 3.2. Summary of annual water usage, energy consumption, and total cost of all study irrigation schemes.

	No-irrigation	Daily constant	Soil-moisture-controlled	Soil-temperature-controlled
Water usage (m^3 m^{-2})	0	1.04	1.09	1.79
Energy consumption (kWh m^{-2})	1405.8	1335.7	1336.3	1321.6
Annual total cost ($ m^{-2})	151.29	143.28	143.32	142.44

3.3.1.4 Effect of irrigation schemes on outdoor thermal comfort

In addition to alleviating environmental temperature and building energy demand, urban irrigation has important implications for thermal comfort of pedestrians in outdoor urban environment. With a large city size, warm and dry climate, and significant amount of clear days, Phoenix is among the hubs of urban heat islands in the United States where people experience intense thermal discomfort during hot days in outdoor or non-air-conditioned indoor environments (Brazel et al. 2000). The quantification of outdoor thermal comfort in urban areas is complicated, due to many environmental factors, including but not limited to temperature, humidity, wind speed, radiative exposure, and ambient evaporative and sensible fluxes (Mishra and Ramgopal 2013). Evaluation of the outdoor thermal comfort may be performed using various indices. In this study, the Index of Thermal Stress (ITS) developed by Givoni (1963) is selected to identify the impact of urban irrigation on outdoor thermal comfort for Phoenix. ITS is a measure of the rate at which the human body must give up moisture to the environment in order to maintain thermal equilibrium, defined by:

$$ITS = E \times \exp\left[0.6\left(\frac{E}{E_{max}} - 0.12\right)\right], \tag{1.5}$$

where E is the cooling rate produced by sweat which is required for equilibrium, and E_{max} is the evaporative capacity of the air. E is given by:

$$E = M - W + R_n + C, \tag{1.6}$$

where M is the body's metabolic rate, W is the energy transformed into mechanical work, R_n and C are the environmental heat exchanges due to radiation and convection, respectively. Detailed calculation of E_{max}, R_n and C using meteorological variables can be

59

found in (Shashua-Bar et al. 2011), where the net metabolic heat gain (M-W) is taken as a constant 70 W m^{-2} for the pedestrian. Pearlmutter et al. (2007) has employed the index to assess outdoor thermal comfort condition in urban canyon with different geometries.

Table 3.3. Summary of monthly averaged ITS of all study irrigation schemes.

Month	ITS (W m^{-2})			
	No-irrigation	Daily constant	Soil-moisture-controlled	Soil-temperature-controlled
January	172.2	169.6	168.9	170.7
February	237.7	233.8	233.0	235.2
March	338.4	333.5	332.3	335.2
April	452.8	438.7	436.9	439.6
May	578.0	554.4	553.9	555.1
June	658.9	627.1	626.4	625.3
July	628.8	605.2	603.2	602.9
August	614.0	595.2	594.0	590.7
September	531.5	533.4	534.1	529.1
October	358.6	345.7	346.4	348.7
November	235.5	229.5	229.0	231.8
December	151.7	149.8	149.0	150.3

The ITS for pedestrians doing gentle outdoor activities (e.g. walking) in the street canyon is calculated. Monthly averaged ITS in different irrigation schemes are

summarized in Table 3.3. Givoni (1963) conducted a series of empirical experiments to correlate ITS with subjective thermal sensation. An ITS between 280 and 400 W m^{-2} indicates a "hot" thermal condition and above 400 W m^{-2} is "very hot". Following their definition, outdoor thermal comfort condition will be very hot for pedestrians from April to September in Phoenix.
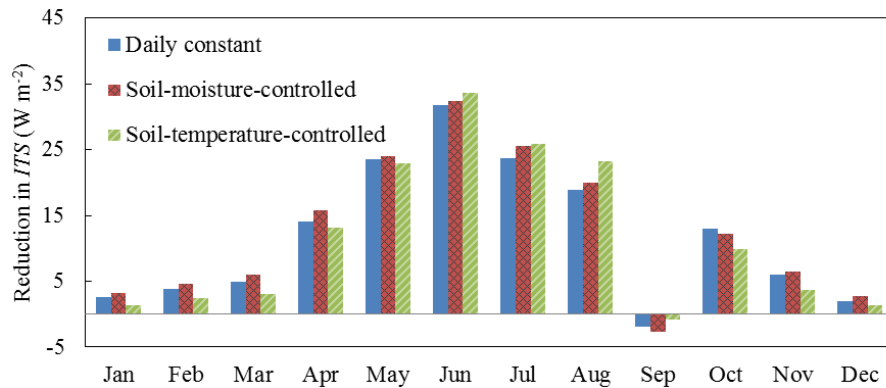
Figure 3.7. Monthly reduction of ITS by various irrigation schemes as compared to the no-irrigation case.

Reduction of ITS by different irrigation schemes as compared to the no-irrigation case is shown in Fig. 3.7. By reducing environmental temperature and increasing humidity, urban irrigation leads to reduction in ITS throughout the year except for September. Due to four major rainfall events, September has a significantly higher relative humidity than other months. Further moisture brought by irrigation under the humid condition thus results in degradation of outdoor thermal comfort. In hot summer, reduction of ITS by the soil-temperature-controlled scheme is more significant than that of other two schemes. Maximum reduction is about 35 W m^{-2} in June. It is noteworthy

61

that outdoor human thermal comfort is a rather subjective measure that is related to physiological aspects of pedestrians, which can vary from region to region. The results of this study indicate a rather qualitatively positive impact of urban irrigation on outdoor thermal comfort in Phoenix.

3.3.2 Optimal soil temperature for the soil-temperature-controlled irrigation

The comparative analysis in section 3.3.1 indicates that the soil-temperature-controlled irrigation is the best scheme in terms of annual total saving. The governing mechanism of the scheme is to generate saving in cooling energy in summers as well as to minimize heating penalty during winters. The use of water to cool a city in summers necessarily points to the intricate balance of water-energy nexus. Is there an optimal temperature regulating the soil-temperature-controlled irrigation that can maximize the combined saving of energy and water resources? To address this question, a set of simulations with six controlling top-soil temperatures (in addition to the initial controlling temperature of 22 ℃) is carried out, namely 20, 21, 23, 24, 25, and 26 ℃, above which the soil-temperature-controlled irrigation will be activated.

Figure 3.8 demonstrates the annual saving in energy, water and the combined cost by different soil-temperature-controlled irrigation schemes as compared to the no-irrigation case. Positive values in the graph denote net saving. At a lower activating temperature, the soil-temperature-controlled scheme consumes more water during hot periods. Due to the nonlinear distribution of temperature, cost of water decreases more rapidly at a lower soil temperature. The combined annual saving exhibits a nonlinear trend as a function of activating soil temperature. Water usage with an activating

temperature of 26 °C is only about 18% of that with an activating temperature of 20 °C. The latter consumes 17.1 kWh m^{-2} less energy than the former. Maximum annual saving is about $9.20 per square meter wall area at 23 °C, while minimum saving of $6.47 per square meter wall area is found with an activating temperature of 20 °C.
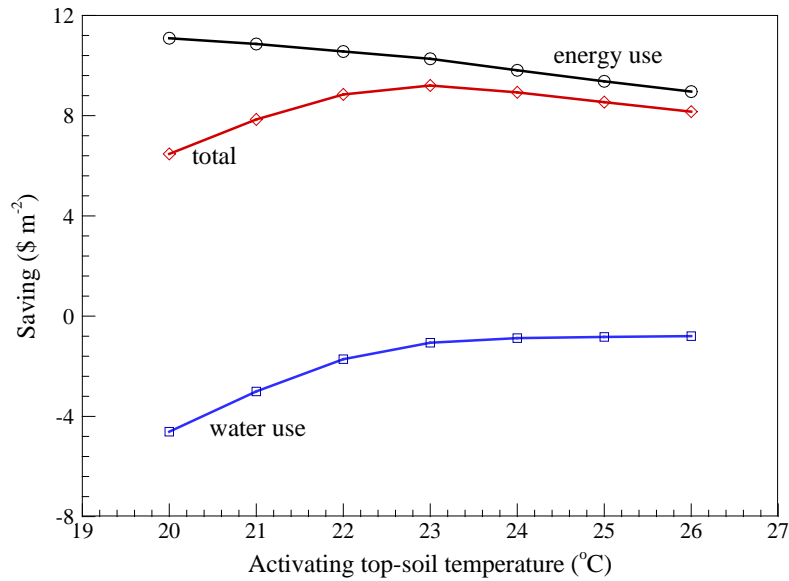
Figure 3.8. Annual saving in cost of water consumption, energy cost and total cost by soil-temperature-controlled irrigation scheme with various activating soil temperatures as compared to the no-irrigation case.

Comparing with the annual saving of $8.01 m^{-2} by daily constant scheme, the activating top-soil temperature needs to be carefully determined in order to yield the optimal irrigation scheme using temperature control in terms of the trade-off between water and energy. It is worth to mention that optimal activating soil temperature depends on meteorological conditions and thus can vary vastly for different seasons or different climatic zones. Analysis here using a yearly constant activating temperature serves as a

first step towards optimizing irrigation schemes for building energy efficiency. Further

studies on a temporally varying activating soil temperature are needed.

3.4. Summary

In this Chapter, the enhanced urban canopy model developed in Chapter 2 was used

to identify the environmental effect of urban irrigation for the Phoenix metropolitan area.

The performance of various uncontrolled and controlled irrigation schemes on mesic

residential landscapes was investigated, including (1) daily constant irrigation, (2) soil-

moisture-controlled irrigation, and (3) soil-temperature-controlled irrigation. In general,

irrigating mesic landscape in urban areas cools the urban environment via enhanced

evapotranspiration. Maximum cooling effect on canyon air temperature can be more than

$3 \, ^{\circ}C$ in summer. Results show that the soil-temperature-controlled irrigation can reduce

annual building energy consumption and the combined energy-water cost of the no

irrigation case by about 6%, which is the most efficient among investigated schemes. By

design, the soil-temperature-controlled scheme activates irrigation during hot periods and

helps to preserve water during cold seasons, thus optimizes the trade-off between energy

and water use. Annual saving can be up to about \$1.19 per square meter wall area

compared to the current irrigation practice (daily constant) in Phoenix. The total saving of

the soil-temperature-controlled scheme requires a fine balance in energy-water use. Site-

specific analysis is therefore required to determine the optimal activating soil

temperatures.

It is noteworthy that estimated saving in this Chapter provides a qualitative rather

than quantitative guidance for water-energy trade-off in urban irrigation, due to (i) the

simplifications made in estimating the building energy consumption, and (ii) the neglect of the uncertainty inherent in model physics and the parameter space. In addition, modelling results, especially those for the daily constant irrigation scheme, are based on the monthly available in-situ measurement of irrigation over mesic residential landscapes. Timing, duration and amount of actual irrigation vary from neighbour to neighbour thus the results cannot be directly up-scaled to extract monetary saving for the entire city. Having more detailed data availability in other study areas will help to validate and improve the proposed irrigation schemes in this study. Nevertheless the analysis in this Chapter deepens our insight into the trade-off between energy and water use and facilitates a development of new paradigm for urban irrigation.

CHAPTER 4 REGIONAL EFFECT OF GREEN ROOFS ON TWO CITIES IN CONTRASTING CLIMATES

4.1. Introduction

    Impact of green roofs on building energy efficiency and urban climate at the city scale has been accessed in Chapter 2. However, studied in an offline (i.e., not dynamically coupled to the overlying atmosphere) setting, simulation results in Chapter 2 did not account for the interaction between the land and atmospheric system, and the potential omission of important feedback mechanisms can lead to significant uncertainty and potential errors (Brubaker and Entekhabi 1996). To model the exchanges between the land surface and the atmosphere, mesoscale atmospheric and urban canopy models need to be coupled, whereby mesoscale models compute meteorological forcings for the surface, while urban canopy models provide the lower boundary conditions for the overlying atmospheric system (Best 2005, Chen et al. 2011). In the literature, there have been only a handful of studies investigating climatic (Georgescu et al. 2014, Georgescu 2015) and meteorological (Li et al. 2014) impacts of green roofs in a coupled atmosphere-urban modelling framework. Georgescu et al. (2014) explored the benefits of green roofs and the potential to offset urban-induced warming at seasonal and annual timescales across the contiguous U.S. Nevertheless, assuming green roofs were infinitely evaporating without water constraint, their results represented the maximum potential benefits of evaporating rooftop water pools rather than green roofs. Li et al. (2014) investigated the effectiveness of green roofs by coupling the Princeton urban canopy model into the WRF system. They focused on a 3-day summer heat wave event whereas the long-term performance of green roofs was not addressed. More importantly, urban

hydrological processes were not adequately represented in these studies (e.g., urban

irrigation and urban oasis effect), leading to potential uncertainty in the findings.

It is therefore imperative to implement green roofs into a coupled atmosphere-urban

modelling system to investigate their impacts under a fully interacting environment. In

addition, the effect of hydrological processes (described in Chapter 2) on urban regional

hydroclimate needs to be addressed. In this chapter we coupled the enhanced SLUCM

developed in Chapter 2 into the integrated WRF-Urban modelling system to: (1) evaluate

the impact of hydrological processes on prediction of urban hydrometeorological

variables, and (2) assess the effect of green roofs at the regional scale with seasonal

variability. To investigate model results under different geographical and climatic

conditions, simulations are conducted for two major cities in the United States, namely,

Phoenix and Houston.

4.2. Methodology

4.2.1 WRF-Urban modelling system

WRF is a fully compressible, non-hydrostatic modelling system that has been used

for a variety of applications, ranging from local to global scale (Skamarock and Klemp

2008). At this stage, four urban parametrization options are available in the WRF-urban

modelling system that are coupled to the Noah land surface model, namely the bulk

parametrization, the single layer urban canopy model (Masson 2000, Kusaka et al. 2001),

the multi-layer urban canopy model (Building Energy Prediction, BEP) (Martilli et al.

2002), and BEP plus indoor-outdoor exchange building energy model (Salamanca et al.

2010). The coupled WRF-urban modelling system has been applied to major

metropolitan regions and its performance has been validated against ground-based observations, atmospheric soundings, and wind-profiler measurements (Lin et al. 2008, Miao and Chen 2008, Kusaka et al. 2012a). Mid- to end-of-century urban climates have also been studied with the modelling system (Georgescu et al. 2012, Kusaka et al. 2012b).

Here we used WRF version 3.4.1 to conduct simulations over study metropolitan areas. Initial meteorological conditions for the WRF simulations were obtained from the National Centers for Environmental Prediction Final Operational Global Analysis data, which were available on a $1^o \times 1^o$ resolution with a 6-hour temporal frequency (details can be found on http://rda.ucar.edu/datasets/ds083.2/). The Noah land surface model, coupled with the single layer urban canopy model, was used to simulate land surface processes after initiation. Note that we adopted an enhanced version of SLUCM as described in Chapter 2, which featured the integration of (1) anthropogenic latent heat, (2) urban irrigation, (3) evaporation from water-holding engineered pavements, (4) urban oasis effect, and (5) multilayer green roof system. Other major physical parameterization schemes used in this study include: (1) the new Thompson scheme for microphysics (Thompson et al. 2008); (2) the rapid radiative transfer model for longwave radiation (Mlawer et al. 1997); (3) the Dudhia scheme for shortwave radiation (Dudhia 1989); (4) the MM5 similarity scheme for surface layer and (5) the Yonsei University scheme for planetary boundary layer (Hong et al. 2006). Cumulus parametrization is turned on only for the outer and middle domain, using the Kain-Fritsch scheme (Kain 2004).

4.2.2 Experiment design

To compare the effect of urban hydrological processes under different geographical and climatic conditions, we selected Phoenix and Houston as our study sites. These two are among the top ten most populous cities in the U.S., whose urban heat island and hydroclimate has been extensively studied in the literature (Salamanca et al. 2011, Georgescu et al. 2012, Yang et al. 2016a). Distinct conditions in two regions (e.g., inland semi-arid for Phoenix and coastal humid for Houston) facilitate a better understanding of urban hydrological processes under different geographical and climatic conditions.

For both areas, we used a two-way nested grid configuration with all three domains centered on the city (see Fig. 4.1). Spatial resolution for the outer, middle, and inner domains was 32 km, 8 km, and 2 km, respectively. The outer domain covered a surface area of 1856 km $\times$ 1856 km, and the inner domain had a size of 212 km $\times$ 212 km. As the outer and middle domains cover portions of Mexico, MODIS global land cover data was used (Friedl et al. 2002). For the inner domain, we used the National Land Cover Database (NLCD) 2006 (Fry et al. 2011) to represent the heterogeneous urban landscape which is subdivided into 3 categories (see Fig. 4.1c and Fig. 4.1d). We selected year 2006 for this study to represent a normal annual climatic condition for both cities. Simulations were initiated on 0000 UTC, 1 November, 2005 and concluded at 0000 UTC, 1 December, 2006. November 2005 was the spin-up period and not included in subsequent analysis. Considering the time span of simulations and geographical locations, sea surface temperature was updated at an interval of 1 day. In this Chapter, our analysis focused on the inner domain and results of the other two domains are not discussed.
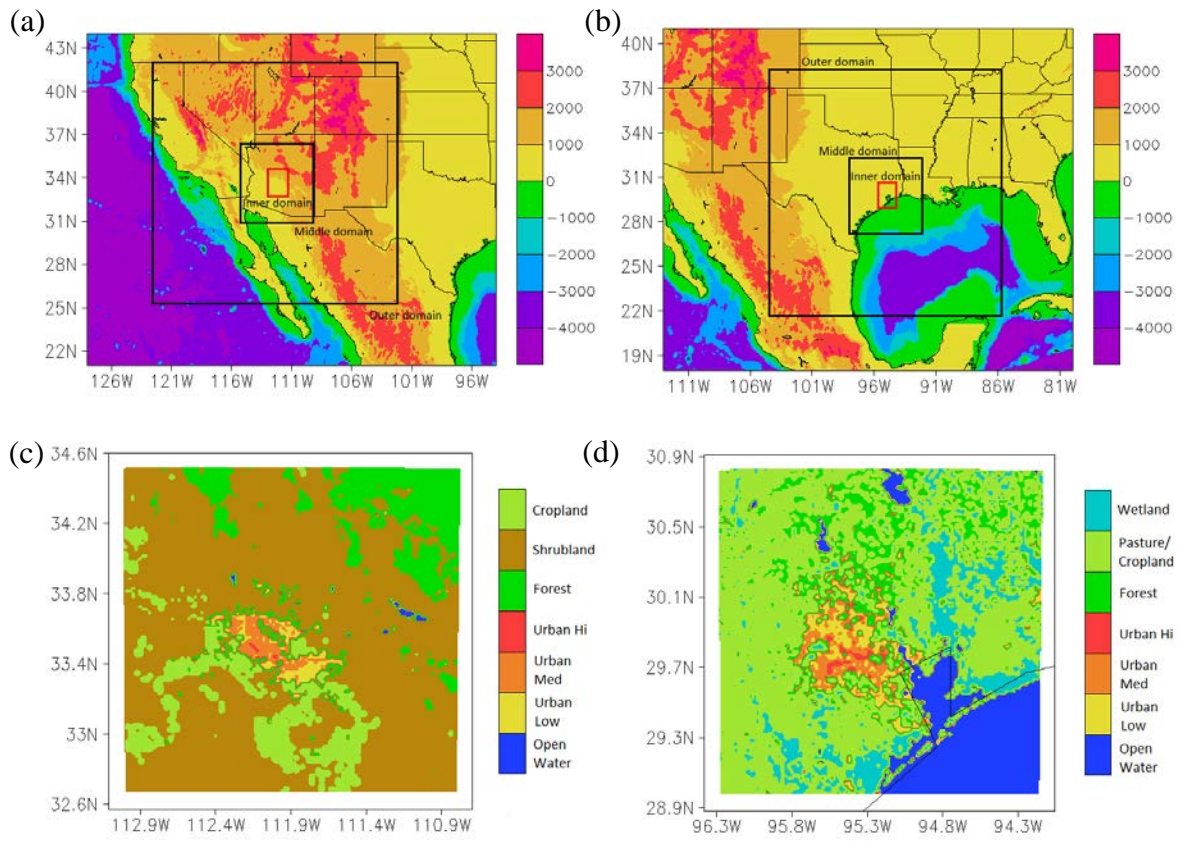
Figure 4.1. Geographical representation of the domain extent with topography (in meters) overlaid for (a) Phoenix, and (b) Houston. Land use land cover information of the inner domain for (c) Phoenix, and (d) Houston.

For each city, a total of three sets of simulation were conducted (see Table 4.1). The first case was a control run with the default SLUCM (hereafter 'Old SLUCM') in WRF. The second case employed the recently enhanced SLUCM ((Yang et al. 2015a), hereafter 'New SLUCM') with a more realistic representation of urban hydrological processes. The last case assumed a 100% areal fraction of green roof deployment over the study cities using the new SLUCM. With this experiment design, the impact of hydrological

processes can be readily obtained by comparing results from the first and second cases. And the difference in results between the second and last cases renders the regional impact of green roofs.

Table 4.1. Summary of numerical experiments performed.

Case number	Model	Hydrological process
1	Old SLUCM	Same as default WRF 3.4.1
2	New SLUCM	Case 1 + anthropogenic latent heat + urban irrigation + evaporation from water-holding engineered pavements + urban oasis effect
3	New SLUCM	Case 2 + multilayer green roof system

4.3. Impact of Urban Hydrological Processes

Performance of the WRF simulations was evaluated against hourly meteorological observations from ground-based weather stations. Simulated 2-m air temperature (T_2) and 2-m dewpoint temperature (T_{d2}) at one hour frequency were available for direct comparison to observed data. These two variables were selected because of their importance in fire weather prediction (Cheng and Steenburgh 2005). Besides, they are essential inputs to a variety of hydrological and ecological models for resolving evapotranspiration process and plant productivity (Dodson and Marks 1997). For Phoenix, we utilized data from Arizona Meteorological Network (AZMET) and NOAA's National Centers for Environmental Information (NCEI).

71

Table 4.2. Summary of name, location, and land use type of meteorological stations used in this study.

City	Station name	Source	Lat	Lon	Land use
	Encanto	AZMET	33.479	-112.096	Urban
	Mesa	AZMET	33.387	-111.867	Urban
	Skyharbor airport	NCEI	33.428	-112.004	Urban
Phoenix	Buckeye	AZMET	33.400	-112.683	Rural
	Waddell	AZMET	33.618	-112.460	Rural
	Greenway	AZMET	33.621	-112.108	Rural
	Desert ridge	AZMET	33.733	-111.967	Rural
	Pearland	NCEI	29.519	-95.242	Urban
	D.W. Hooks	NCEI	30.068	-95.556	Urban
Houston	William	NCEI	29.638	-95.282	Urban
	Intercontin	NCEI	29.980	-95.360	Rural
	Suger	NCEI	29.622	-95.657	Rural

Details of the meteorological stations are summarized in Table 4.2. Based on NLCD 2006 land use classification, 4 stations were identified as urban and the rest as rural. With respect to Houston, only data from NCEI were used, among which 3 stations were urban and 2 were rural. Arithmetic average of ground-based measurements is compared against that of simulation results at corresponding model grids for evaluation.

Figure 4.2. Comparison of annual average diurnal profiles of simulated and observed (a) urban T_2, (b) urban T_{d2}, (c) rural T_2, and (d) rural T_{d2} for Phoenix.

Figure 4.2 compares the simulated annual average diurnal profiles of T_2 and T_{d2} with the old and new SLUCM against the observations for Phoenix. Hydrological processes are expected to reduce air temperature and increase dewpoint temperature at the 2 m level of urban areas, nevertheless Fig. 4.2 shows that the effect on 2-m air temperature is negligible. One important reason for this phenomenon is the limited effective area and time of hydrological processes. Among the implemented urban hydrological processes,

73

urban irrigation and oasis effect are effective over vegetated area, which is only 20% of the urban land surface in Phoenix. Evaporation from water-holding engineered pavements functions during and shortly after rainfall, therefore its long-term average impact is trivial. Another critical reason is the parameterization schemes in the WRF model. The WRF model adopts a "tile" approach, where fluxes over built and vegetated surfaces are weighted by their respective areal fractions to calculate the total flux arise from the urban land surface. In this case, surface temperature and air temperature are largely determined by the built surface, whose areal fraction and temperature are significantly larger than those over the vegetated surface. Anthropogenic latent heat is directly added to the latent heat flux term that it does not modify partitioning of solar radiation into different fluxes over the urban area. On the other hand, moisture and humidity over the urban land surface are primarily controlled by the vegetated part, as there is no evaporation over the built surface most of the time.

In terms of T_{d2}, it is clear from Fig. 4.2 that modelled T_{d2} is significantly underestimated in WRF simulations with the old SLUCM. Diurnal minimum T_{d2} is found at 1600 local time, which corresponds to maximum T_2. After accounting for urban hydrological processes, model prediction agrees better with observations. Increase of T_{d2} can be up to about 1.5 $^\circ$C for the urban area across the diurnal cycle. Via urban-rural circulations, urban hydrological processes also have detectable effects on rural T_{d2}, though with a smaller magnitude. Results for Houston are plotted in Fig. 4.3. Located in a coastal area, Houston has a lower air temperature and a higher dewpoint temperature than Phoenix. Daytime onshore flow provides moisture for the urban area, therefore weakens

74

the influence of urban hydrological processes. Increase in T_{d2} by hydrological processes is about 0.3 $^{\circ}$C for Houston.

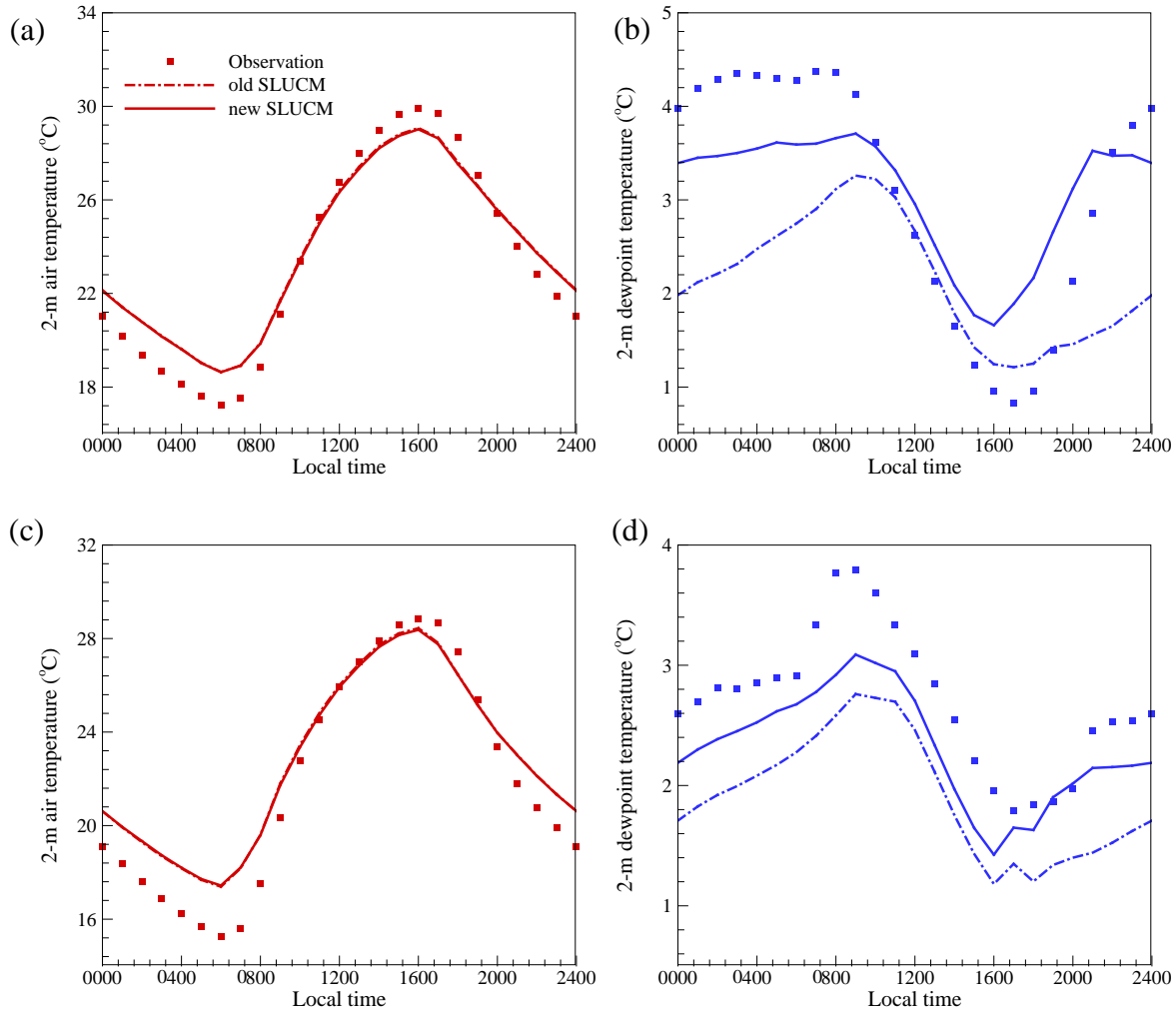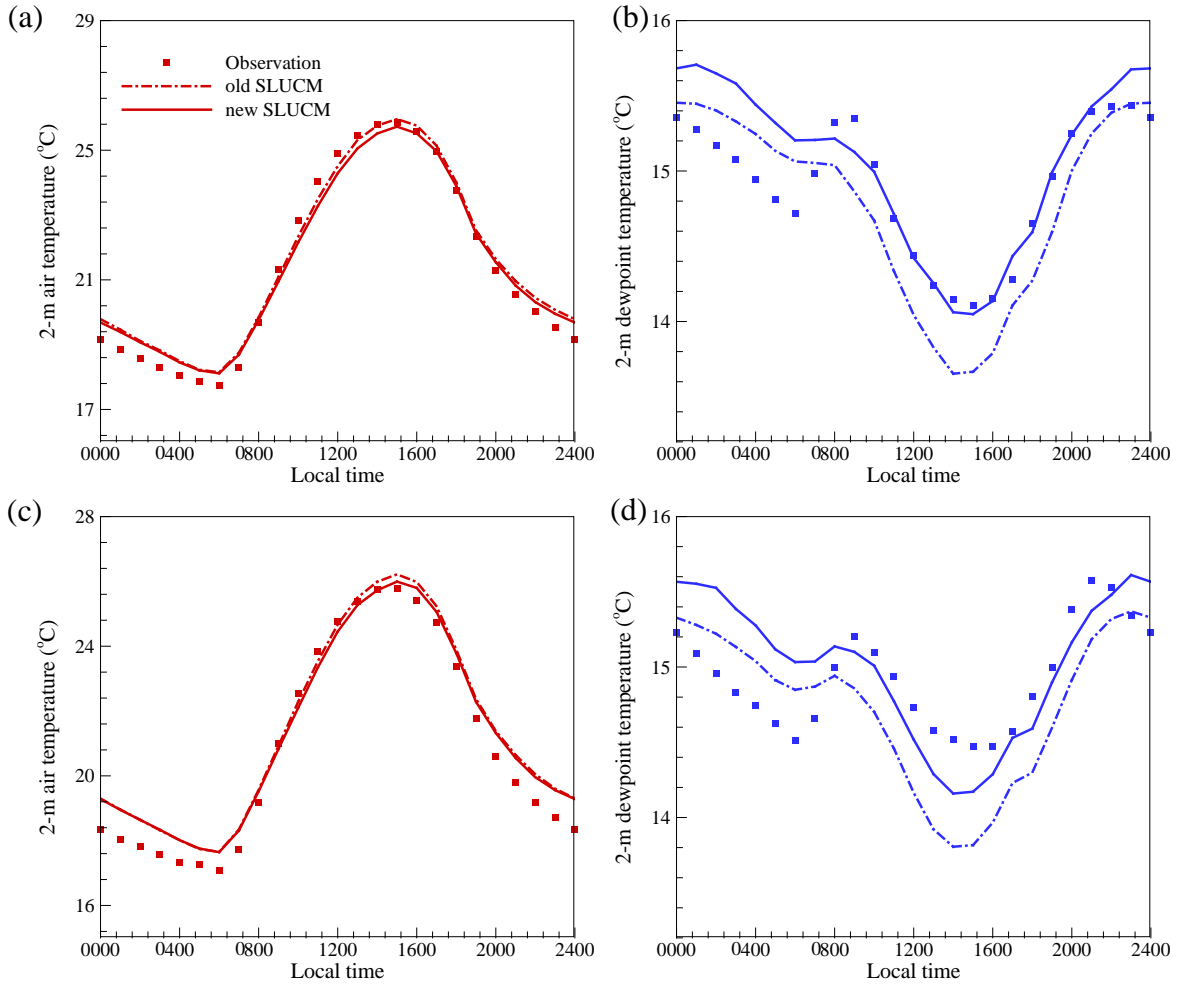Figure 4.3. Comparison of annual average diurnal profiles of simulated and observed (a) urban T_2, (b) urban T_{d2}, (c) rural T_2, and (d) rural T_{d2} for Houston.

Figures 4.2 and 4.3 illustrate that urban hydrological processes have limited effects on T_2. Therefore we used the daily maximum, mean and minimum 2-m dewpoint temperatures for statistical analysis in this Chapter. Evaluating these temperatures is very

useful as they are indices for climate extremes (Alexander et al. 2006; Perkins et al. 2007). Seasonally-averaged results for Phoenix and Houston are summarized in Table 4.3, which shows that with the old SLUCM, WRF simulations considerably underestimate daily maximum and mean T_{d2}. The new SLUCM with enhanced urban hydrological modelling enables improved predictions for the entire simulation period.

Table 4.3. Summary of average daily maximum, mean, and minimum T_{d2} (^{o}C) for different seasons. Obs is short for observation, Old and New denote simulation results with the old and new SLUCM, respectively.

City	T_{d2}	Daily maximum			Daily mean			Daily minimum		
		Obs	Old	New	Obs	Old	New	Obs	Old	New
Phoenix	DJF	-1.91	-3.15	-1.61	-5.71	-6.63	-5.50	-9.12	-10.22	-9.28
	MAM	4.69	3.67	4.10	0.62	-0.07	0.36	-3.66	-3.75	-3.37
	JJA	15.54	13.02	13.33	11.81	10.36	10.64	7.83	7.68	7.93
	SON	8.86	7.87	8.49	4.92	4.52	5.18	0.94	1.15	1.79
Houston	DJF	10.94	11.51	11.92	6.25	6.27	6.8	1.58	1.15	1.74
	MAM	18.25	19.65	19.75	15.64	15.9	16.02	12.47	11.79	11.93
	JJA	23.54	22.41	22.45	22.01	19.76	19.83	20.1	15.84	15.94
	SON	18.57	18.22	18.47	15.59	14.17	14.44	12.25	9.89	10.27

For Phoenix, increase in daily maximum and mean T_{d2} is about 1.2, 0.4, 0.3, and 0.6 ^{o}C for winter (DJF), spring (MAM), summer (JJA), and fall (SON), respectively. With respect to daily minimum T_{d2}, the improvement is less clear. Improvement is observed in winter while degradation is reported for fall. In Houston, the impact of urban

hydrological processes is weak due to the presence of sea-land breezes. During spring

and summer when temperature difference is distinct between the land and sea surface,

strong onshore flow makes the effect of urban hydrological processes negligible. For fall

and winter, average daily maximum, mean and minimum T_{d2} is increased by about 0.6

and 0.3 °C, respectively.

4.4. Regional Hydroclimatic Effect of Green Roofs

On the basis of the demonstrated skill of the modelling system in capturing the

urban meteorological field, we conducted simulations to investigate the regional effect of

green roofs for both Phoenix and Houston. Our hypothetical scenario assumes that all

rooftops of the two cities are replaced by green roofs, with results indicating the

maximum possible effect. Here we select short grasses for green roof vegetation type

with a 0.3-m deep loam soil layer. Sensitivity of green roof performance to parameters

related to soil and vegetation type is referred to the previous study (Yang and Wang

2014a).

Figure 4.4 shows the seasonal variability of impacts of green roofs on land surface

temperature T_s at 1400 LT for Phoenix. We present the result at 1400 LT as subsequent

analysis find the time corresponds to diurnal maximum effect (see Fig. 4.13). From Fig.

4.4 it is clear that green roofs can reduce T_s of the urban area by more than 4 °C

throughout the year (please refer to Fig. 4.1c for the urban area in Phoenix). Compared to

other seasons, fall (SON) has the smallest reduction in T_s, primarily due to the extensive

amount of precipitation simulated in this season. Simulated accumulated precipitation

depth for spring, summer, fall, and winter is about 47.9, 59.4, 100.5, and 4.8 mm,

77

respectively. Seasonal variation of precipitation in green roof case is similar to that of control case (see Table 4.4). Compared to in-situ measurements, model prediction underestimates precipitation in summer and overestimates it in fall for Phoenix. The deviation in precipitation pattern can be caused by various physical parametrizations, such as microphysics, planetary boundary layer, and cumulus schemes. Closing the gap between simulated and observed precipitation requires a thorough sensitivity analysis in the future and is beyond the scope of this study.

Figure 4.4. Simulated impact of green roofs on land surface temperature at 1400 LT for Phoenix during (a) winter, (b) spring, (c) summer, and (d) fall.

78

Table 4.4. Summary of observed and simulated precipitation (mm) for different seasons. Obs is short for observation, New and GR denote simulation results using the new SLUCM with and without green roofs, respectively.

City	Precipitation	Obs	New	GR		Precipitation	Obs	New	GR
	DJF	1.6	4.8	4.8		DJF	185.7	134.5	132.8
	MAM	39.7	47.9	46.5		MAM	141.2	172.7	165.3
Phoenix					Houston				
	JJA	82.3	59.4	55.6		JJA	307.6	205.3	202.7
	SON	79.4	100.5	99.0		SON	365.5	301.6	268.7

Chapter 2 suggested a green roof cooling of Phoenix metropolitan area by about 8 °C at 1400 LT in summer. This significant difference between offline and online simulation results indicates that feedback between the atmospheric system and land surface has notable influences on the performance of green roofs. Results in this Chapter, derived from the fully coupled WRF-urban modelling system, are more representative of actual effects. To demonstrate impacts during nighttime hours, results at 0200 LT are shown in Fig. 4.5.

Figure 4.5. Simulated impact of green roofs on land surface temperature at 0200 LT for Phoenix during (a) winter, (b) spring, (c) summer, and (d) fall.

With additional soil layers on top of buildings, green roofs are able to store extra solar energy during daytime as compared to conventional roofs. The energy is released and causes a considerable warming effect at night. Figure 4.5 demonstrates that increase in T_s is about 1 - 2 ℃ from spring to fall and is less than 1 ℃ in winter. The magnitude of nighttime warming is much smaller than that of daytime cooling by green roofs for Phoenix. These results are consistent with recent high-resolution simulations for urbanizing regions in California, which similarly indicated an increased nighttime

warming tendency for green roofs deployment that was considerably smaller in

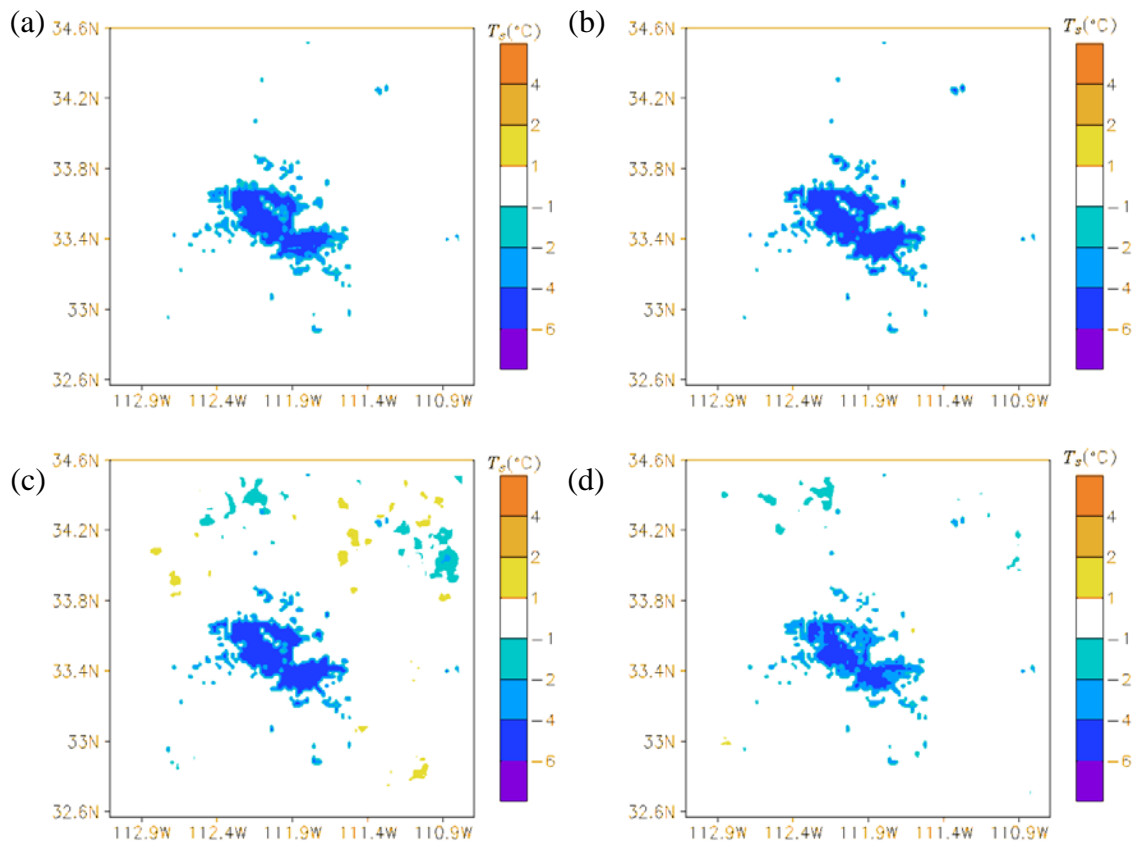magnitude relative to daytime cooling (Georgescu 2015).

Figure 4.6. Simulated impact of green roofs on land surface temperature at 1400 LT for

Houston during (a) winter, (b) spring, (c) summer, and (d) fall.

Cooling effect of green roofs on T_s at 1400 LT for Houston is shown in Fig. 4.6

(please refer to Fig. 4.1d). Compared to Phoenix, temperature reduction in fall and winter

for Houston is much lower. Evaporative cooling of green roofs is mainly controlled by

two factors: available energy and availability of water at the surface. As precipitation for

Houston is abundant throughout the year, evapotranspiration arising from green roofs is

largely determined by the available solar radiation. Houston is known to have a much

cloudier weather and thus less total available solar radiation than the desert city Phoenix. In winter, when the sun angle is lower, solar radiation intensity decreases significantly and green roofs become relatively less effective. Precipitation also plays a role in determining the cooling effect. During the simulation period, Houston receives nearly double the amount of rainfall in fall as compared to spring (see Table 4.4), which indicates less clear days on average, leading to ineffectiveness of green roofs.

Figure 4.7. Simulated impact of green roofs on 2-m air temperature at 1400 LT for Phoenix during (a) winter, (b) spring, (c) summer, and (d) fall.

Difference in simulated 2-m air temperature between 0% and 100% green roof fraction cases at 1400 LT for Phoenix is shown in Fig. 4.7. Opposite to the trend of

surface temperature, it is found that the strongest cooling effect on T_2 of more than 1.2 ℃ occurs in winter, while the smallest reduction is less than 0.8 ℃ in summer. A reason for this phenomenon is that non-linear relation exists between surface temperature and 2-m air temperature. When green roofs reduce T_s, buoyancy effect is also reduced such that the reduction of T_2 is smaller than the reduction of T_s.
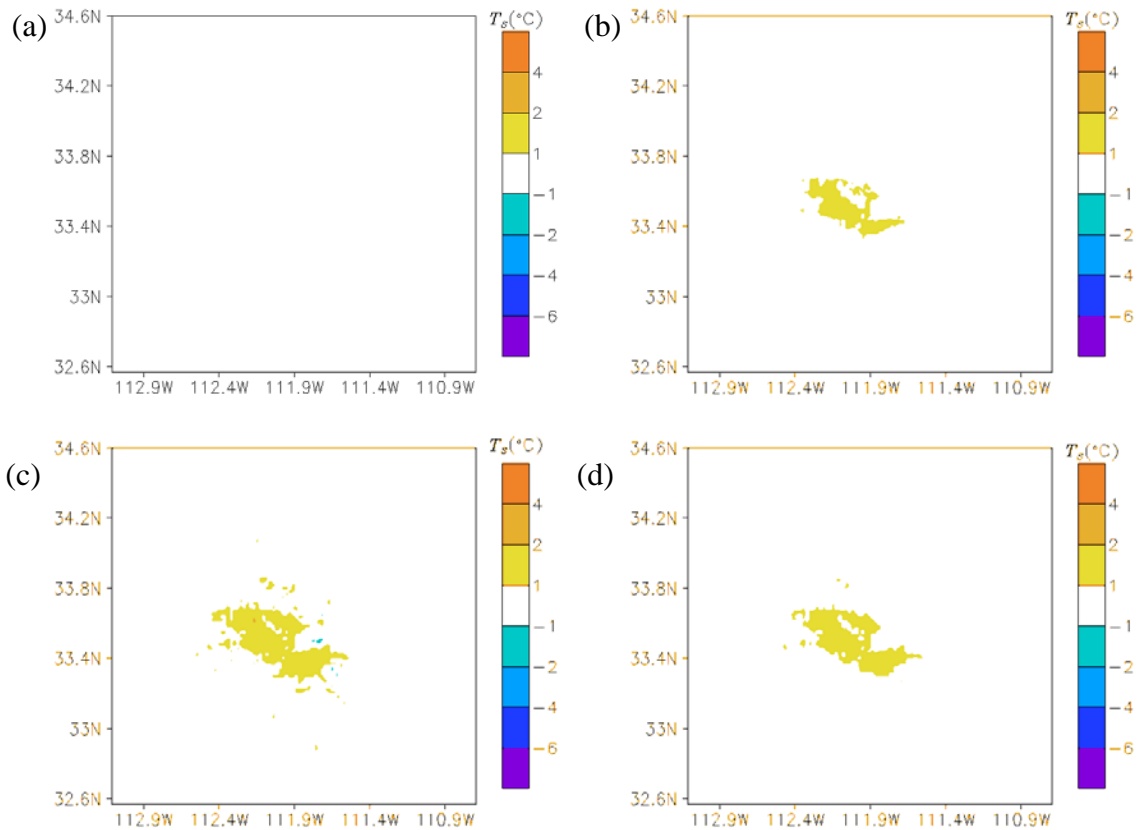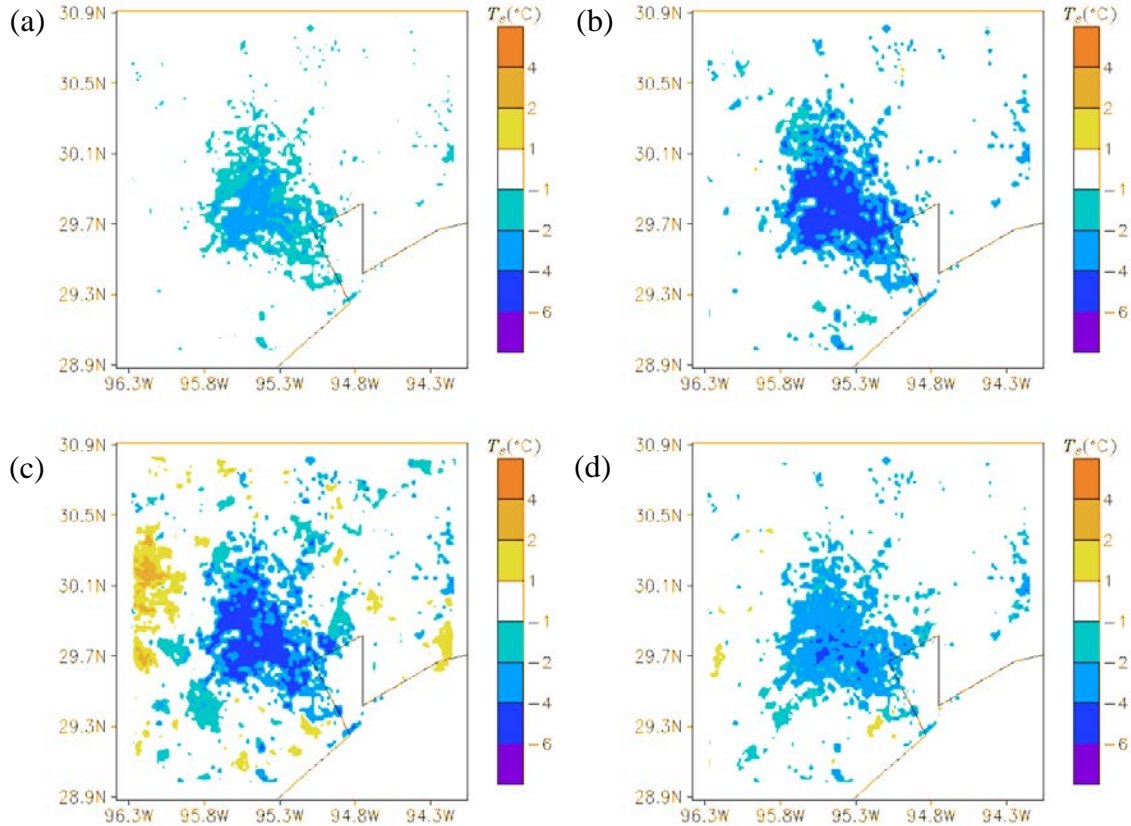

Figure 4.8. Simulated impact of green roofs on 2-m air temperature at 0200 LT for Phoenix during (a) winter, (b) spring, (c) summer, and (d) fall.

Another critical factor contributing to the phenomenon is the warming effect caused by green roofs at night, as demonstrated in Fig. 4.8. Compared to winter, the urban land

surface in summer receives a considerably enhanced solar radiative flux, which is stored

via large thermal mass of manmade structures, and is subsequently released at night. In

the absence of incoming solar radiation, vertical mixing over urban terrain in nighttime is

weak that evolution of air temperature is steady (Poulos et al. 2002). As a consequence,

increase in T_2 by heat released from green roofs dissipates slowly until sunrise when

surface heating modifies the stability condition of the boundary layer. Figure 4.8 clearly

illustrates that increase in T_2 in summer is more significant than that in winter, in terms of

both the influence area and the magnitude. This nighttime warming impedes cooling of

air temperature in daytime, and results in the stronger cooling of T_2 in winter as compared

to summer.

Figure 4.9 demonstrates the regional effect of green roofs on T_2 at 1400 LT for

Houston. It is noteworthy that unlike in Phoenix, the order of reduction in T_2 among

different seasons generally follows that of T_s for Houston. This is primarily due to the

negligible nighttime warming of air temperature in Houston throughout the year (results

not shown here). In a coastal area, different surface cooling over land and sea results in a

temperature gap in overlying air layers and consequently leads to nighttime advection of

marine air. Simulated 10-m wind speed at 2100 LT (sunset around 2000 LT) for Houston
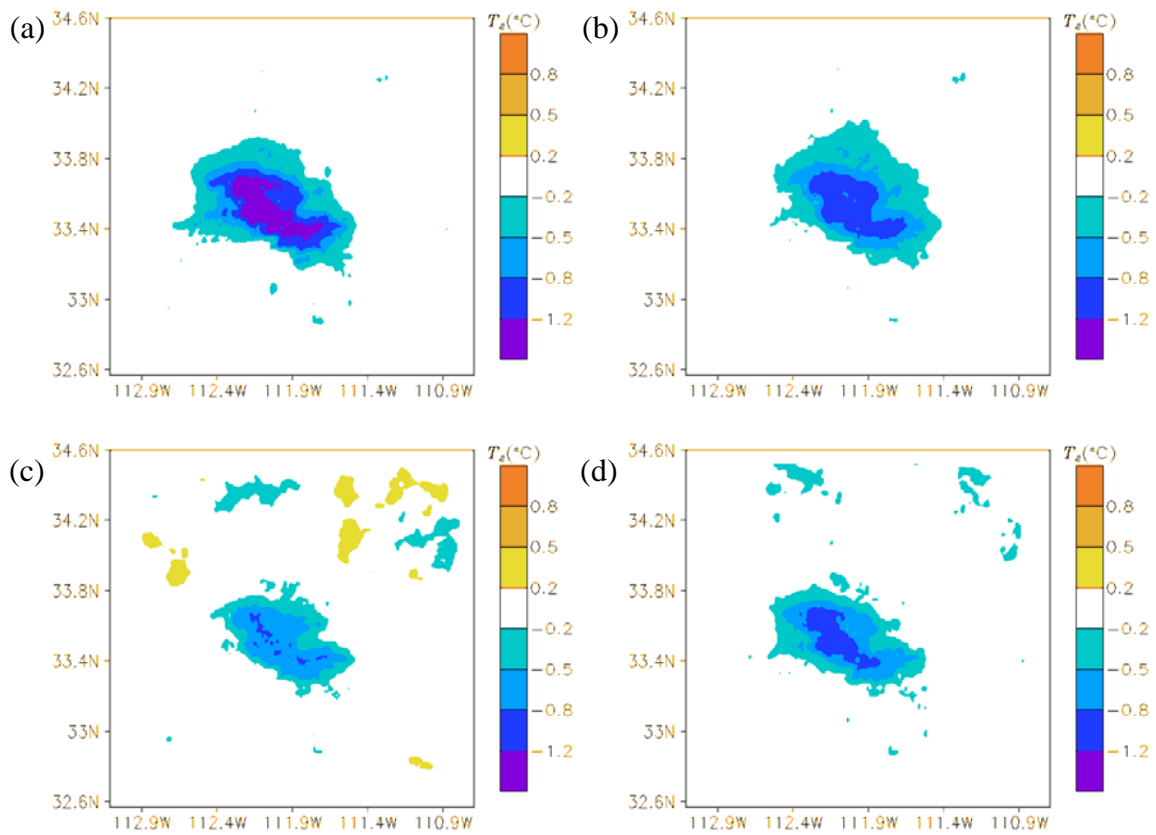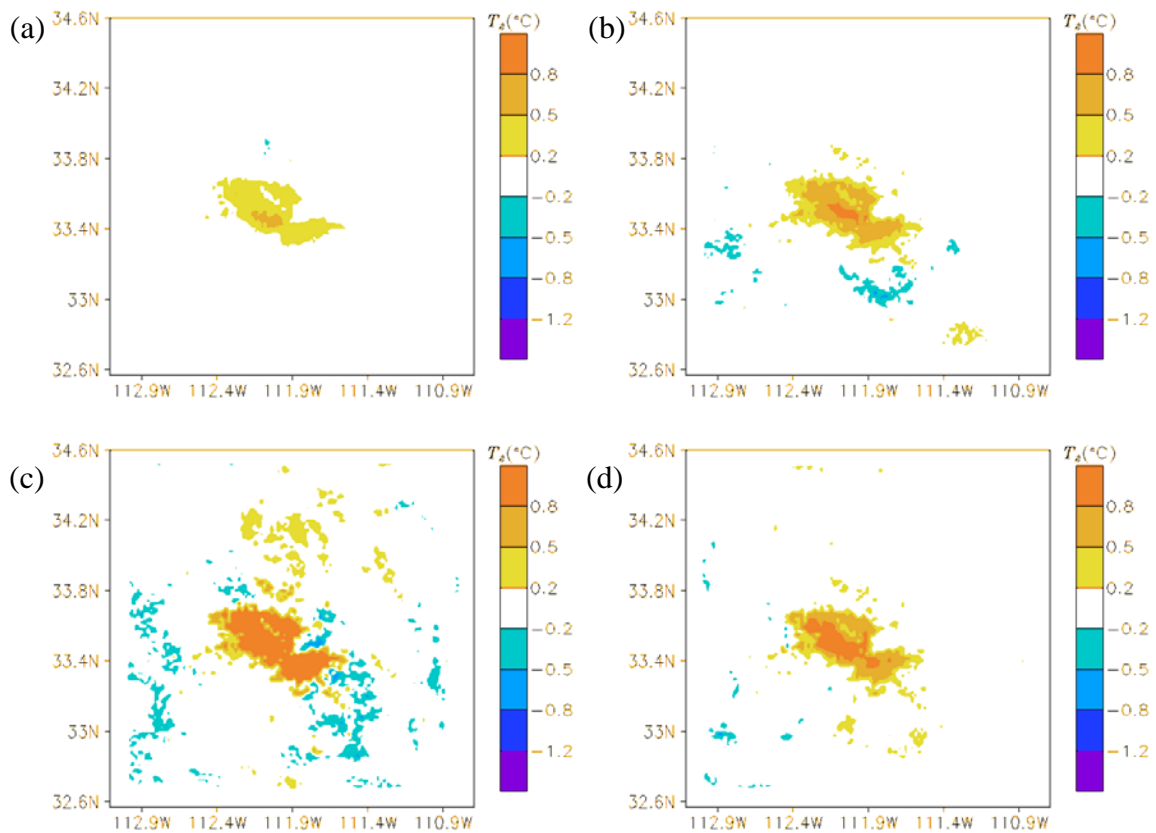
during summer is presented in Fig. 4.10.

Figure 4.9. Simulated impact of green roofs on 2-m air temperature at 1400 LT for Houston during (a) winter, (b) spring, (c) summer, and (d) fall.
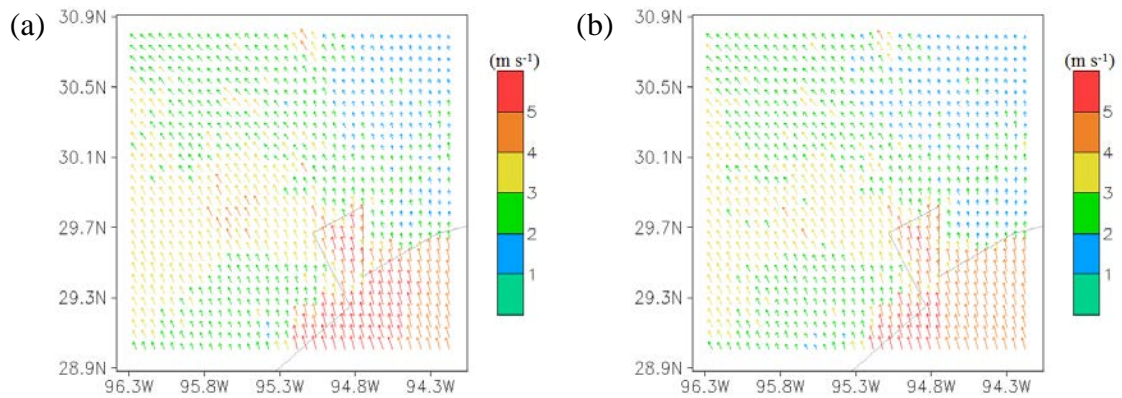
Figure 4.10. Simulated 10-m wind speed at 2100 LT for Houston during summer: (a) control case without green roofs, and (b) green roof case.

Advection of marine air towards the land tends to reduce T_2 over sea and increase T_2 over land. As illustrated in Fig. 4.8, green roofs tend to increase T_2 over urban areas at night. The increase in T_2 narrows the gap in air temperatures over land and sea. As a consequence, nighttime advection of marine air is slowed down, which in turn offsets the warming effect on T_2 over urban areas. Figure 4.10 shows that green roofs decrease 10-m wind speed by about 1 m s^{-1} in the bay area. The combined effect of green roofs on nocturnal T_2 is therefore insignificant. With an insignificant nighttime warming, daytime cooling of T_2 follows the trend of reduction in T_s. Reduction in T_2 at 1400 LT for Houston is less than 0.8 ºC in winter, and can be up to more than 1.2 ºC in summer. It is worth mentioning that cooling effect on T_2 has a larger spatial coverage in Houston due to the existence of land-sea circulation, especially in spring and summer when there is a considerable gap between land and sea surface temperature.

Impact of green roofs on 2-m dewpoint temperature for Phoenix at 1400 LT is shown in Fig. 4.11. Through evaporative cooling, green roofs are able to increase moisture and decrease temperature of near-surface air layer, thus leading to a substantial rise in T_{d2} for the entire simulation period. Sunwoo et al. (2006a, b) suggested that to avoid dryness of the eyes and skin, relative humidity should be maintained at greater than 30%. Therefore increased air humidity can enhance the thermal comfort of pedestrians in a dry environment, such as the pre-monsoon season in Phoenix (relative humidity ≈ 12%). However, extra moisture in the monsoon season can aggravate the thermal discomfort of residents, as illustrated in the analysis on urban irrigation in Chapter 3. This two-sided effect of green roofs needs special attentions, especially in humid regions like Houston.

86
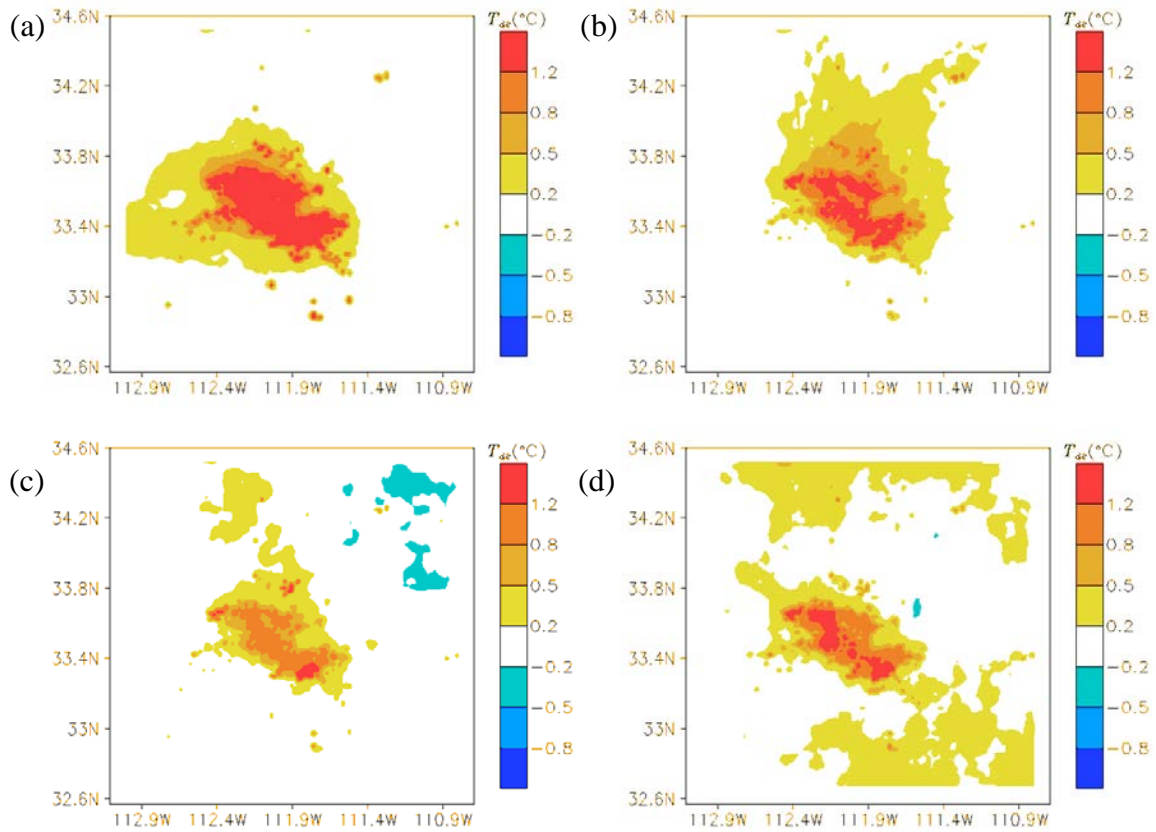
Figure 4.11. Simulated impact of green roofs on 2-m dewpoint temperature at 1400 LT for Phoenix during (a) winter, (b) spring, (c) summer, and (d) fall.

Figure 4.11 demonstrates that increase of T_{d2} can be up to more than 1.2 ^{o}C across the year. It is easy to recognize that seasonal variation of increase in T_{d2} is similar to that of decrease in T_2 for Phoenix, due to the non-linear relationship between saturated vapour pressure with air temperature. According to the Clausius-Clapeyron equation, a same amount of increase in absolute humidity of air will cause a larger increase of dewpoint temperature at a lower air temperature. At night, evapotranspiration rate becomes much slower as the driving force (solar radiation) disappears, influence of green roofs on T_{d2} thus become insignificant (results not shown here). Figure 4.12 presents the results at

1400 LT for Houston. The relation between green roofs' effects on T_{d2} and T_2 is consistent in both cities.
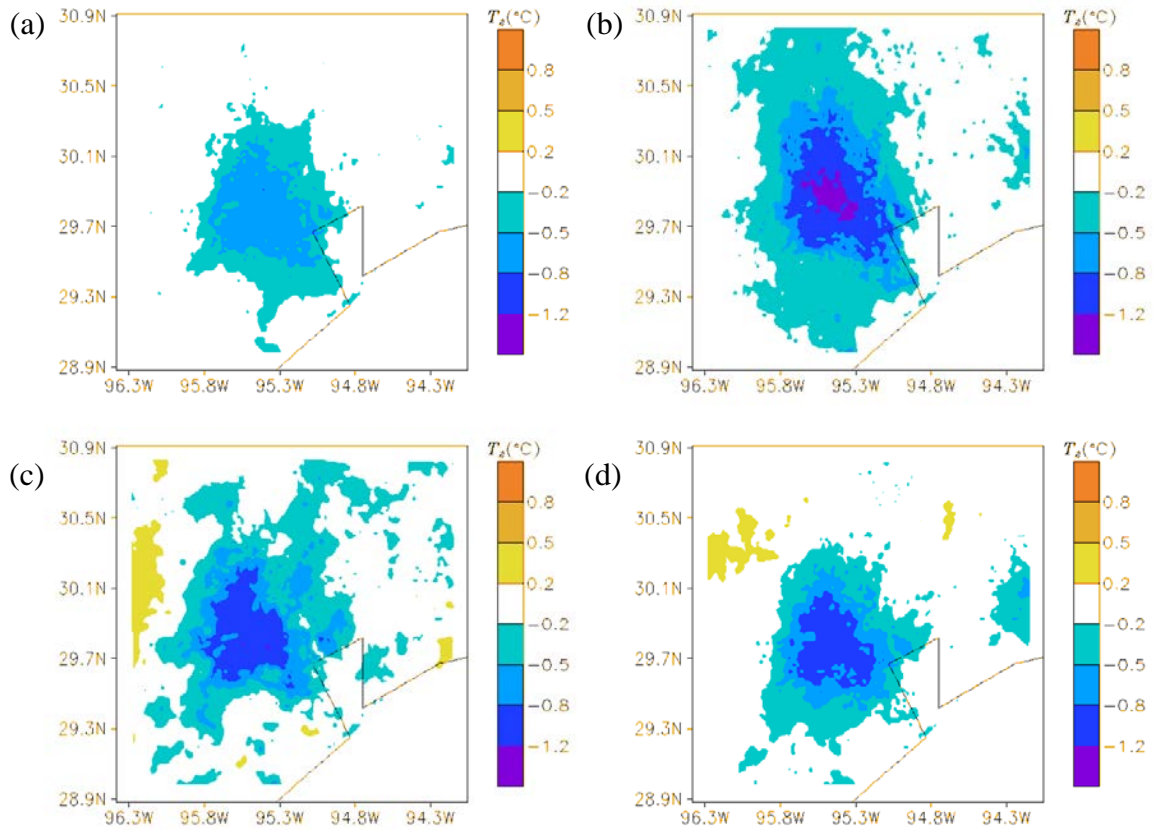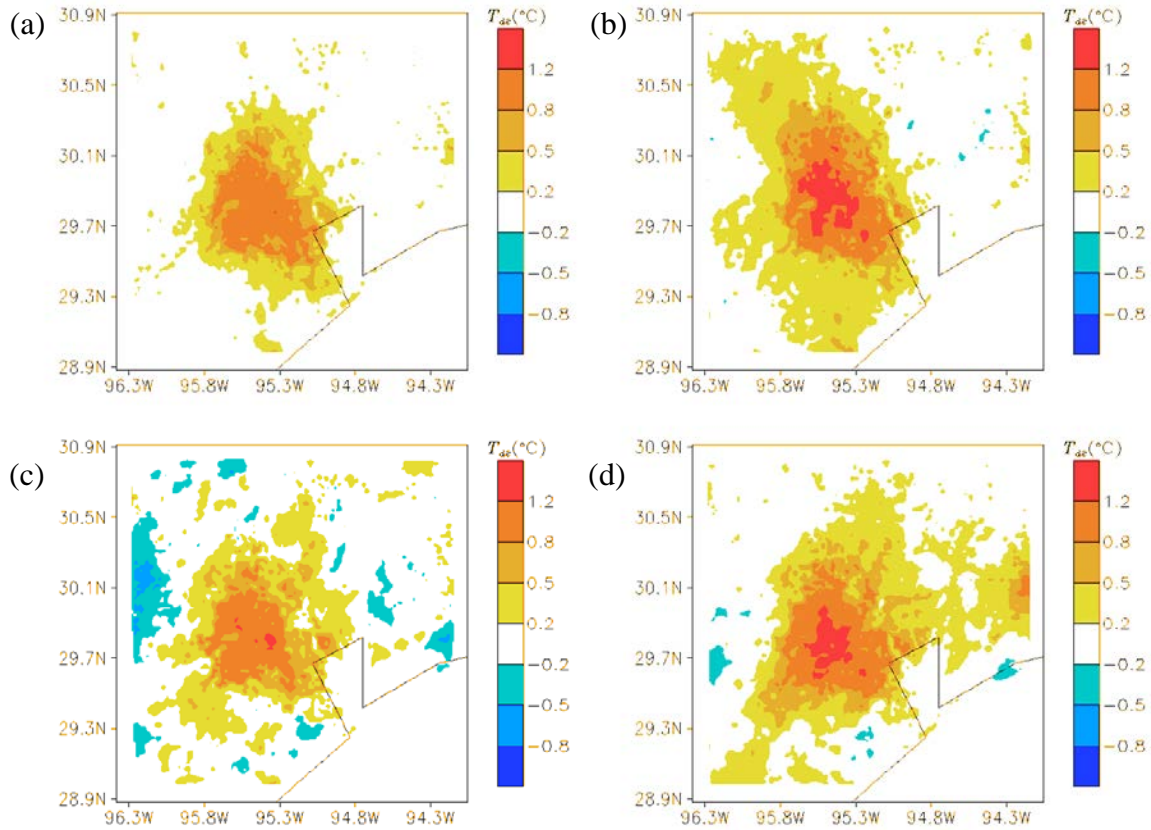

Figure 4.12. Simulated impact of green roofs on 2-m dewpoint temperature at 1400 LT for Houston during (a) winter, (b) spring, (c) summer, and (d) fall.

Besides spatial variation, temporal variation of the impact of green roofs is investigated. Realizing the maximum and minimum effects of green roofs in a temporal cycle has important implications for urban planning. In fact, the time at which spatial effect of green roofs was presented (e.g., 1400 and 0200 LT in above context) is selected based on diurnal results in Fig. 4.13.

Figure 4.13. Diurnal variation of average impact of green roofs on (a) LE, (b) T_s, (c) T_2, and (d) T_{d2} over the entire Phoenix metropolitan area.

Figure 4.13 demonstrates the diurnal impact of green roofs averaged over the entire Phoenix urban area. As expected, latent heat flux (LE) from green roofs increases with intensity of solar radiation at the surface that the largest increment of more than 70 W m^{-2} is found in summer. Additionally, daytime sunshine duration controls the effective period of green roofs. It is indicated from Fig. 4.13a that green roofs function about 4 hours more in summer than in winter.

While increase in LE is the largest in summer, it does not necessarily lead to the greatest reduction in T_s. As shown in Fig. 4.13b, the strongest cooling of the urban land surface by green roofs occurs in spring instead of summer, owing to the monsoon period from July to September in Arizona. The extensive amount of precipitation in fall also results in a smaller reduction of T_s than that in winter. With respect to the nighttime warming, increase of T_s by green roofs from the largest to the smallest is summer, fall, spring, and winter. The order is the same for increase in nighttime T_2. Average increment of nighttime T_2 is about $1.1\,^{\circ}C$ in summer and about $0.3\,^{\circ}C$ in winter. As aforementioned, the difference in nighttime warming has implications for daytime cooling process. Consequently, the largest reduction of daytime T_2 and the largest increase of T_{d2} by green roofs occur in winter. From December 2015 to February 2016, Phoenix was in an abnormally dry condition. Evapotranspiration from green roofs is low under the circumstance that a few rainfall events in this period cause large variations in latent heat flux, which lead to the spike in Fig. 4.13d.

Average impact of green roofs on studied variables for Houston is qualitatively similar to that for Phoenix; however, seasonal variation of the impact differs considerably. With sufficient supply of water from precipitation, effectiveness of green roofs in Houston largely depends on duration and strength of incoming solar radiation. Figure 4.14a shows that increased LE by green roofs can be up to more than 130 W m^{-2} in spring and summer, which is remarkably larger than the increase of about 80 W m^{-2} in fall. With respect to T_s, Fig. 4.14b demonstrates that daytime cooling effect is the strongest in summer and the weakest in winter, while nighttime warming is almost negligible. Diurnal impact of green roofs on T_2 across various seasons is similar to that on T_s. Peak cooling

effect is found to be about 1 °C in spring and summer. As land-sea circulation mixes the air layer of coastal area, increased T_{d2} by green roofs has a relatively limited seasonal variation.
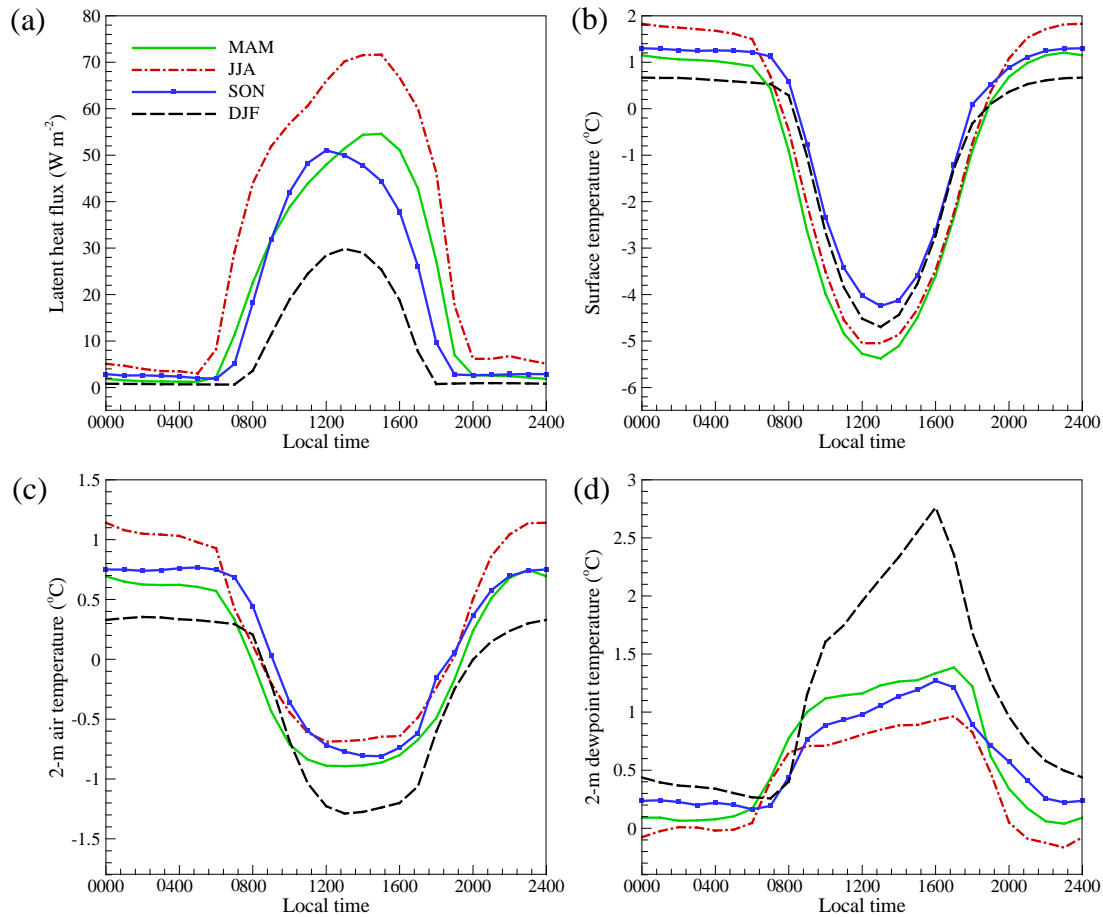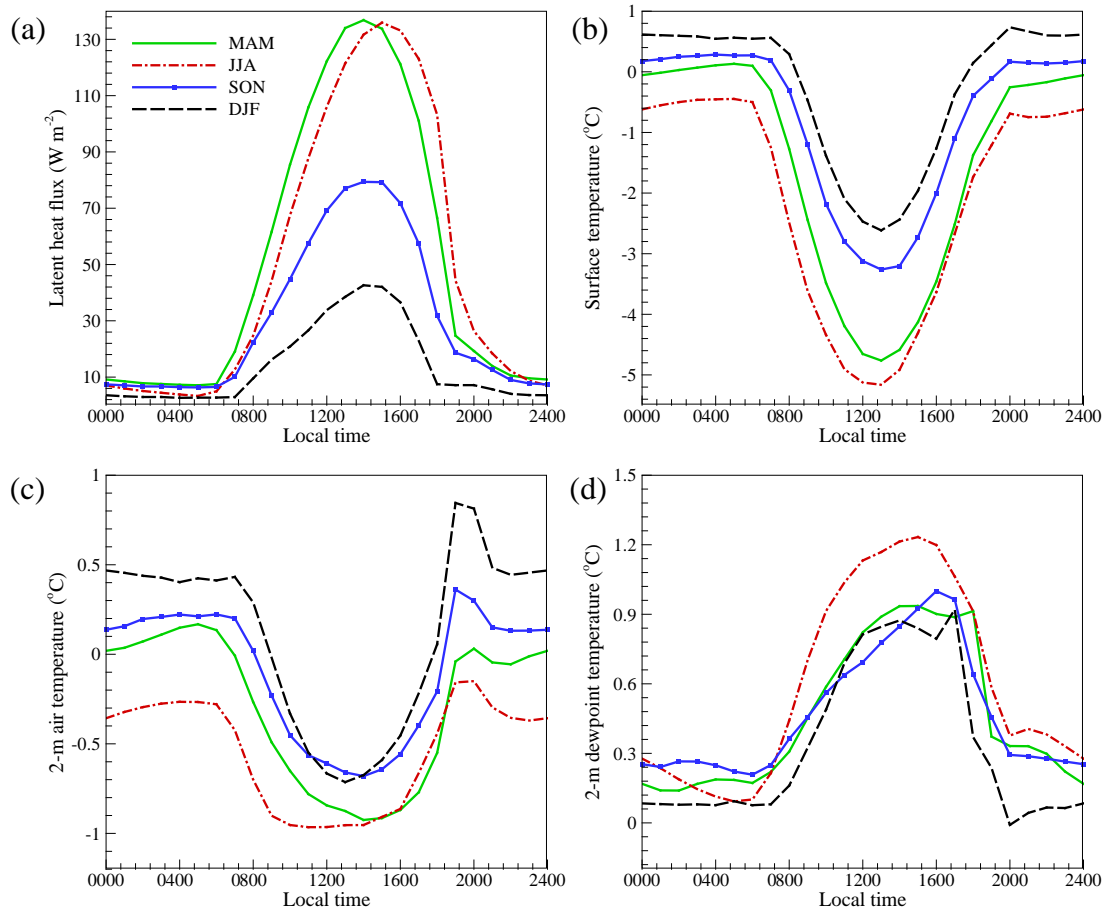

Figure 4.14. Diurnal variation of average impact of green roofs on (a) LE, (b) T_s, (c) T_2, and (d) T_{d2} over the entire Houston metropolitan area.

4.5. Summary

In this Chapter, we applied the WRF modelling framework with the enhanced single layer urban canopy model developed in Chapter 2 to assess the effect of hydrological

processes on urban meteorology. Evaluation against field measurements illustrates that including hydrological processes can improve prediction of the 2-m dewpoint temperature. Based on the tested simulations, regional impact of green roofs is investigated at the annual scale for Phoenix and Houston. Model results demonstrate that green roofs are effective in reducing daytime air temperature and increasing dewpoint temperature over urban areas. The effect of green roofs shows strong diurnal and seasonal variations, and varies with geographical and climatic conditions. It is noteworthy that urban vegetation is largely represented by short grasses in the WRF-urban modelling system, whereas physical resolution of more diverse urban vegetation types, e.g. shade trees, and their hydrometeorological effect, such as on radiative energy exchange, remains an open challenge (Wang 2014b).

Comparing results from this Chapter and Chapter 2, it is indicated that land-atmosphere interactions cannot be ignored in quantifying the influence of surface hydrological process. In coastal area, land-sea circulation mixes the near-surface air layer that effect of hydrological processes on meteorological field is weaker compared to that of inland area. To accurately evaluate sustainable adaptation/mitigation strategies for urban area, numerical experiments should be carried out with a fully interacting land-atmosphere modelling system. Modification of urban landscape has implications for hydrometeorology of surrounding rural areas, which requires serious consideration and planning before implementation.

CHAPTER 5 POTENTIAL WATER BUFFERING CAPACITY OF URBAN GREEN INFRASTRUCTURE

5.1. Introduction

Previous Chapters demonstrate that urban green infrastructure provides valuable benefits for the built environment via evaporative cooling and reducing the urban heat island. Yet, the watering demand of green infrastructure raises practical concerns of the water resource management, especially for cities located in the semiarid or arid environment. Under the potential, to certain extent actualizing, challenges of the global climate changes, water scarcity is becoming a widespread reality for global cities with rapid population growths (Vörösmarty et al. 2000). Chapter 3 investigates the intricate balance of water-energy nexus when using outdoor irrigation to cool the desert city Phoenix. Nevertheless, the trade-off between water and energy resources is only one of many aspects in the convoluted activities of an urban system that water pervades (see Fig. 5.1). Efficient management of water is an integral component as well as a critical challenge of multisector sustainability for cities (Brown et al. 2009). While increasing studies demonstrate the effectiveness of green infrastructure in cooling urban environments (Shashua-Bar and Hoffman 2000, Oberndorfer et al. 2007), only a handful of them have looked into its impact on urban water resources in detail (Gober et al. 2012, Yang and Wang 2015).

The populous desert metropolitan area of Phoenix, Arizona is studied in this Chapter mainly due to: (1) land use conversion in the past decades has created a significant UHI in this region (Wang et al. 2016), and (2) typical landscape management practices in the study area, ranging from oasis to desert landscaping, impose vastly different requirement

for outdoor irrigation of green infrastructure (Brazel et al. 2000). In the 21st century, high

temperature, low precipitation, and decreased runoff result in increased aridity of the

southwest United States (MacDonald 2010). On the other hand, Arizona's Sun Corridor

is the fastest growing megapolitan area, anchored by the Phoenix and Tucson

metropolitan areas at its geographical termini (Grimm et al. 2008). Even without

reductions in river flows caused by climate change, political decisions and actions are

imperative for water sustainability of Phoenix in 2030 (Gober and Kirkwood 2010).
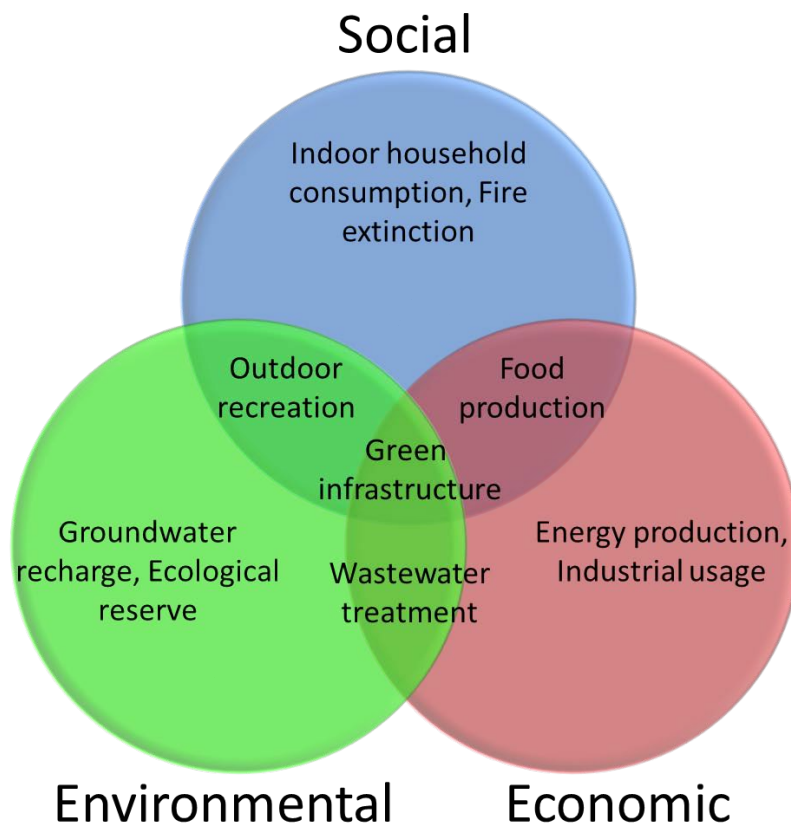
Figure 5.1. A schematic for water consuming activities in the complex urban network.

Recognizing that a more native desert landscaping facilitates amelioration of water shortage, the city of Mesa offers financial incentives for xeriscaping homeowners (City of Mesa, 2013). On the other hand, though the widespread adoption of water-intensive mesic landscape has adverse impacts on the long-term water sustainability, it enhances the thermal comfort in the built environment over all spatial and temporal scales (Chow and Brazel 2012). The city of Phoenix has initialized a Tree and Shade master plan to achieve a tree canopy cover of 25% by 2030 (City of Phoenix, 2010). In the context of water-energy-climate repercussions, the tradeoff between water conservation and UHI mitigation inevitably exerts profound impacts on multisector components in the urban network. Assessment of the water usage associated with urban green infrastructure is thus of crucial importance for the water resource management as well as the sustainable development of the Phoenix metropolitan area.

Towards this end, in this Chapter we used the integrated WRF-UCM modelling system, with a realistic representation of urban hydrological processes, to access the water usage of urban green infrastructure in the Phoenix metropolitan area. Our objective here is to quantify the potential water buffering capacity, i.e. the possible range of variability in the water resource demand, of urban green infrastructure in arid environments and its implication to sustainable urban development.

5.2. Numerical Experiment Design

The same experimental setup used in Chapter 4 (see Fig. 4.1a) was adopted here. With the WRF-UCM modelling system, three scenarios are simulated in this Chapter: (1) the control case: mixed ground infrastructure (cropland/natural vegetation mosaic)

95

representing the current urban practice of landscape management with daily irrigation in the Phoenix metropolitan area; (2) the hypothetic water-saving scenario, i.e. all xeriscaping (open shrubland) with no irrigation; and (3) the fully-greening scenario with 100% coverage of green roofs (short-grass) and mesic landscaping (grassland), both irrigated daily. Following the setup in Chapter 4, irrigation is scheduled at night and the daily amount is equal to an increase in moisture of a 0.4 m thick soil layer to a threshold value where transpiration will not be limited by the water availability. Areal fraction of green infrastructure varies with urban land use categories, whose parameters are summarized in Table 5.1.

Table 5.1. Summary of canopy parameters in different urban land use categories.

Canopy parameters	Unit	High-density	Medium-density	Low-density
h (building height)	m	17.0	7.5	5.0
l_{roof} (roof width)	m	10.0	9.4	8.3
l_{road} (road width)	m	10.0	9.4	8.3
f_{urb} (urban fraction)	-	0.95	0.85	0.70
α (albedo of building materials)	-	0.16	0.18	0.18
k (thermal conductivity of building materials)	$W\ m^{-1}\ K^{-1}$	1.8	1.3	1.3
C (heat capacity of building materials)	$MJ\ m^{-3}\ K^{-1}$	2.8	2.1	2.1
ε (emissivity of building materials)	-	0.90	0.90	0.90
Anthropogenic heat	$W\ m^{-2}$	35	30	20

Simulated water consumption for outdoor irrigation and corresponding

hydroclimatic condition related to individual green infrastructure scenarios are expected

to be highly informative for analysts in urban planning by answering fundamental

questions, such as 'What is the potential (maximum possible) degree of cooling by fully-

greening Phoenix and at what price (of water usage)?'.

5.3. Regional Climate Modelling

Capacity of the WRF-UCM model in reproducing the hydroclimate of the study area

is evaluated against field measurements obtained by ground-based stations in Chapter 4.

Thus we are confident to apply the model to investigate hydroclimatic consequences of

hypothesized urban green infrastructure scenarios. Simulations were conducted for

summertime (June, July and August) when frequent irrigation is conducted to compensate

heat-induced rapid moisture loss. A summer of normal climatic condition, year 2012, is

studied to obtain general findings applicable for other years.

5.3.1 Hydroclimatic impacts

With different irrigation schedules and green infrastructure types, the two simulated

hypothetic scenarios exhibit distinct hydroclimatic responses in the study area. Compared

to the control case, the fully-greening scenario with ample irrigation promotes

evaporative cooling during daytime (Fig. 5.2a), leading to significant alleviation of urban

thermal stress. The mean daily maximum cooling of the 2-m air temperature (T_2) and

increase of the 2-m dewpoint temperature (T_{d2}) is about 1.4 and 2.9 $^{\circ}$C respectively. The

reduction in air temperature, as demonstrated in Chapter 3, has promising implications for building energy consumption, and a meticulous life cycle analysis of the water-energy nexus is capable of determining an optimal urban irrigation scheme. The nocturnal cooling of air temperature, in comparison, is considerably lower than the daytime counterpart, as the energy source for evapotranspiration diminishes.

On the other hand, Figure 5.2b shows that the self-supportive xeriscaping infrastructure with no irrigation leads to consistently higher T_2 and lower T_{d2} in a water-saving city. It is noteworthy that simulated mean daytime maximum temperature of 2012 summer is about 39.6 ℃, where the additional warming of about 1 ℃ by xeriscaping is critical for heat-related morbidity and mortality (Golden et al. 2008), especially for low-income citizens without access to air conditioning systems. Throughout the mean diurnal cycle, the potential warming induced by the hypothetic xeriscaping scenario is close to the potential cooling by irrigated mesic green infrastructure. This indicates that the existing urban green infrastructure and irrigation schemes play a crucial role in regulating the current hydroclimate of the Phoenix metropolitan area. To further improve the thermal environment, if the coverage of green infrastructure at the ground level is not increased, deployment of green roofs will require extensive engineering and maintenance efforts.
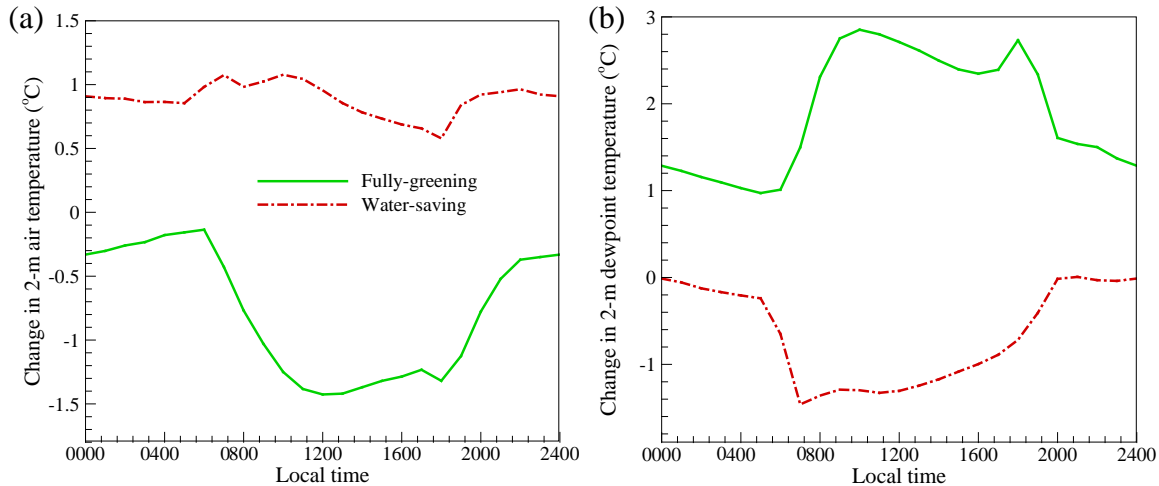
Figure 5.2. Simulated difference in (a) T_2, and (b) T_{d2} between study cases and the control case averaged over the Phoenix metropolitan area during the 2012 summer.

5.3.2 Potential water buffering capacity

The potential water buffering capacity of urban green infrastructure is estimated as the difference of water usage between the water-saving (xeriscaping) and the fully-greening scenarios. Despite the variation of urban morphology, the potential water buffering capacity per unit area is relatively constant over the study area, mainly due to the substantial water consumption related to the green infrastructure on the roof level. To completely replace the xeric landscapes by the mesic/oasis ones, together with the deployment of green roofs, it consumes about 240 mm depth of outdoor irrigation per unit area in the summer (Fig. 5.3a). Summing over the entire Phoenix metropolitan area, this demand of outdoor irrigation amounts to $4.24 \times 10^8 \, \mathrm{m}^3$ of water (Table 5.2). Most of the irrigated water is converted to air humidity via evapotranspiration (Fig. 5.3b) and creates cooling benefits for the built environment. The variability between the xeric and mesic green infrastructure leads to markedly different hydroclimatic patterns in the desert

99

city (Table 5.2). The simulated maximum difference is observed at the metropolitan

center, covering Tempe, Mesa, Glendale, and a large portion of the city of Phoenix.
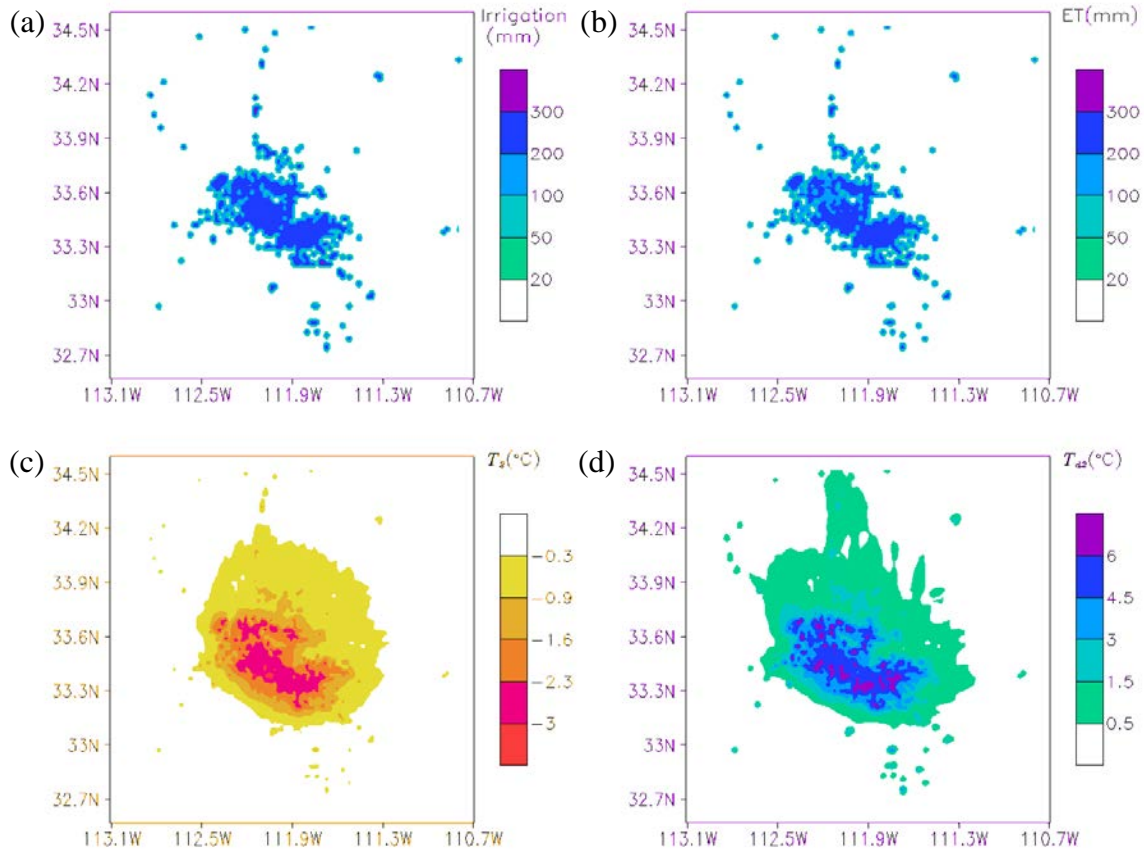
Figure 5.3. Spatial variation of simulated difference in (a) total irrigation depth, (b)

cumulative evapotranspiration, (c) daytime mean T_2, and (d) daytime mean T_{d2} between

fully-greening and water-saving cases during the 2012 summer.

The maximum cooling of daytime mean T_2 and the warming of T_{d2} are about 3.1

(Fig. 5.3c) and 6.5 °C (Fig. 5.3d), respectively. This effect generally diminishes with the

distance away from the metropolitan center. Via the urban-rural air circulation, the

change of urban green infrastructure also alters the hydroclimate of surrounding rural areas. The prevailing wind generates a more evident difference in the northern and western outskirts of the Phoenix metropolitan. The spatial patterns provide a good demonstration of the potential variability of regional hydroclimatic responses to the landscape planning.

Table 5.2. Water usage and corresponding hydroclimatic condition of the Phoenix metropolitan area in different simulated scenarios.

Case name	Irrigation amount (m^3)	Cumulative ET (mm)	Daytime mean T_2 (^{o}C)	Daytime mean T_{d2} (^{o}C)
Control	1.61×10^8	84.2	34.45	9.51
Water-saving	0	12.6	35.42	8.90
Fully-greening	4.24×10^8	218.4	33.34	11.43

5.4. Implications to Water Resource Management

The water resource management in urban networks necessitates complex tradeoffs among social, economic, and environmental components (Fig. 5.1). Previous studies of urban green infrastructure have largely focused on unraveling the environmental-economic tradeoff (e.g., water vs. electricity consumption), leaving the implications to the environmental-social and socio-economic nexuses comparatively less explored. To illustrate the environmental-social tradeoff, here we quantify the water usage required by urban green infrastructure as equivalent to the population to be supported by the same amount of water. Estimated water required to support residential densities in the Phoenix is given by (Gober and Kirkwood 2010):

$$y = 155.2 \ln(x) + 842.38, \qquad\qquad (3.1)$$

where y is annual water use per person in m^3, and x is the density of persons per hectare.

An urban density of 37-74 housing per ha in Phoenix amounts to a mean annual

consumption of about 75 m^3 of water per person (Gober and Kirkwood 2010). The high

per capita water use is unexceptional as compared to many other low-density

Southwestern urban areas; and is representative for future urban development in the study

area. Under this circumstance, conserved water resource from xeriscaping infrastructure

is able to support the demand of 2.15 million new residents, which is about 82% of

projected population growth (2.62 million) by 2050 in the medium series (ADOA, 2015).

This number agrees well with previous findings (Gober and Kirkwood 2010) from a

water supply and demand model (WaterSim) that changes in lifestyle would allow the

region to avoid water shortage. In contrast, the excessive amount of irrigation water

required by fully-greening the city during summer is equal to the annual water

consumption of 3.51 million residents, which can fulfill the demand of emerging

population even in the projected high growth series (ADOA, 2015). Water users in the

Phoenix metropolitan area have relied heavily on groundwater, which supplies about 31%

of the water demand (0.85 billion m^3) in 2006 (ADWR, 2014). Future modification on

green infrastructure will also have substantial influence on the continuous overdraft

groundwater resource projected through 2025 (ADWR, 2014).

5.5. Summary

   Despite the inherent uncertainties associated with the modelling approach, the

analysis in this Chapter quantifies the potential water buffering capacity of urban green

infrastructure in the Phoenix metropolitan area and its hydroclimatic and social

implications. Such information is crucial for the long-term water sustainability under the

challenge of future climate change and population growth. The adoption of complete

xeriscaping land use significantly reduces the vulnerability of water shortage induced by

the projected population growth in the region; notwithstanding the intensive summertime

urban thermal environment in the semiarid region will be further exacerbated. With the

potential water buffering capacity of urban green infrastructure in mind, the dilemma is

still left to be solved by decision makers by pondering how much the cost of water

resource need to be paid in order to sustain a cooler environment, or vice versa.

CHAPTER 6 CONCLUSIONS AND PERSPECTIVES

6.1. Conclusions and Recommendations

We presented in this dissertation a comprehensive effort focused on the implementation, evaluation, and application of hydrological processes and green infrastructure in the urban environment. The Weather Research and Forecasting (WRF) system coupled with the single layer urban canopy model, a numerical framework widely applied to major metropolitan regions worldwide, was used as the underlying numerical tool in this study. Recognizing the importance of the realistic representation of urban hydrological processes in accurately simulating urban hydroclimate, we incorporated the following processes into the WRF-Urban modelling system: (1) evaporation over engineered pavements, (2) urban irrigation, (3) anthropogenic heat, and (4) urban oasis effect. Comparisons against field measurements from multiple metropolitan areas showed that the enhanced model is more accurate in predicting urban hydroclimatic variables, especially those related to the water budget, in both offline and online experimental setup. Nevertheless, the presence of model-measurement deviation in specific cities, e.g. Vancouver in Chapter 2, calls for further development of hydrological processes such as snow/ice in the numerical tool.

The environmental performance of green roofs exhibits strong diurnal and seasonal variations, and is subject to change in geographical and climatic conditions. Through the combined evaporative cooling and insulation effect, installation of green roofs decreases daytime temperature and increases nighttime temperature in the urban areas. This leads to the effective reduction of both summer cooling demand and winter heating demand for buildings. Considerable differences found between offline results in Chapter 2 and online

simulations in Chapter 4 demonstrates the ineligible impact of the land-atmosphere interactions on quantifying the benefits of urban green infrastructure. Based on that, we therefore recommend future numerical studies on urban green infrastructure to be conducted in a fully interacting land-atmosphere system.

In Chapter 3, the environmental sustainability of a variety of uncontrolled and controlled urban irrigation schemes is investigated in terms of the combined monetary saving for the desert city of Phoenix. Among investigated irrigation schemes, the soil-temperature-controlled irrigation is the most efficient in reducing annual building energy consumption. It is found that the saving of cooling energy in this scheme outweighs the cost of water resources, but a careful analysis is required in order to yield the optimal net saving in terms of the trade-off between water and energy. It is noteworthy that water is a precious resource for semiarid environments that the water-energy nexus is only one aspect of the intricate relationship among various components in the urban network. Future development of cities is inevitably constrained by the limited availability of water resources, concomitant with emergent climate changes and continuous population and urban growths. Water conservation through xeriscaping allows the Phoenix metropolitan region to accommodate the water shortage caused by population growth, at a cost of exacerbated urban living environment.

Simulated water consumption and corresponding hydroclimatic condition related to individual green infrastructure scenario in this dissertation is highly informative for analysts in urban planning. We expected the results to provide useful guidance for green infrastructure over metropolitan areas with similar geographical and climatic conditions. Compared to another popular strategy of using reflective materials to mitigate UHI (Yang

et al. 2016b), it is found that green infrastructure has a smaller cooling impact in summer. Nevertheless, reflective materials tend to make winters colder and thus lead to potential heating penalties in terms of building energy consumption. Both strategies have unintended consequences, green infrastructure emits volatile organic compounds, while reflected radiation from reflective materials can impair outdoor thermal comfort in urban environments. It is therefore debatable that what the best UHI mitigation strategy is, and potential benefits of various solutions should be compared to come up with the optimum strategy for mitigating UHI for a specific city.

It is also noteworthy that the effect of all mitigation strategies, including green infrastructure and reflective materials, can change with the scale of its deployment (Yang et al. 2015b). Strategies applied on a single building will not exhibit same hydrothermal behavior as those on the entire city, and vice versa. For example, the placement of a single white roof could enhance local vertical mixing, increased surface temperature on building walls by bringing warm air from other roofs to the street level (Botham-Myint et al. 2015). When white roofs were deployed on all buildings, this phenomenon disappeared that temperatures on all urban facets were decreased. In terms of hydroclimate, large-scale deployment of green roofs reduces vertical mixing significantly, leading to reduction in boundary layer height. When green roofs are applied over a single building, this impact will not happen as the reduction of mixing is not strong enough to affect overall turbulent fluxes arising from the city. This apparent size effect necessitates the use of different experimental and numerical tools for characterizing and simulating mitigation strategies at different scales. Following findings in this study and applying a "one-size-fits-all" approach will likely result in undesired

consequences and lower-than-expected benefits for other urban regions and at other scales. Further experimentation should be prompted at a case-by-case basis to test the overall value of urban green infrastructure in sustaining development of study regions.

6.2. Future Work

This dissertation hitherto focused on short vegetation (e.g. grasses) at the ground and roof levels in the built environment. Shade trees and green walls constitute a considerable fraction of existing urban green infrastructure that physical resolution of their hydrometeorological effect in an integrated modelling framework is necessary in the future. Recent years have seen only a handful of urban canopy models that takes into account the presence of trees in urban canopies (Krayenhoff et al. 2014, Wang 2014a). The Monte Carlo method used in these studies works reasonably well in capturing the effect of trees on sky view factors between different surfaces in street canyons. Nevertheless, the evapotranspirative cooling and trees' ability to tap into deeper soil layers for water are largely ignored in existing models. Faithful implementation of urban tress into urban canopy models will allow applications to investigate the benefit of trees as an urban heat-island mitigation strategy. On the other hand, representation of green infrastructure in the current modeling framework can be further improved. For example, as plant grows and withers, dynamic of evapotranspiration varies vastly with the change in leaf areas and root water uptake (Peñuelas and Filella 2009). Such seasonal variation should be accounted for in the simulation of green infrastructure.

Thanks to the rapid development in computational capacity, online simulation applying coupled atmosphere-urban models over large domains at the annual scale

107

becomes feasible. However, uncertainty of simulation results in this dissertation is not adequately addressed after fulfilling the fine spatial resolution and long simulation period in experimental setup. The regional simulation using WRF-Urban system in this dissertation is constrained by accuracy of the initial and boundary conditions; errors in the input reanalysis data are propagated into the simulation results. Another concern is that the simulation in this dissertation relies on a single set of parameterizations. This raises questions regarding the reliability of drawing conclusions based on a single integration as different parameterizations vary vastly in model configuration and and no single scheme outperforms others under all conditions (Yang and Arritt 2002). Sensitivity of environmental performance of urban green infrastructure to initial and boundary conditions, and to physical parameterizations in the numerical model thus requires further examination. An ensemble approach can help reduce the uncertainty and provide a better quantitative estimation in future work.

Last but not least, urban green infrastructure features multi-scale ecological, economic and social benefits as compared to other mitigation strategies (e.g. reflective engineering materials) for UHI. For example, green infrastructure maintains the integrity of habitat systems and contributes to conservation of urban biological diversity (Tzoulas et al. 2007). Previous studies provided evidence of a positive relationship between citizens' longevity and green space (de Vries et al. 2003). Economic valuation has also identified that investment of green infrastructure benefits the region as a whole (Vandermeulen et al. 2011). Convoluted relations between social, economic, and environmental activities in the urban environment require urban planners and decision makers to balance issues of city development, environmental protection, and quality of

life. Existing studies usually focus on one of these issues that the dilemma on overall sustainability of cities is still left. The intricate nexus in urban network necessitates the development of a comprehensive tool to advance sustainable water management and urban planning under the challenge of global climate change.

REFERENCES

Akbari H (2009) Cooling our communities. A guidebook on tree planting and light-colored surfacing. Lawrence Berkeley National Laboratory, pp. 245

Alexander LV, Zhang X, Peterson TC, Caesar J, Gleason B, Klein Tank AM, Haylock M, Collins D, Trewin B, Rahimzadeh F, Tagipour A (2006) Global observed changes in daily climate extremes of temperature and precipitation. J Geophys Res: Atmos 111:D05109

Arizona Department of Adminstration (2015) Empolyment and population statistics. Available at http://population.az.gov/population-projections. Accessed April 11, 2016.

Arizona Department of Water Resources (2014) Fourth management plan. Available at http://www.azwater.gov/AzDWR/WaterManagement/AMAs/FourthManagementPlan.htm. Accessed April 11, 2016.

Arnfield AJ (2003) Two decades of urban climate research: A review of turbulence, exchanges of energy and water, and the urban heat island. Int J Climatol 23:1-26

Bateni SM, Entekhabi D (2012) Relative efficiency of land surface energy balance components. Water Resour Res 48:W04510

Bergeron O, Strachan IB (2012) Wintertime radiation and energy budget along an urbanization gradient in Montreal, Canada. Int J Climatol 32:137-152

Best MJ (2005) Representing urban areas within operational numerical weather prediction models. Boundary-Layer Meteorol 114:91-109

Bonfils C, Lobell DB (2007) Empirical evidence for a recent slowdown in irrigation-induced cooling. Proc Natl Acad Sci USA 104:13582-13587

Botham-Myint D, Recktenwald GW, Sailor DJ (2015) Thermal footprint effect of rooftop urban cooling strategies. Urban Clim 14:268-277

Bowler DE, Buyung-Ali L, Knight TM, Pullin AS (2010) Urban greening to cool towns and cities: A systematic review of the empirical evidence. Landscape Urban Plan 97:147-155

Brazel A, Selover N, Vose R, Heisler G (2000) The tale of two climates - Baltimore and Phoenix urban LTER sites. Clim Res 15:123-135

Brown R, Keath N, Wong T (2009) Urban water management in cities: historical, current and future regimes. Water Sci Tech 59:847-855

Brubaker KL, Entekhabi D (1996) Analysis of feedback mechanisms in land-atmosphere interaction. Water Resour Res 32:1343-1357

Chen F, Dudhia J (2001) Coupling an advanced land surface-hydrology model with the Penn State-NCAR MM5 modeling system. Part I: Model implementation and sensitivity. Mon Weather Rev 129:569-585

Chen F, Kusaka H, Bornstein R, Ching J, Grimmond CSB, Grossman-Clarke S, Loridan T, Manning KW, Martilli A, Miao SG, Sailor D, Salamanca FP, Taha H, Tewari M, Wang XM, Wyszogrodzki AA, Zhang CL (2011) The integrated WRF/urban modelling system: development, evaluation, and applications to urban environmental problems. Int J Climatol 31:273-288

Cheng WY, Steenburgh WJ (2005) Evaluation of surface sensible weather forecasts by the WRF and the Eta models over the western United States. Wea Forecasting 20:812-821

Chow WT, Brazel AJ (2012) Assessing xeriscaping as a sustainable heat island mitigation approach for a desert city. Build Environ 47:170-181

Chow WT, Volo TJ, Vivoni ER, Jenerette GD, Ruddell BL (2014) Seasonal dynamics of a suburban energy balance in Phoenix, Arizona. Int J Climatol 34: 3863-3880

City of Mesa (2013) Residential grass to xericscape rebate. Available at http://www.mesaaz.gov/residents/ water-conservation/residential-grass-to-xeriscape-rebate. Accessed April 11, 2016.

City of Phoenix (2010) Tree and shade master plan, pp. 53.

de Vries S, Verheij RA, Groenewegen P, Spreeuwenberg P (2003) Natural environments–healthy environments? An exploratory analysis of the relationship between greenspace and health. Environ Plan 35:1717-1731

Diem JE, Brown DP (2003) Anthropogenic impacts on summer precipitation in central Arizona, USA. Prof Geogr 55:343-355

Dodson R, Marks D (1997) Daily air temperature interpolated at high spatial resolution over a large mountainous region. Clim Res 8:1-20

Dudhia J (1989) Numerical study of convection observed during the winter monsoon experiment using a mesoscale two-dimensional model. J Atmos Sci 46:3077-3107

Dvorak B, Volder A (2010) Green roof vegetation for North American ecoregions: A literature review. Landscape Urban Plan 96:197-213

Eigenbrod F, Bell VA, Davies HN, Heinemeyer A, Armsworth PR, Gaston KJ (2011) The impact of projected increases in urbanization on ecosystem services. Proc R Soc Lond B: Biol Sci :rspb20102754

European Commission (2012) Energy, transport and environment indicators, Eurostat, Italy, pp. 234

Field CB, Barros VR, Mach K, Mastrandrea M (2014) Climate change 2014: impacts, adaptation, and vulnerability. Working Group II Contribution to the IPCC 5th Assessment Report – Technical Summary, pp 76

Friedl MA, McIver DK, Hodges JC, Zhang XY, Muchoney D, Strahler AH, Woodcock CE, Gopal S, Schneider A, Cooper A, Baccini A (2002) Global land cover mapping from MODIS: algorithms and early results. Remote Sens Environ 83:287-302

Fry JA, Xian G, Jin S, Dewitz JA, Homer CG, Limin Y, Barnes CA, Herold ND, Wickham JD (2011) Completion of the 2006 national land cover database for the conterminous United States. Photogramm Eng Remote Sens 77:858-864

Fung WY, Lam KS, Hung WT, Pang SW, Lee YL (2006) Impact of urban temperature on energy consumption of Hong Kong. Energy 31:2623-2637

Georgescu M, Mahalov A, Moustaoui M (2012) Seasonal hydroclimatic impacts of Sun Corridor expansion. Environ Res Lett 7:034026

Georgescu M, Morefield PE, Bierwagen BG, Weaver CP (2014) Urban adaptation can roll back warming of emerging megapolitan regions. P Natl Acad Sci 111:2909-2914

Georgescu M (2015) Challenges associated with adaptation to future urban expansion. J Climate 28:2544-2563

Geros V, Santamouris M, Karatasou S, Tsangrassoulis A, Papanikolaou N (2005) On the cooling potential of night ventilation techniques in the urban environment. Energy Build 37:243-257

Givoni B (1963) Estimation of the effect of climate on man: Development of a new thermal index. PhD Thesis, Israel Institute of Technology

Gober P, Brazel A, Quay R, Myint S, Grossman-Clarke S, Miller A, Rossi S (2010) Using watered landscapes to manipulate urban heat island effects: How much water will it take to cool Phoenix?. J Am Plan Assoc 76:109-121

Gober P, Kirkwood CW (2010) Vulnerability assessment of climate-induced water shortage in Phoenix. Proc Natl Acad Sci USA 107:21295-21299

Gober P, Middel A, Brazel A, Myint S, Chang H, Duh JD, House-Peters L (2012) Tradeoffs between water conservation and temperature amelioration in Phoenix and Portland: implications for urban sustainability. Urban Geogr 33:1030-1054

Golden JS, Hartz D, Brazel A, Luber G, Phelan P (2008) A biometeorology study of climate and heat-related morbidity in Phoenix from 2001 to 2006. Int J Biometeorol 52:471-480

Goodwin NR, Coops NC, Tooke TR, Christen A, Voogt JA (2009) Characterizing urban surface cover and structure with airborne LIDAR technology. Can J Remote Sens 35:297-309

Grimm NB, Faeth SH, Golubiewski NE, Redman CL, Wu J, Bai X, Briggs JM (2008) Global change and the ecology of cities. Science 319:756-760

Grimmond CSB, Oke TR (1986) Urban water balance: 2. Results from a suburb of Vancouver, British Columbia. Water Resour Res 22:1404-1412

Grimmond CSB (1992) The suburban energy balance: Methodological considerations and results for a mid-latitude west coast city under winter and spring conditions. Int J Climatol 12:481-497

Grimmond CSB, Blackett M, Best MJ, Barlow J, Baik JJ, Belcher SE, Bohnenstengel SI, Calmet I, Chen F, Dandou A, Fortuniak K, Gouvea ML, Hamdi R, Hendry M, Kawai T, Kawamoto Y, Kondo H, Krayenhoff ES, Lee SH, Loridan T, Martilli A, Masson V, Miao S, Oleson K, Pigeon G, Porson A, Ryu YH, Salamanca F, Shashua-Bar L, Steeneveld GJ, Tombrou M, Voogt J, Young D, Zhang N (2010) The international urban energy balance models comparison project: First results from Phase 1. J Appl Meteorol Clim 49:1268-1292

Grimmond CSB, Blackett M, Best MJ, Baik JJ, Belcher SE, Beringer J, Bohnenstengel SI, Calmet I, Chen F, Coutts A, Dandou A, Fortuniak K, Gouvea ML, Hamdi R, Hendry M, Kanda M, Kawai T, Kawamoto Y, Kondo H, Krayenhoff ES, Lee SH, Loridan T, Martilli A, Masson V, Miao S, Oleson K, Ooka R, Pigeon G, Porson A, Ryu YH, Salamanca F, Steeneveld GJ, Tombrou M, Voogt JA, Young DT, Zhang N (2011) Initial results from Phase 2 of the international urban energy balance model comparison. Int J Climatol 31:244-272

Hagishima A, Narita KI, Tanimoto J (2007) Field experiment on transpiration from isolated urban plants. Hydrol Process 21:1217-1222

Harriman III LG, Plager D, Kosar D (1997) Dehumidification and cooling loads from ventilation air. ASHRAE J 39:37-45

Hirano Y, Fujita T (2012) Evaluation of the impact of the urban heat island on residential and commercial energy consumption in Tokyo. Energy 37:371-383

Hong SY, Noh Y, Dudhia J (2006) A new vertical diffusion package with an explicit treatment of entrainment processes. Mon Weather Rev 134:2318-2341

Imhoff ML, Zhang P, Wolfe RE, Bounoua L (2010) Remote sensing of the urban heat island effect across biomes in the continental USA. Remote Sens Environ 114:504-513

Jim CY, He H (2010) Coupling heat flux dynamics with meteorological conditions in the green roof ecosystem. Ecol Engineer 36:1052-1063

Johnson TD, Belitz K (2012) A remote sensing approach for estimating the location and rate of urban irrigation in semi-arid climates. J Hydrol 414:86-98

Kain JS (2004) The Kain-Fritsch convective parameterization: an update. J Appl Meteorol 43:170-181

Karlessi T, Santamouris M, Apostolakis K, Synnefa A, Livada I (2009) Development and testing of thermochromic coatings for buildings and urban structures. Sol Energy 83:538-551

Krayenhoff ES, Christen A, Martilli A, Oke TR (2014) A multi-layer radiation model for urban neighbourhoods with trees. Boundary-Layer Meteorol 151:139-178

Kusaka H, Kondo H, Kikegawa Y, Kimura F (2001) A simple single-layer urban canopy model for atmospheric models: Comparison with multi-layer and slab models. Boundary-Layer Meteorol 101:329-358

Kusaka H, Chen F, Tewari M, Dudhia J, Gill DO, Duda MG, Wang W, Miya Y (2012a) Numerical simulation of Urban Heat Island effect by the WRF Model with 4-km grid increment: an inter-comparison study between the urban canopy model and slab model. J Meteorol Soc Japan 90B:33-45

Kusaka H, Hara M, Takane Y (2012b) Urban climate projection by the WRF model at 3-km horizontal grid increment: Dynamical downscaling and predicting heat stress in the 2070's August for Tokyo, Osaka, and Nagoya metropolises. J Meteorol Soc Japan 90B:47-63

LADWP (City of Los Angeles Department of Water and Power) (2001) Urban water management plan: fiscal year 2000-2001 annual update. City of Los Angeles, California

Lantz N, Wang J (2010) Land cover information extraction using high resolution satellite data in Montreal. EPiCC Technical Report No. 5, pp 28. Available from http://www.epicc.ca/media-centre/presentations#TechDocs

Lee SH, Park SU (2008) A vegetated urban canopy model for meteorological and environmental modelling. Boundary-Layer Meteorol 126:73-102

Lemonsu A, Belair S, Mailhot J, Leroyer S (2010) Evaluation of the town energy balance model in cold and snowy conditions during the Montreal urban snow experiment 2005. J Appl Meteorol Clim 49:346-362

Li D, Bou-Zeid E (2013) Synergistic interactions between urban heat islands and heat waves: The impact in cities is larger than the sum of its parts. J Appl Meteorol Climatol 52:2051-2064

Li D, Bou-Zeid E, Oppenheimer M (2014) The effectiveness of cool and green roofs as urban heat island mitigation strategies. Environ Res Lett 9:055002

Lin CY, Chen F, Huang JC, Chen WC, Liou YA, Chen WN, Liu SC (2008) Urban heat island effect and its impact on boundary layer development and land–sea circulation over northern Taiwan. Atmos Environ 42:5635-5649

Lin TP, Matzarakis A, Hwang RL (2010) Shading effect on long-term outdoor thermal comfort. Build Environ 45:213-221

Lobell DB, Bonfils C (2008) The effect of irrigation on regional temperatures: A spatial and temporal analysis of trends in California 1934-2002. J Clim 21:2063-2071

Loridan T, Grimmond CSB, Grossman-Clarke S, Chen F, Tewari M, Manning K, Martilli A, Kusaka H, Best M (2010) Trade-offs and responsiveness of the single-layer urban canopy parametrization in WRF: An offline evaluation using the MOSCEM optimization algorithm and field observations. Q J R Meteorol Soc 136:997-1019

Ma Y, Zhang X, Zhu B, Wu K (2002) Research on reversible effects and mechanism between the energy-absorbing and energy-reflecting states of chameleon-type building coatings. Sol Energy 72:511-520

MacDonald GM (2010) Water, climate change, and sustainability in the southwest. Proc Natl Acad Sci USA 107:21256-21262

Martilli A, Clappier A, Rotach MW (2002) An urban surface exchange parameterisation for mesoscale models. Boundary-Layer Meteorol 104:261-304

Masson V (2000) A physically-based scheme for the urban energy budget in atmospheric models. Boundary-Layer Meteorol 94:357-397

Mayer PW, Deoreo WBE (1999) Residential end uses of water. American Water Works Association, Denver, pp 310

Mell IC (2010) Green infrastructure: concepts, perceptions and its use in spatial planning. Ph.D. Thesis, Newcastle University, Newcastle, 291 pp.

Mentens J, Raes D, Hermy M (2006) Green roofs as a tool for solving the rainwater runoff problem in the urbanized 21st century?. Landscape Urban Plan 77:217-226

Miao S, Chen F (2008) Formation of horizontal convective rolls in urban areas. Atmos Res 89:298-304

Miao S, Dou J, Chen F, Fan S (2012) Analysis of observations on the urban surface energy balance in Beijing. Sci China Earth Sci 55:1881-1890

Miao S, Chen F (2014) Enhanced modeling of latent heat flux from urban surfaces in the Noah/single-layer urban canopy coupled model. Sci China Earth Sci 57: 2408-2416

Middel A, Häb K, Brazel AJ, Martin CA, Guhathakurta S (2014) Impact of urban form and design on mid-afternoon microclimate in Phoenix Local Climate Zones. Landscape Urban Plan 122:16-28

Mishra AK, Ramgopal M (2013) Field studies on human thermal comfort—An overview. Build Environ 64:94-106

Mitchell V, Mein RG, McMahon TA (2001) Modelling the urban water cycle. Environ Modell Softw 16: 615-629

Mitchell V, Cleugh H, Grimmond C, Xu J (2008) Linking urban water balance and energy balance models to analyse urban design options. Hydrol Process 22:2891-2900

Mlawer EJ, Taubman SJ, Brown PD, Iacono MJ, Clough SA (1997) Radiative transfer for inhomogeneous atmospheres: RRTM, a validated correlated-k model for the longwave. J Geophys Res: Atmos 102:16663-16682

Moriwaki R, Kanda M, Senoo H, Hagishima A, Kinouchi T (2008) Anthropogenic water vapor emissions in Tokyo. Water Resour Res 44:W11424

Myint SW, Gober P, Brazel A, Grossman-Clarke S, Weng QH (2011) Per-pixel vs. object-based classification of urban land cover extraction using high spatial resolution imagery. Remote Sens Environ 115:1145-1161

Nazaroff WW (2013) Exploring the consequences of climate change for indoor air quality. Environ Res Lett 8:015022

Niachou A, Papakonstantinou K, Santamouris M, Tsangrassoulis A, Mihalakakou G (2001) Analysis of the green roof thermal properties and investigation of its energy performance. Energy Build 33:719-729

Oberndorfer E, Lundholm J, Bass B, Coffman RR, Doshi H, Dunnett N, Gaffin S, Köhler M, Liu KKY, Rowe B (2007) Green roofs as urban ecosystems: ecological structures, functions, and services. BioScience 57:823-833

Oke TR (1979) Advectively-assisted evapotranspiration from irrigated urban vegetation. Boundary-Layer Meteorol 17:167-173

Oke TR (1988) The urban energy balance. Prog Phys Geog 12:471-508

Park M, Hagishima A, Tanimoto J, Narita KI (2012) Effect of urban vegetation on outdoor thermal environment: field measurement at a scale model site. Build Environ 56:38-46

Pearlmutter D, Berliner P, Shaviv E (2007) Integrated modeling of pedestrian energy exchange and thermal comfort in urban street canyons. Build Environ 42:2396-2409

Perkins SE, Pitman AJ, Holbrook NJ, McAneney J (2007) Evaluation of the AR4 climate models' simulated daily maximum temperature, minimum temperature, and precipitation over Australia using probability density functions. J Clim 20:4356-4376

Peñuelas J, Filella I (2009) Phenology feedbacks on climate change. Science 324:887-888.

Poulos GS, Blumen W, Fritts DC, Lundquist JK (2002) CASES-99: A comprehensive investigation of the stable nocturnal boundary layer. Bull Am Meteorol Soc 83:555-581

Ramamurthy P, Bou-Zeid E (2014) Contribution of impervious surfaces to urban evaporation. Water Resour Res 50:2889-2902

Ramamurthy P, Bou-Zeid E, Smith JA, Wang Z, Baeck ML, Saliendra NZ, Hom JL, Welty C (2014) Influence of subfacet heterogeneity and material properties on the urban surface energy budget. J Appl Meteorol Climatol 53:2114-2129

Retzlaff R (2008) Green building assessment systems: A framework and comparison for planners. J Am Plan Assoc 74:505-519

Rizwan AM, Dennis LY, Chunho LIU (2008) A review on the generation, determination and mitigation of Urban Heat Island. J Environ Sci 20:120-128

Roy S, Byrne J, Pickering C (2012) A systematic quantitative review of urban tree benefits, costs, and assessment methods across cities in different climatic zones. Urban For Urban Gree 11:351-363

Sacks WJ, Cook BI, Buenning N, Levis S, Helkowski JH (2009) Effects of global irrigation on the near-surface climate. Clim Dyn 33:159-175

Sailor DJ, Lu L (2004) A top-down methodology for developing diurnal and seasonal anthropogenic heating profiles for urban areas. Atmos Environ 38:2737-2748

Sailor DJ, Hart M (2006) An anthropogenic heating database for major US cities. In: Sixth Symposium on the Urban Environment, Atlanta, Georgia, 28 January - 3 February 2006

Sailor DJ, Brooks A, Hart M, Heiple S (2007) A bottom-up approach for estimating latent and sensible heat emissions from anthropogenic sources. In: Seventh Symposium on the Urban Environment, San Diego, California, 10-13 September 2007

Salamanca F, Krpo A, Martilli A, Clappier A (2010) A new building energy model coupled with an urban canopy parameterization for urban climate simulations-part I. formulation, verification, and sensitivity analysis of the model. Theor Appl Climatol 99:331-344

Salamanca F, Martilli A, Tewari M, Chen F (2011) A study of the urban boundary layer using different urban parameterizations and high-resolution urban canopy parameters with WRF. J Appl Meteorol Clim 50:1107-1128

Santamouris M, Pavlou C, Doukas P, Mihalakakou G, Synnefa A, Hatzibiros A, Patargias P (2007) Investigating and analysing the energy and environmental performance of an experimental green roof system installed in a nursery school building in Athens, Greece. Energy 32:1781-1788

Santamouris M (2014) Cooling the cities-a review of reflective and green roof mitigation technologies to fight heat island and improve comfort in urban environment. Sol Energy 103:682-703

Sarrat C, Lemonsu A, Masson V, Guedalia D (2006) Impact of urban heat island on regional atmospheric pollution. Atmos Environ 40:1743-1758

Senay GB, Budde M, Verdin JP, Melesse AM (2007) A coupled remote sensing and simplified surface energy balance approach to estimate actual evapotranspiration from irrigated fields. Sensors 7:979-1000

Seto KC, Fragkias M, Guneralp B, Reilly MK (2011) A meta-analysis of global urban land expansion. PLoS One 6:e23777

Seto K, Dhakal S (2014) Chapter 12: Human Settlements, Infrastructure, and Spatial Planning, in: Climate Change 2014: Mitigation of Climate Change. Contribution of Working Group III to the Fifth Assessment Report of the Intergovernmental Panel on Climate Change, pp. 67-76

Shashua-Bar L, Hoffman ME (2000) Vegetation as a climatic component in the design of an urban street: An empirical model for predicting the cooling effect of urban green areas with trees. Energy Build 31:221-235

Shashua-Bar L, Pearlmutter D, Erell E (2011) The influence of trees and grass on outdoor thermal comfort in a hot-arid environment. Int J Climatol 31:1498-1506

Sivak M (2008) Where to live in the United States: Combined energy demand for heating and cooling in the 50 largest metropolitan areas. Cities 25:396-398

Skamarock WC, Klemp JB (2008) A time-split nonhydrostatic atmospheric model for weather research and forecasting applications. J Comput Phys 227:3465-3485

Song J, Wang ZH (2015) Interfacing the urban land–atmosphere system through coupled urban canopy and atmospheric models. Boundary-Layer Meteorol 154:427-448

Sun T, Bou-Zeid E, Wang ZH, Zerba E, Ni GH (2013) Hydrological determinants of green roof performance via a vertically-resolved model for heat and water transport. Build Environ 60:211-224

Sunwoo Y, Chou C, Takeshita J, Murakami M, Tochihara Y (2006a) Physiological and subjective responses to low relative humidity in young and elderly men. J Physiol Anthropol 25:229-238

Sunwoo Y, Chou C, Takeshita J, Murakami M, Tochihara Y (2006b) Physiological and subjective responses to low relative humidity. J Physiol Anthropol 25:7-14

Synnefa A, Santamouris M, Livada I (2006) A study of the thermal performance of reflective coatings for the urban environment. Sol Energy 80:968-981

Synnefa A, Dandou A, Santamouris M, Tombrou M, Soulakellis N (2008) On the use of cool materials as a heat island mitigation strategy. J Appl Meteorol Climatol 47:2846-2856

Tan J, Zheng Y, Tang X, Guo C, Li L, Song G, Zhen X, Yuan D, Kalkstein AJ, Li F, Chen H (2010) The urban heat island and its impact on heat waves and human health in Shanghai. Int J Biometeorol 54:75-84

Thompson G, Field PR, Rasmussen RM, Hall WD (2008) Explicit forecasts of winter precipitation using an improved bulk microphysics scheme. Part II: Implementation of a new snow parameterization. Mon Weather Rev 136:5095-5115

Tooke TR, Coops NC, Goodwin NR, Voogt JA (2009) Extracting urban vegetation characteristics using spectral mixture analysis and decision tree classifications. Remote Sens Environ 113:398-407

Topak R, Suheri S, Acar B (2010) Comparison of energy of irrigation regimes in sugar beet production in a semi-arid region. Energy 35:5464-5471

Tran H, Uchihama D, Ochi S, Yasuoka Y (2006) Assessment with satellite data of the urban heat island effects in Asian mega cities. Int J Appl Earth Obs Geoinf 8:34-48

Tzoulas K, Korpela K, Venn S, Yli-Pelkonen V, Kaźmierczak A, Niemela J, James P (2007) Promoting ecosystem and human health in urban areas using Green Infrastructure: A literature review. Landscape Urban Plan 81:167-178

United Nations (2012) World urbanization prospects: The 2011 revision. The United Nations' Department of Economic and Social Affairs - Population Division, New York, pp 50

United States Census Bureau, Phoenix quick facts, in: http://quickfacts.census.gov/qfd/states/04/0455000.html, Retrieved October 5, 2016

Vahmani P, Hogue TS (2014) Incorporating an urban irrigation module into the Noah land surface model coupled with an urban canopy model. J Hydrometeorol 15:1440-1456

Vairavamoorthy K, Gorantiwar SD, Pathirana A (2008) Managing urban water supplies in developing countries – Climate change and water scarcity scenarios. Phys Chem Earth 33:330-339

van der Laan M, Tooke TR, Christen A, Coops N, Heyman E, Olchovski I (2011), Statistics on the built infrastructure at the Vancouver EPiCC experimental sites. EPiCC Technical Report No. 4, pp 30. Available from http://www.epicc.ca/media-centre/presentations/#TechDocs

Vandermeulen V, Verspecht A, Vermeire B, Van Huylenbroeck G, Gellynck X (2011) The use of economic valuation to create public support for green infrastructure investments in urban areas. Landscape Urban Plan 103:198-206

Volo TJ, Vivoni ER, Martin CA, Earl S, Ruddell BL (2014) Modeling soil moisture, water partitioning and plant water stress under irrigated conditions in desert urban areas. Ecohydrol 7:1297-1313

Vörösmarty CJ, Green P, Salisbury J, Lammers RB (2000) Global water resources: vulnerability from climate change and population growth. Science 289:284-288

Wang ZH, Bou-Zeid E, Smith JA (2011a) A spatially-analytical scheme for surface temperatures and conductive heat fluxes in urban canopy models. Boundary-Layer Meteorol 138:171-193

Wang ZH, Bou-Zeid E, Au SK, Smith JA (2011b) Analyzing the sensitivity of WRF's single-layer urban canopy model to parameter uncertainty using advanced Monte Carlo simulation. J Appl Meteorol Clim 50:1795-1814

Wang ZH, Bou-Zeid E, Smith JA (2013) A coupled energy transport and hydrological model for urban canopies evaluated using a wireless sensor network. Q J R Meteorol Soc 139:1643-1657

Wang ZH (2014a) Monte Carlo simulations of radiative heat exchange in a street canyon with trees. Sol Energy 110:704-713

Wang ZH (2014b) A new perspective of urban–rural differences: The impact of soil water advection. Urban Clim 10:19-34

Wang ZH, Zhao X, Yang, J, Song J (2016) Cooling and energy saving potentials of shade trees and urban lawns in a desert city. Appl Energy 161:437-444

Wang ZX, Jiang YH, Li J, Liu WD, Wang Q (2009) On the measurement of urban boundary layer radiation of the meteorological tower in Beijing (in Chinese). Plateau Meteorol 28:20-27

Wang C, Myint SW, Wang Z-H, Song J (2016) Spatio-temporal modeling of the urban heat island in the Phoenix metropolitan area: Land use change implications. Remote Sens 8:185.

Wilmers F (1988) Green for melioration of urban climate. Energy Build 11:289-299

Wong NH, Cheong DW, Yan H, Soh J, Ong CL, Sia A (2003) The effects of rooftop garden on energy consumption of a commercial building in Singapore. Energy Build 35:353-364

Yang Z, Arritt RW (2002) Tests of a perturbed physics ensemble approach for regional climate modeling. J Clim 15:2881-2896

Yang J, Wang ZH, Lee TW (2013) Relative efficiency of surface energy partitioning over different land covers. Brit J Environ Clim Change 3:86-102

Yang J, Wang ZH (2014a) Parameterization and sensitivity of urban hydrological models: Application to green roof systems. Build Environ 75:250-263

Yang J, Wang ZH (2014b) Land surface energy partitioning revisited: A novel approach based on single depth soil measurement. Geophys Res Lett 41:8348-8358

Yang J, Wang ZH (2015) Optimizing urban irrigation schemes for the trade-off between energy and water consumption. Energy Build 107:335-344

Yang J, Wang ZH, Chen F, Miao S, Tewari M, Voogt J, Myint S (2015a) Enhancing hydrologic modeling in the coupled Weather Research and Forecasting - urban modeling system. Boundary-Layer Meteorol 155:87-109

Yang J, Wang ZH, Kaloush KE (2015b) Environmental impacts of reflective materials: Is high albedo a 'silver' bullet for mitigating urban heat island?. Renew Sustain Energy Rev 47:830-843

Yang J, Wang ZH, Georgescu M, Chen F, Tewari M (2016a) Assessing the impact of enhanced hydrological processes on urban hydrometeorology with application to two cities in contrasting climates. J Hydrometeorol 17:1031-1047

Yang J, Wang ZH, Kaloush KE, Dylla H (2016b) Effect of pavement thermal properties on mitigating urban heat islands: A multi-scale modelling case study in Phoenix. Build Environ 108:110-121

Yang J, Yu Q, Gong P (2008) Quantifying air pollution removal by green roofs in Chicago. Atmos Environ 42:7266-7273